BNWL-750

FAST FLUX
TEST FACILITY
PROJECT REPORT

5-

[redacted]

THERMAL-HYDRAULIC AND MECHANICAL ASPECTS OF FTR FUEL PIN SPACER DESIGN

OCTOBER 1968

[redacted]

AEC RESEARCH & DEVELOPMENT REPORT

R. A. Jones	33747	3706	JAN 12 1970

BATTELLE NORTHWEST
BATTELLE MEMORIAL INSTITUTE
PACIFIC NORTHWEST LABORATORY
BATTELLE BOULEVARD, P. O. BOX 999, RICHLAND, WASHINGTON 99352

BNWL-750

INFORMATION CONCERNING USE OF THIS REPORT

PATENT STATUS

This document copy, since it is transmitted in advance of patent clearance, is made available in confidence solely for use in performance of work under contracts with the U.S. Atomic Energy Commission. This document is not to be published nor its contents otherwise disseminated or used for purposes other than specified above before patent approval for such release or use has been secured, upon request to the Chief, Chicago Patent Group, U. S. Atomic Energy Commission, 9800 So. Cass Avenue, Illinois.

PRELIMINARY REPORT

This report contains information of a preliminary nature prepared in the course of work under Atomic Energy Commission Contract AT(45-1)-1830. This information is subject to correction or modification upon the collection and evaluation of additional data.

LEGAL NOTICE

This report was prepared as an account of Government sponsored work. Neither the United States, nor the Commission, nor any person acting on behalf of the Commission:

A. Makes any warranty or representation, expressed or implied, with respect to the accuracy, completeness, or usefulness of the information contained in this report, or that the use of any information, apparatus, method, or process disclosed in this report may not infringe privately owned rights; or

B. Assumes any liabilities with respect to the use of, or for damages resulting from the use of any information, apparatus, method, or process disclosed in this report.

As used in the above, "person acting on behalf of the Commission" includes any employee or contractor of the Commission, or employee of such contractor, to the extent that such employee or contractor of the Commission, or employee of such contractor prepares, disseminates, or provides access to, any information pursuant to his employment or contract with the Commission, or his employment with such contractor.

PACIFIC NORTHWEST LABORATORY
RICHLAND, WASHINGTON
operated by
BATTELLE MEMORIAL INSTITUTE
for the
UNITED STATES ATOMIC ENERGY COMMISSION UNDER CONTRACT AT(45-1)-1830

PRINTED BY/FOR THE U.S. ATOMIC ENERGY COMMISSION

84-1050-016 (4-68)
AEC-RL RICHLAND, WASH

BNWL-750

THERMAL-HYDRAULIC AND MECHANICAL ASPECTS OF FTR FUEL PIN SPACER DESIGN

by

P. D. Cohn
T. J. Bennett
M. A. Fischer
G. L. Fox
R. J. Jackson
M. T. Jakub
N. L. Johnson
D. C. Kolesar
D. L. Koreis
R. J. Lobsinger
W. E. McClung
M. K. Millhollen
H. G. Powers
J. B. Shafer
W. H. Sutherland
D. R. Wilson

Approved by

P. L. Hofmann

October 1968

BATTELLE MEMORIAL INSTITUTE
PACIFIC NORTHWEST LABORATORY
RICHLAND, WASHINGTON

TABLE OF CONTENTS

LIST OF FIGURES

THERMAL-HYDRAULIC AND MECHANICAL ASPECTS OF FTR FUEL PIN SPACER DESIGN

SUMMARY

This document presents detailed analytical and experimental data and current program status of the hydraulic, mechanical, and thermal aspects of the FTR fuel pin and spacer design. The document deals primarily with the wire wrap spacers. A satisfactory grid system has not yet been proposed and therefore cannot be analyzed. The results of the analyses and tests to date show that the reference wire wrap spacer system for the FTR fuel subassemblies will perform reliably throughout the fuel lifetime. Development of a grid spacer system comparable in performance to the wire wrap can also be expected. Hydraulic and subsequent thermal analyses have shown temperature gradients caused by excess flow around the assembly perimeter to be severe but acceptable from a mechanical stress standpoint. Another major technical requirement, accommodation of fuel pin diametral growth, has been demonstrated both by analytical and experimental data to be adequate for the wire wrap system. While extensive analysis and testing remains to be done, the thorough analysis and experiments completed to date have shown the present spacer system to date to be feasible.

INTRODUCTION

SUMMARY DESCRIPTION OF THE FTR FUEL ASSEMBLY[1]

The main component of the fuel assembly, the subassembly, is a closely packed hexagonal array of fuel pins contained in a hexagonal flow duct. The pins are separated by wire wrap spacers designed to assure adequate cooling for each pin and promote inter-channel mixing. The pins are made of stainless steel tubing approximately 6 ft long. About half of that length contains PuO_2-UO_2. The pellets are compacted to a density sufficient to provide the required fuel loading while accommodating transient fuel melting, retaining fission product swelling, and providing relief of fission gases at appropriate temperatures. Immediately above the fuel column and insulating uranium oxide pellet is a 6-in. long neutron reflector in the form of a nickel or high-nickel alloy rod inserted into the stainless steel cladding. Adequate clearance between the reflector and cladding permits passage of fission gas. Approximately 2 equivalent feet of vacant tube for fission gas plenum occupy the tube above the nickel reflector. End caps are welded into the ends of the cladding tube and the wire wrap spacer is wound around the pin and welded to the end caps.

The pins, assembled in a hexagonal array, are structurally bonded together at their base with a grid assembly. A slotted grid at the top of the assembly allows all but the three anchor pins to expand axially and independently of each other while restraining lateral movement. The pin assembly is attached structurally to the coolant duct by welding between the pin lower grids and the coolant duct wall. Sodium coolant enters the subassembly through the bottom of each duct at the rate of about 1.6×10^5 lb/hr and at a velocity of 25-30 ft per second. The core pin-bundle pressure drop is from 60 to 100 psi. The

coolant experiences an average core temperature rise of 300-350 °F for operation at the design point.

Additional components of the fuel assembly include the lower coolant duct extension providing assembly radial position and coolant inlet passages in the high pressure plenum, the upper coolant duct extension housing the instrument package and providing coolant outlet passages, and the hanger rod attached to the reactor cover supporting the fuel assembly and serving as the upper structural member. Table I lists the reference design characteristics of the FTR fuel subassembly.

TABLE I. FFTF Fuel Subassembly Characteristics

Reactor Power, MW_t	350-450		
Pin OD, in.	0.250		
Cladding ID, in.	0.218		
Pin Separation:			
Method	wire wrap, all pins (0.030 in. triangular pitch		
Center-to-Center Spacing, in.	0.28		
Nominal Rod Separation, in.	0.030		
Pin Support Span, in.	2		
Sodium Coolant:			
Flow Direction	up		
Average Velocity, ft/sec	26		
Core Pressure Drop, psi	60-100		
Pin Linear Power, kW/ft:			
average	7.85		
maximum	14.4		
maximum (with OPF)	18.0		
Heat Flux, 10^6 Btu/hr-ft^2:			
average	0.409		
maximum	0.750		
maximum (with OPF)	0.936		
Nuclear Power Peaking Factors:			
Axial	1.24		
Radial	1.3	1.84	2.30
Engineering, Hot Spot-Hot Channel	1.14 (max)		
Overpower Factor (OPF)	1.25 (steady state)		(max with overpower)
Fuel Subassembly Data:			
Pins/Subassembly	217		
Active Fuel Length, in.	32		
Fuel Pin Length, ft	6-7		
Plenum Length, in.	24 (equivalent, plus 6-in. Ni or high Ni alloy reflector) (~30 in. actual length)		
Location	top		
Other Supporting Data:			
Coolant Temperature			
Inlet, °F	550		
Outlet (average), °F	900		
maximum operating Na-cladding interface (with hot channel), °F	1060		

Spacing Width

The present reference design incorporates a 30-mil spacing width to satisfy the FTR fuel packing requirement. Wire diameters from 30-50 mils yielding a pitch-to-diameter of 1.12 to 1.20, respectively, are being considered. An intensive program is underway to evaluate all aspects of spacing width, including pressure drop, core fissile load, channel blockage, pin bowing, and assembly considerations.

At present, no unfavorable aspects have been uncovered for the 30-mil wire wrap spacers. Thermal-hydraulic studies have indicated the following:

Design Conditions	30-mil Wire Wrap (P/D = 1.12)	50-mil Wire Wrap (P/D = 1.20)
Min particle size for blockage	51 mils	66 mils
Max overtemperature for tangent touched pins	100 °F	50-100 °F
Max growth to exceed 20% hot channel flow criteria	3%+	4-5%
Radial pin gradient to produce tangent touching pins within support span	>100 °F	~100 °F
Pressure drop for reference design over subassembly length	60 psi	20 psi

Figure 1 shows the relative flow areas for 30, 40, and 50-mil wire wrap spacers.

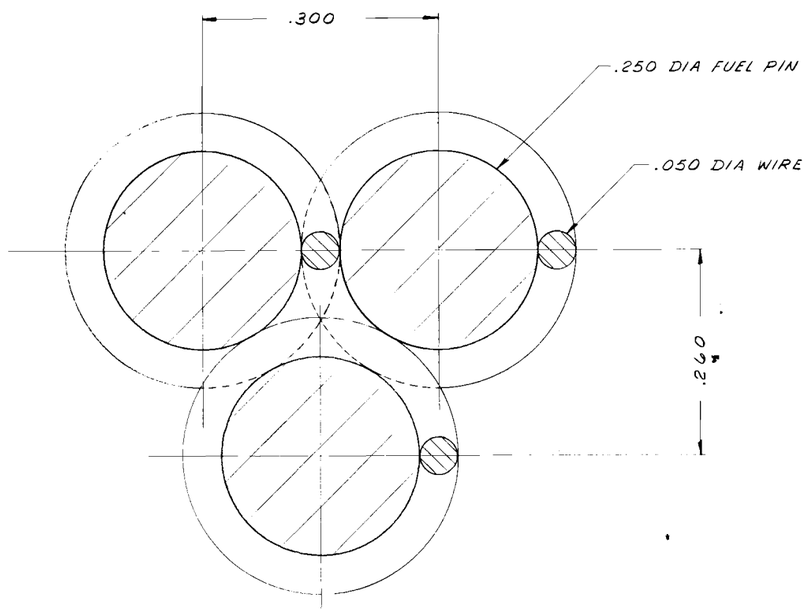

ARRANGEMENT 1

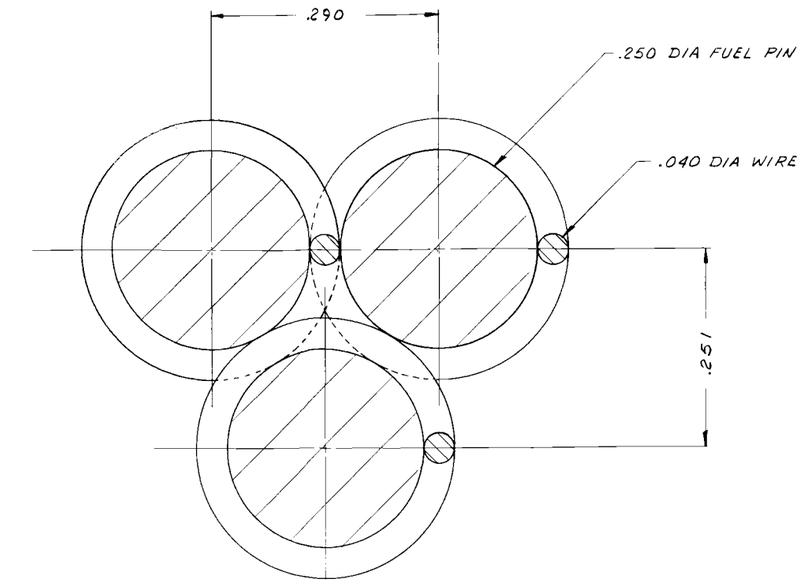

ARRANGEMENT 2

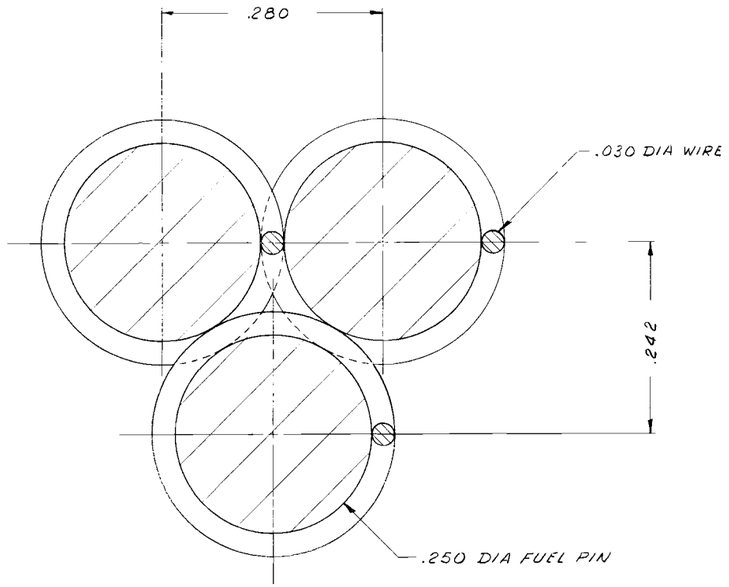

ARRANGEMENT 3

FIGURE 1. *Fuel Rod-Wire Wrap Spacer Arrangement*

WIRE WRAP SPACERS

The reference spacers are individual 30-mil wires wrapped around each fuel pin at a pitch of 1 ft. They serve (1) to maintain spacing in the fuel pin array, and (2) to promote inter-channel mixing. The design of this component is shown on Drawings SK-3-13187 (Figure 2) and 13188 (Figure 3). The characteristics of the wire wrap spacers are listed in Table II.

TABLE II. Wire Wrap Spacers

Size	0.030 ± 0.001 in. diam, length to fit
Pitch	1 ft
Material	304 SS
Type of Connection	TIG weld at each end (PNL-75, PNL Provisional Product Description - Welding 10/20/67)
Specification	ASTM A 478-63 (carbon controlled to 0.04-0.06%)
Material Condition	Fully annealed, <5% C.W. No internal voids or inclusions No surface cracks, laps, or scratches exceeding 0.0005 in. in depth
Operating Conditions (including overpower)	Temperature range, 550-1160 °F Total allowable material loss 0.001 in. per yr
Special Conditions	Maximum tension on wire, when applied, not to exceed 7 lb

Wire wrap spacers serve to:

- Permit uniform pin compliance
- Lower pressure drop characteristics
- Provide positive mixing vectors
- Permit continuous mixing over pin length

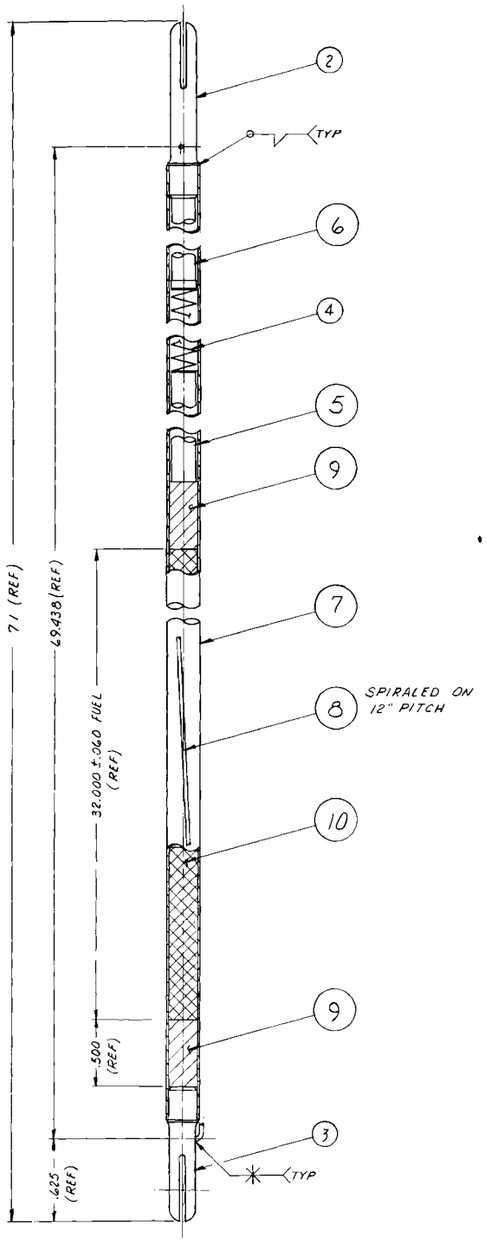

(1) ASSEMBLY

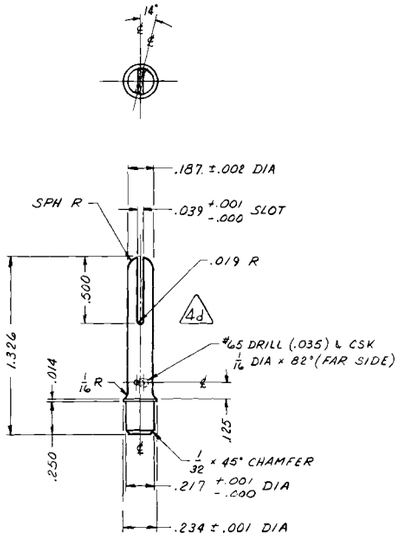

(2) 304 SST

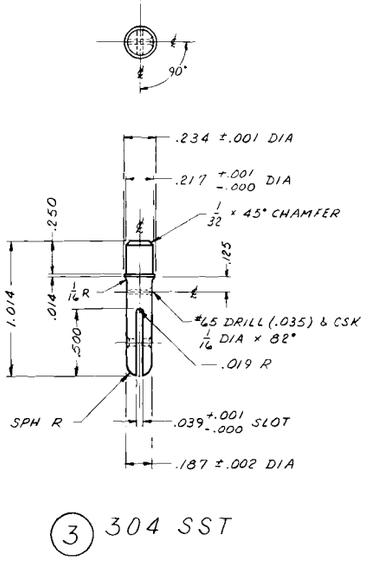

(3) 304 SST

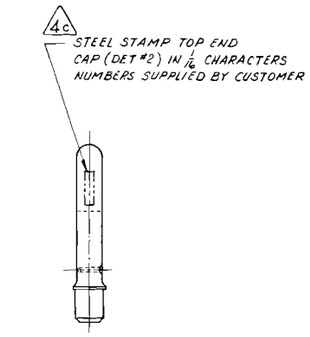

TYP PIECE MARK

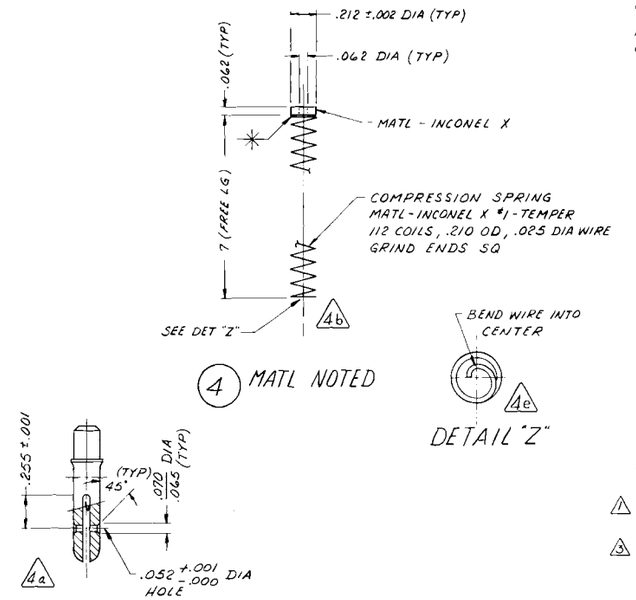

(4) MATL NOTED

DETAIL "Z"

QTY	PART NO.	DESCRIPTION	MATL	REF
X	1	ASSEMBLY		
1	2	END CAP - TOP		
1	3	END CAP - BOTTOM		
1	4	SPRING		
1	5	ROD .212 ±.001 DIA x 6" LONG	NICKEL	
1	6	TUBE .187 ±.002 OD x .014 WALL x 23.594 LG	304 SST	
1	7	TUBE .250 ±.001 OD x .218 ±.001 ID x 69.160 LG	↓	
AR	8	WIRE .030 ±.001 DIA	↓	
AR	9	INSULATOR PELLETS - UO_2		H-3-27832
AR	10	FUEL PELLETS - UO_2-PuO_2		H-3-27831

GENERAL NOTES

ALL PARTS, UNLESS OTHERWISE SPECIFIED, SHALL CONFORM TO THE FOLLOWING:

1. TOLERANCES, FRACTIONAL ±1/64 DECIMAL ±.005 ANGULAR ±0°30'
2. REMOVE ALL BURRS AND BREAK SHARP EDGES TO 1/64 MIN RADIUS, EXCEPT WELD PREP AREA (TUBE END & LIPS)
3. ALL MACHINED SURFACES 32√ (ASA B46.1-1962)
4. ALL MATERIAL TO BE AS SPECIFIED, OR APPROVED EQUAL QUALITY.
5. MATERIAL 304 SST TO BE ASTM SPEC, MODIFIED A 213-65 (CARBON 0.04-0.06)
6. MAXIMUM ACCEPTABLE TUBING OVALITY SHALL BE .002" MEASURED AS THE DIFFERENCE BETWEEN THE MAX AND MIN SPECIFIED INSIDE DIAMETER.
7. MAXIMUM ACCEPTABLE TUBING ECCENTRICITY SHALL BE .002" MEASURED AS THE DIFFERENCE BETWEEN THE SPECIFIED MAX AND MIN WALL THICKNESS AT ANY CROSS-SECTION OF THE TUBES.
8. TUBES SHALL SHOW A MAXIMUM BOW NOT TO EXCEED .010" PER LINEAL FOOT.
9. END CAP WELD DIAMETER SHALL NOT EXCEED MAXIMUM ALLOWABLE TUBE DIA BY MORE THAN .001.
10. INTERNAL ROD ATMOSPHERE SHALL BE WELDING GRADE, OR PURER, HELIUM.
11. SLOTS IN END CAPS SHALL BE PARALLEL TO ℄ OF TUBE TO WITHIN 0°15' AFTER WELDING.
12. ℄ IN END CAPS SHALL BE SYMMETRICAL TO THE ℄ OF THE SLOTS WITHIN A TOLERANCE OF .001.

SK-3-13187

FIGURE 2. Split Core Fuel Pin Assembly and Details

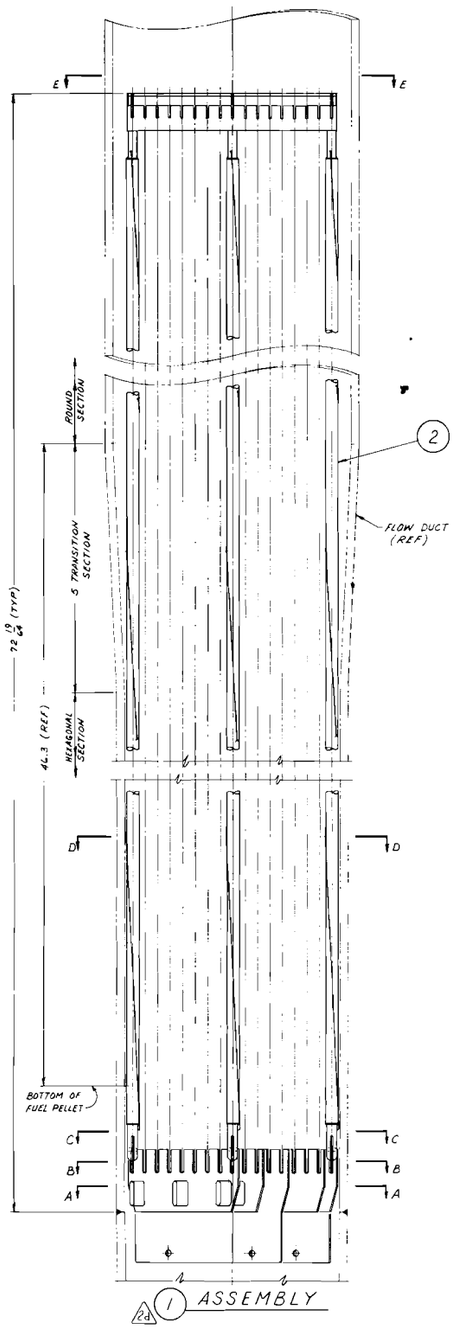

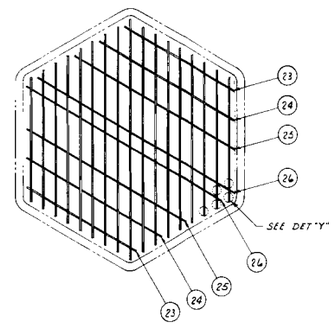

SECTION "B-B"
(LAYER LOCKING GRID)

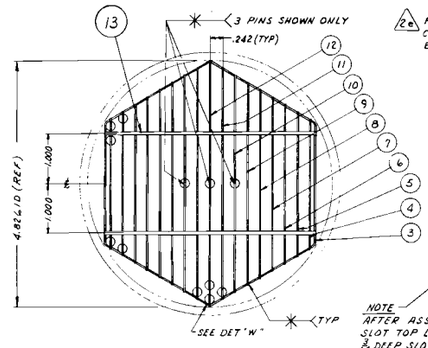

SECTION "E-E"
(TOP LOCKING GRID)

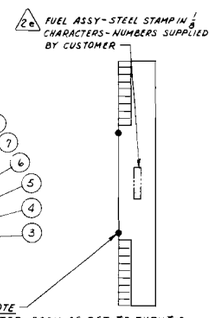

QTY	PART NO.	DESCRIPTION	MATL	REF
X	1	FUEL CLUSTER ASSY		
217	2	FUEL PIN ASSY		SK-3-13187
1	3	RETAINER BAND		SH #2
2	4	STRIP - TOP		
2	5			
2	6			
2	7			
2	8			
2	9			
2	10			
2	11			
1	12			
2	13	ROD 3/32 DIA x 4.204 LONG	304 SST	
2	14	STRIP-LAYER		SH #2
2	15			
2	16			
2	17			
2	18			
2	19			
2	20			
2	21			
1	22			
2	23	STRIP-LOCKING		
2	24			
2	25			
2	26			
3	27	STRIP-SUPPORT		
217	28	PIN .050 ±.001 DIA x .200 ± .005 LONG	304 SST	

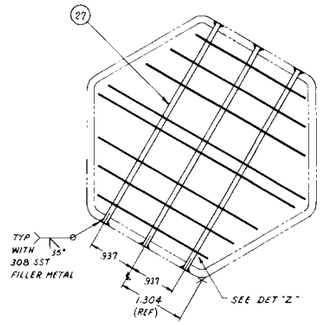

SECTION "A-A"
(ELEMENT SUPPORT)

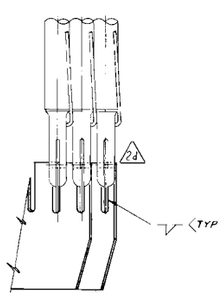

DETAIL "Y"

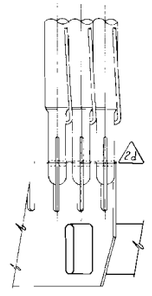

DETAIL "Z"

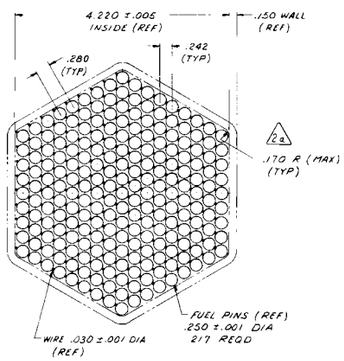

SECTION "D-D"

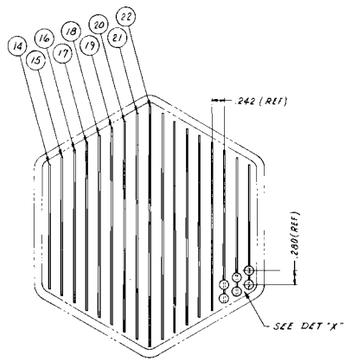

SECTION "C-C"
(LAYER SPACING GRID)

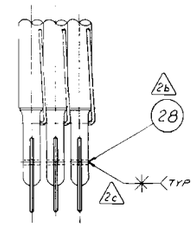

DETAIL "X"

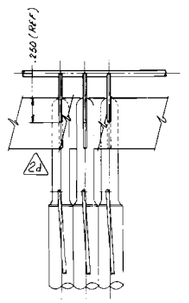

DETAIL "W"

SK-3-13188

FIGURE 3. Split Core Driver Fuel Subassembly
(Sheet 1 of 2)

- Facilitate fabrication
- Permit tightest fuel packing (required for FTR flux [power density]).

Wire wrap used in a triangular pin array on a 12-in. pitch offers, on a 60° progression, support to a pin and its neighbors at 2-in. intervals. Wire wrap spaced subassemblies present the following problems:

- Wire fixity only at the end points
- Possibility of channel blockage during in-channel repositioning
- Poor compliance compared to compliant grid spacers.

GRID SPACERS

Westinghouse Corporation, under Contract AT-(30-1)-3684, is presently examining compliant grid spacers for use in the FTR.[2] These spacers may consist of alternating ring or web-type spacers placed between the fuel pins. Hydraulic testing will be necessary, as in the case of wire wrap, to establish the grid spacer pressure drop characteristics. Wire wrap spacers were chosen for the reference design since this type of spacer demonstrates a favorable pressure drop characteristic when compared to grid spacers.[3] Honeycomb spacers, evaluated in Reference (2), had a 50% higher total absolute pressure drop than a comparable wire wrap system with similar spacing. Analyses of grid spacer design for FTR yielded similar higher pressure drops in wire wrapped systems.

The program presently formulated at PNL includes an evaluation of alternate spacing techniques.

Grid spacers have the attributes of:

- Requiring grid, not pin, compliance
- Compliant characteristics
- Integral support plane.

Problem areas associated with grid spacers involve:

- Requirement of non-standard fabrication methods
- Difficulty in subassembly loading
- Pin scratching
- Possible need for axial fixity may be at each support plane due to pin swelling.
- Relatively high pressure drop
- Less potential for achieving a tight pin spacing.

ANALYTICAL AND EXPERIMENTAL PROGRAMS

The integrated project plan for pin and spacer hydraulic, mechanical, and thermal analysis, water flow, sodium flow, and mechanical testing fuel pins, bundles, and subassemblies is required to establish operating behavior and provide reliable driver fuel for the FTR.[4]

The analytical and testing programs are directed toward solving design uncertainties empirically through tests where analytical techniques are not sufficiently sophisticated to guarantee meeting requirements. Tests are pursued when observation through testing under prototype or near prototype conditions is the only available method for performance prediction.

The analytical and testing programs attempt to simulate all possible FTR fuel operating experiences, and couple results with the effects of irradiation as generated in the FTR fuel and cladding irradiation programs. The problems of erosion and corrosion are examined in light of other reactor operating experience where a temperature gradient is imposed on the fuel assembly. Coupling of the mechanical effects of vibration, fretting corrosion, fretting fatigue, etc. with the vibration and material removal measurements noted in hydraulic and the sodium dynamic tests will be performed. The total fuel operating experience cannot be simulated in any one of these tests,

since a number of the more important operating conditions, such as core ΔT radiation exposure and in-core induced vibrations, are absent. Thermal effects will be further simulated in the heated fuel pin bundle tests.[5] The thermal-hydraulic studies also examine abberated pin bundles, varied spacing, varied spacer geometry, and differences between compliant grid spacers and the reference wire wrap spacers. Data from the tests described in this document and the thermal-hydraulic development tests will be interchanged and used to assure application of the most up-to-date parameters and methods from both studies. By this synthesis analysis and testing method, the total experience for the fuel performance will be predicted.

The aim of the FTR driver fuel subassembly design and testing programs is to assure performance under the following conditions:

First Core Parameters

- An in-reactor life of about 1.25 yr at a plant availability factor of 75%
- Maximum fuel assembly surface material loss not to exceed more than 0.001 in. over the life of the subassembly
- Nominal sodium inlet temperature of 550 °F and core bulk outlet temperature to 900 °F
- Sodium flow velocity of ∿30 fps
- Reactor ΔT up to 400 °F
- Pressure drop over the fuel section of 20 to 30 psi per foot of length
- Sufficient interchannel mixing to prevent flow starving, excessive hot channel factors, or extreme thermal gradients
- No destructive vibration phenomena
- Ability to withstand operational thermal shocks

Upgraded Performance Parameters*

An extension of the preceding requirements include:

- Alternate cladding materials with different allowable material losses
- Nominal sodium inlet temperature of 550 °F, and core bulk outlet temperature to 1200 °F
- Sodium flow velocity up to 45 fps
- Fuel burnup in excess of 100,000 MWd/T
- Fuel pins up to 11 ft in length (extended gas plenum)

The pin spacer analytical evaluation program will continue into FY 1969, with the emphasis shifting to evaluation of the alternate compliant grid spacer. A selection between the wire wrap and grid spacer will be made in November 1968, prior to issue of the preliminary design description for the fuel. Table III describes the testing programs relating to the spacer evaluation.

TABLE III. Test Objectives and Facilities Description

Test Designation	Test Objectives and Facilities
Water Hydraulics	
Water Flow Tests, 7-pin cluster	Investigate flow rate for application of data to 7-pin cluster sodium flow tests (Test No. 2 in Figure 4). The main purpose of this test was to investigate pressure drop characteristics of the assemblies prior to sodium testing. These tests have been conducted in the PNL thermal-hydraulics water test loop providing a flow rate capability of 500 gpm at 100 psi ΔP and temperature capabilities up to 100 °F.

* *Not part of the first core testing and analysis programs*

TABLE III. (contd)

Test Designation	Test Objectives and Facilities
Subassembly Flow Test, Partial and Full Size, Standard and Non-Standard (warped), Wire Wrap and Grid Assemblies	Investigate pressure drop, interchannel mixing, and flow distribution for Standard and non-standard wire wrap and grid assemblies of varied spacing. Both full and partial assemblies will be used. Vibration measurements will be made as per Test No. 9, (see Figure 4 schedule). These tests will be conducted at the PNL thermal-hydraulics facility water test loop. This loop, the same used in the 7-pin test, will have capability for multiple readouts of subchannel velocities and pin vibrations. It is presently capable of measuring pressure drop flow rates over a wide range of parameters and test locations. These tests will be instrumented with the noise analysis equipment for vibration, subchannel, and cross-channel mixing data. The loop is presently equipped to test sections up to 12 ft in length and may be extended to 20 ft.
Sodium Dynamic Tests Sodium Flow Tests, 7- and 19-Pin Clusters	Tests with velocities up to 35 fps in shortened 7- and 19-pin clusters will be run in the PNL sodium loop, with a capability of 25 gpm at 40 psi ΔP, and temperatures up to 1200 °F for grid and variable size wire spacers. First assembly test temperature is at the maximum sodium-clad interface temperature--1060 °F.
Subassembly Flow Tests, Full Size	Full subassembly flow in the Core Component Test Loop (CCTL) at maximum hot channel outlet temperature will be run to examine flow-induced vibration, corrosion, erosion, effect of subassembly tilt, etc. for wire wrap and grid assemblies.

TABLE III. (contd)

Test Designation	Test Objectives and Facilities
	The CCTL has the capability of operating at 800 gpm at 110 psi ΔP, and at temperatures up to 1200 °F. The first wire wrap assembly was delivered to CCTL in March 1968.
Mechanical Tests	
Vibration Test, Single Pins	Test the dynamic characteristics of single pins to determine appropriate test parameters for follow-on mechanical (vibration) tests. These mechanical vibration tests will be conducted on the PNL small vibration tester. This tester applies a force vector of 50 lb at a peak displacement of 0.5 in. and a maximum velocity of 70 in. per second. The maximum capability is 124 g's and the frequency rate is 5 to 10 k (cps). The allowable payloads are 9.6 lb at 5 g's, 4.6 lb at 10 g's, 1.6 lb at 25 g's, and 0.6 lb at 50 g's.
Vibration Tests, 19-Rod Cluster (air and water)	Bench vibration tests of 19-rod clusters, first in air and then in water (if necessary) to calibrate and determine appropriate instrumentation location points (maximum amplitude) for use in vibration measurements in water and possibly the sodium flow tests (Tests 3 and 4 in Figure 4). These tests will use either the large or small PNL vibration test beds described in the preceding and following paragraphs.
Vibration Tests, Full Subassembly (air)	Accelerated (aggravated) vibration tests will be performed on full subassemblies in air. These tests will be performed if vibration characteristics in water and sodium indicate a necessity for accelerated

TABLE III. (contd)

Test Designation	Test Objectives and Facilities
	vibration testing. These mechanical vibration tests will be conducted on the PNL large vibration tester. This tester applies a forced vector of 1500 lb at a peak displacement of 0.5 in. and a maximum velocity of 50 in. per second. The maximum capability is 94 g's and the frequency rate is 5 to 5, cps. The allowable payloads are 134 lb at 10 g's, 59 lb at 20 g's, and 34 lb at 30 g's.
Vibration Tests, Full Subassembly, Water and Sodium	The first 19 months of vibration testing in water and sodium will take place with instrumentation in the water flow tests (Test 3 in Figure 4), and visual observation of wear areas caused by vibrations in the sodium dynamic test. The vibration measurements conducted in the water tests will be in the thermal-hydraulics loop at PNL. Description of this test facility is given with the water test (Test No. 4 in Figure 4).
Heated Pin Tests (Water and Sodium)	The in-sodium tests will simulate first core fuel performance to determine temperature peaking in the tri-cusp flow channel, thermal mixing effects in sodium, etc. Follow-on tests will include flow blockage and loss of flow tests. Test conditions will simulate FTR operation for first core through full performance requirements
Thermal Shock Tests (Not Funded)	Thermal shock tests will be performed with thinner "end of life" cladding in sodium to determine the fatigue and strain characteristics of full subassemblies subjected to shutdown and excursion transients. These tests will be conducted at the GE Thermal Shock Facility, capable of shocking assemblies in the temperature range of 800 to 1300 °F in a 5-in. ID by 4 ft long test cell. The test cell may be enlarged for bigger assemblies.
Thermal Shock Tests, Full Subassembly	

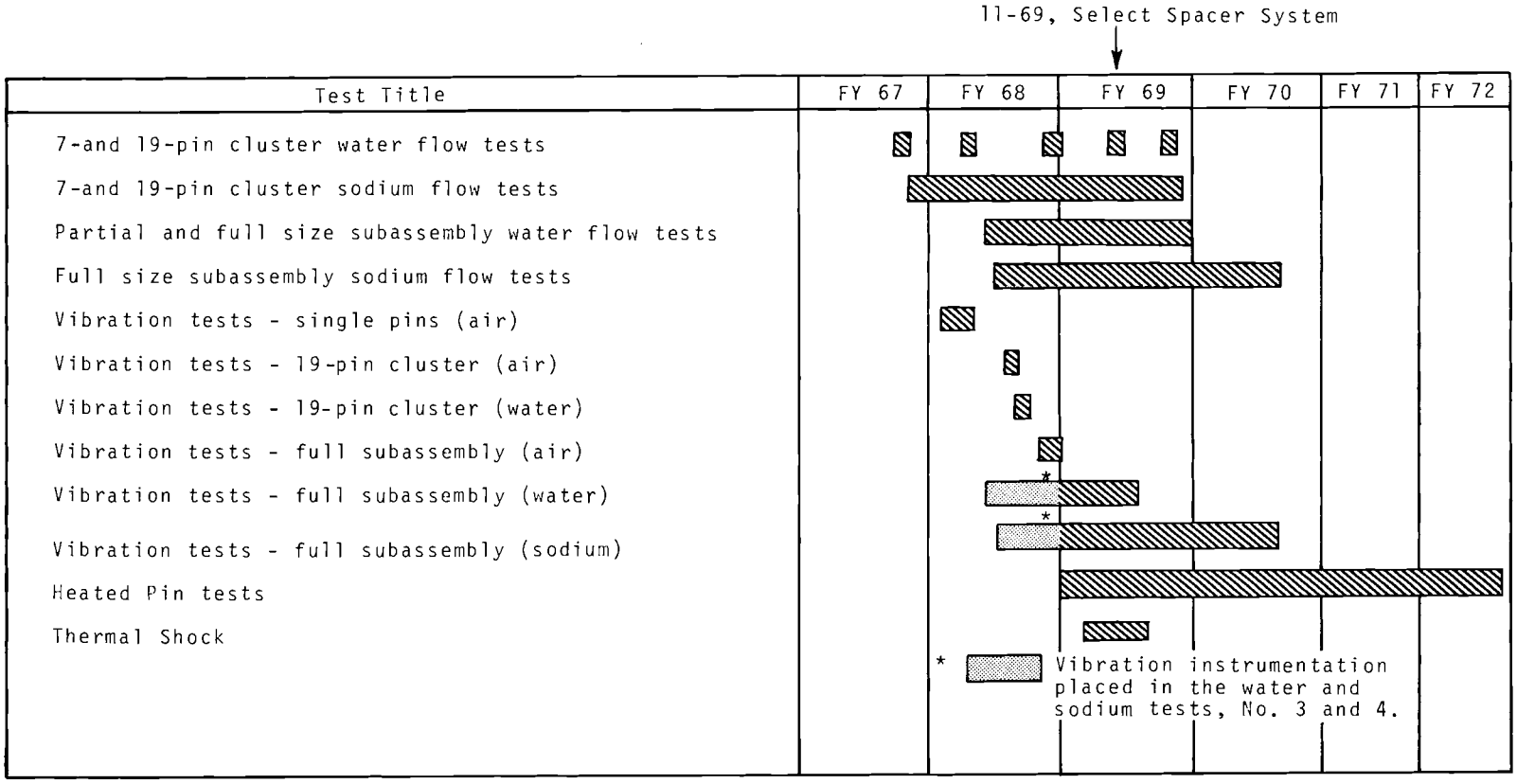

FIGURE 4. Test Program Schedule

PIN BUNDLE PRESSURE DROP ANALYSIS

T. J. Bennett

SUMMARY

Correlation and analysis of wire wrap pin bundle pressure drop data and application of theoretical methods have led to the development of the following equation for the FTR pin bundle pressure drop during normal operation:

$$\Delta P = 49.6 \frac{M^{1.8}}{10^3} + 5.2 \frac{M^2}{10^3},$$

where the flow rate yields velocities in the range of 15 to 45 ft/sec, and M = mass flow rate in lb/sec, and ΔP is in psi, resulting in a pin region pressure drop of 50 psi.

Pressure drop in a pin bundle experiencing fuel pin swelling, such as shown for the peak profiled swelling in a following section, is increased by 9 psi, or by about 14% for the total subassembly.

The pressure drop analysis for compliant grid spacers has demonstrated that, for similar core performance requirements and spacing support span, the core pressure drop is approximately 30% higher for grid spacers than for wire wrap.

Detailed Correlations and Analyses

Pressure Drop Correlations for Uniform Pin Bundles[6,7]

An extrapolation technique applied to 7-, 19-, and 37-pin bundles was employed to generate a friction factor applicable to the FTR 217 pin bundle for the conventional pressure drop relationship:

$$\Delta P = f \frac{LG^2}{2\rho g D_{eq}},$$

where ΔP = Pressure drop, lb force/ft^2

f = Friction factor, unitless

L = Core length, ft

G = Mass flow rate, lb mass/ft^2-sec

ρ = Density, lb mass/ ft^3

g = Gravitational constant, ft - lb mass/lb force - sec^2

D_{eq} = Equivalent diameter - ft

Figure 5 shows the comparison between pressure drops calculated by the extrapolation technique and by the de Stordeur[6] method which is used in the MIDAS code.[8] In the de Stordeur approximation, f in preceding equation is replaced by $\frac{0.307}{R_e^{.2}}$, where R_e is the Reynolds number.

The extrapolation procedure was based on pressure drop data taken at PNL[5] and Karlsruhe,[9] Germany. Pertinent data for the two tests are shown in the following tabulation.

	PNL-1	PNL-2	Karlsruhe
Fluid	water	water	water
Rod O.D., in.	0.200	0.250	0.473
Wire Wrap O.D., in.	0.040	0.030	0.197
Wire Wrap Pitch, in.	12.0	12.0	11.8
Pins/cluster	7	7	7, 19, and 37

Although the rod and wire wrap diameters differ considerably for the two sets of data, the resulting dimensionless plots of log f versus log R_e for both 7-pin clusters show fairly good agreement. Figure 6 shows these f versus R_e plots.

Figure 7, which involves the extrapolation, is a plot of log $\frac{1}{f}$ versus log N, where N is the number of pins per subassembly. Extrapolation was made from N = 37 to N = 217.

Figure 8 shows the friction characteristics of the 7-pin PNL assemblies versus smooth tube friction factors.

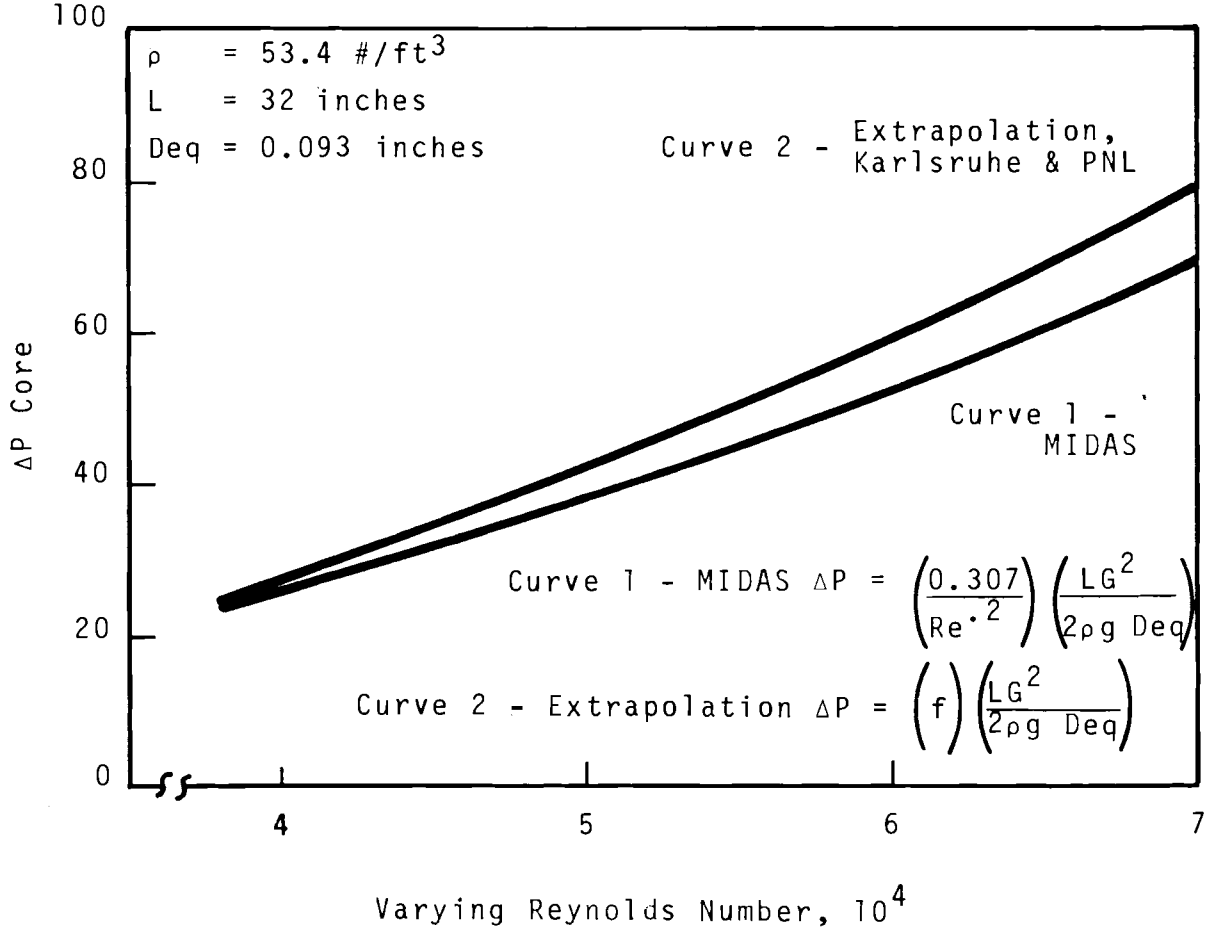

FIGURE 5. December Comparison of Extrapolation and MIDAS Predictions for Subassembly Pressure Drop

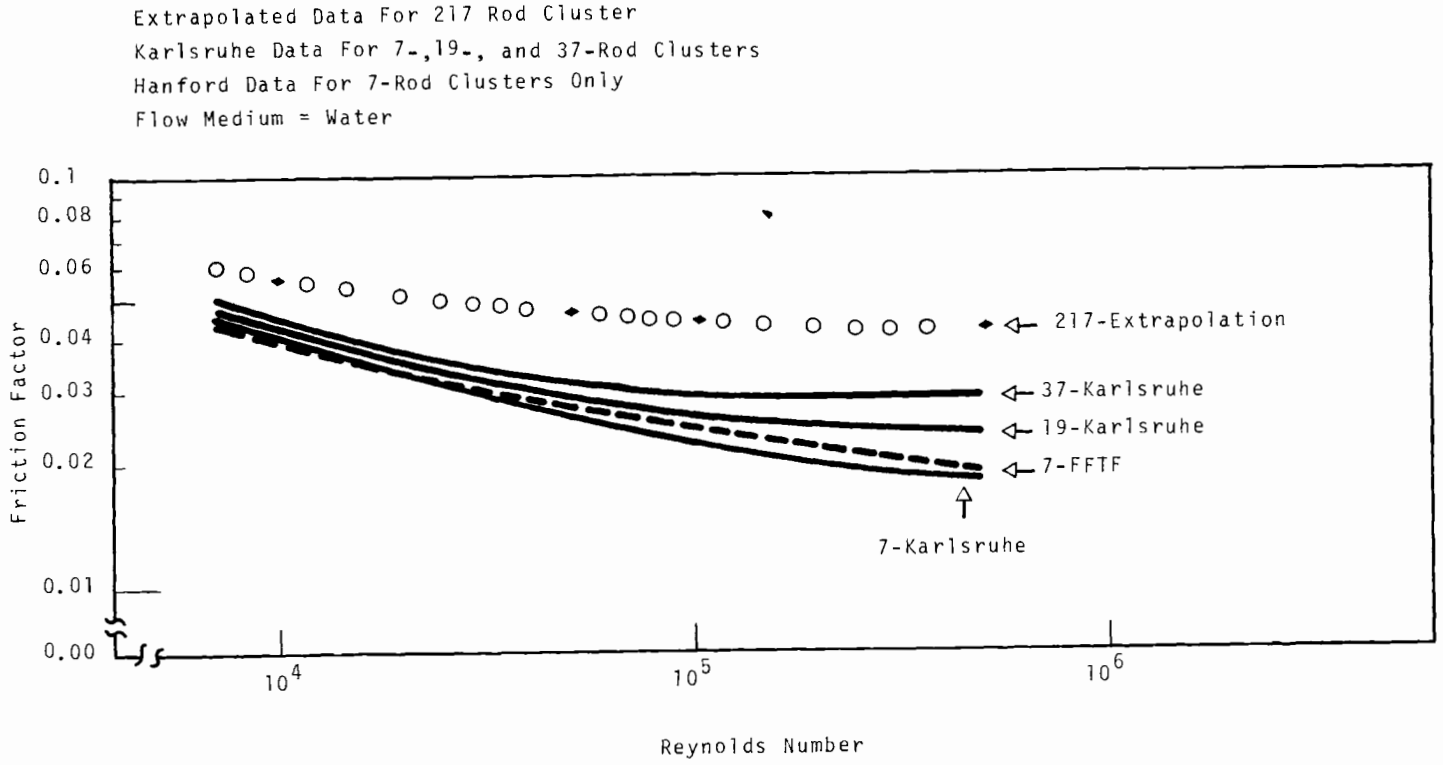

FIGURE 6. Friction Factor Versus Reynolds Number

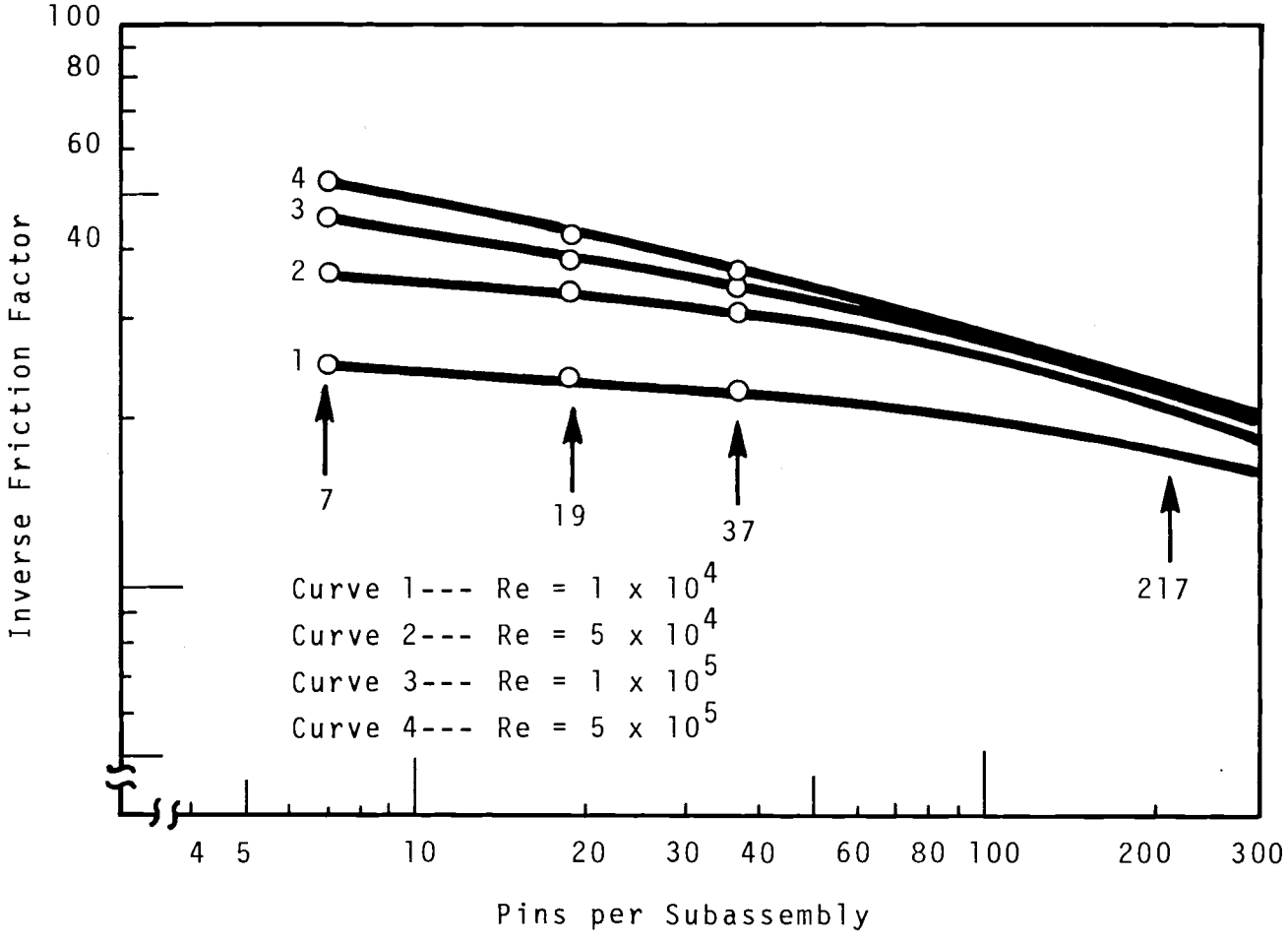

FIGURE 7. Inverse Friction Factor (1/f) Versus Pins Per Subassembly (N) for Varying Reynold's Number (Re)

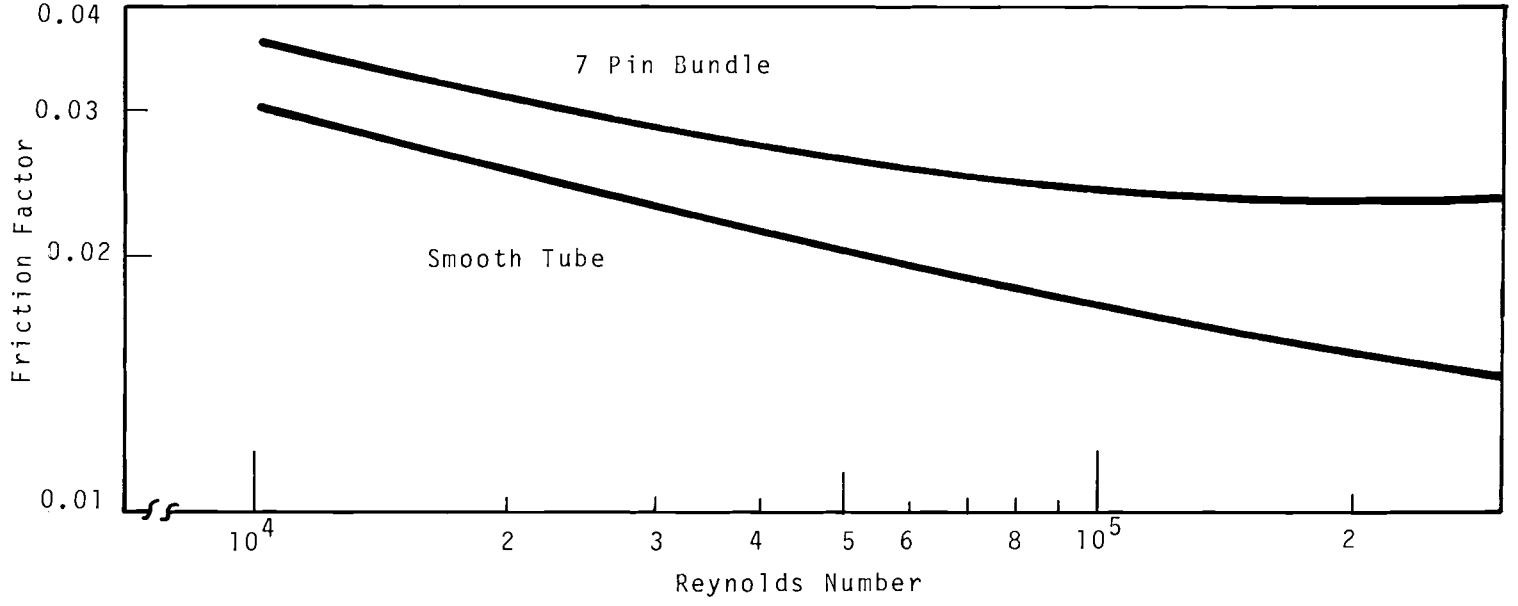

FIGURE 8. Reynolds Number Versus Friction Factor for 7 Pin PNL Bundles in Water

Pressure Drop Analysis for Uniform Pin Bundles

Various techniques and approaches have been used to estimate FFTF core pressure drops at 400 MW. The mean value obtained for core pressure drop is 51 ± 11 psi for the following conditions:

Active Core Length	32 in.
Pin Diam	0.25 in.
Wire Wrap Diam	0.030 in.
Wire Wrap Pitch	12 in.
Na avg Temp	725 °F
Na avg Density	53.4 lb/ft^3
Na avg Velocity	27 ft/sec
Viscosity	0.7 lb/ft-hr
Channel Equiv. Diam	0.0930 in.
Reynolds Number	5.68×10^4

These pressure drop estimates are mean values obtained from the techniques outlined in this section. The subassembly used for this analysis has the following characteristics:

- Flow Duct - hexagonal in shape, 4.220 ± 0.005 in. across inside flats; wall thickness of 0.15 in.
- Pin Assembly in duct - 217 pins, 0.25 in. diam, each wrapped with 0.030-in. wire, with a pitch of 12 in. The pins are arranged in a hexagonal pattern.

Three methods of calculation were used. They are outlined as follows:

- The de Stordeur Approach

The general procedure described on page 76 of de Stordeur's paper[6] was used.

Using his notation, the following values were obtained:

$d = 0.25$ in.	$Ac = 0.0188$ $in.^2$
$d_s = 0.03$ in.	$Ac' = 0.0181$ $in.^2$
$p = 0.28$ in.	$D_{ec} = 0.09515$ in.
$D_{eq} = 20.1$ in.	$D'_{ec} = 0.0823$ in.

$A_w' = 0.02755$ in.^{2} $\quad \Delta P_R = 34.1$ psi

$D_{ew} = 0.09504$ in. $\quad \mu = 0.7$ lb/ft-hr

$f_T = 5.4$ $\quad m_1 = 51$

$L = 32$ in. $\quad m_2 = 189$

$h = 12$ in. $\quad \nu = 5.24 \times 10^{-4}$ in^2/sec

$A_T = 4.65$ in.^{2} $\quad Re_r = 2.97 \times 10^4$

$K_1 = 1.63$ $\quad Re_s = 1.95 \times 10^4$

$K_2 = 1.52$ $\quad C_x = 0.29$

$Q_T = 272\ Q_c$ $\quad S = 0.0704$ in.^{2}

$A_T = 266.5\ Ac'$ $\quad \Delta P_s = 5.1$

$f_M = 0.0234$ $\quad D_{eq_T} = 0.085$ in.

$V = 27$ ft/sec $\quad \rho = 53.4$ psi

$$\Delta P_{core} = \Delta P_R + \Delta P_s = 39.2 \text{ psi}$$

- The MIDAS Equation

The core pressure drop as represented by the equation in MIDAS is

$$\Delta P_{core} = \frac{G^2\ (0.307\ H_1)}{2\rho g\ d_n\ (Re)^{.2}},$$

where $G = \rho V$

$\rho = 53.4$ lb/ft^3 $\quad g = 32.2$ ft/sec^2

$V = 27$ ft/sec $\quad d_n = 0.0930$ in.

$Re = \frac{\rho V d n}{\mu}$ $\quad H_1 = 32$ in.

$\mu = 0.7$ lb/hr-ft

This equation gives a core pressure drop of $\Delta P_{core} = 49.5$ psi ~ 50 psi

- Extrapolation Technique

By the extrapolation technique previously described, the pressure drop may be determined from

$$\Delta P = f\ \frac{LG^2}{2\rho g d_n},$$

where f is determined from the extrapolation technique. For $R_e = 5.7 \times 10^4$, f = 0.043, yielding

$$\Delta P = 62 \text{ psi}$$

- Summary

Method	ΔP
de Stordeur	39
MIDAS	50
Extrapolation	62
Mean (1→3)	51 ± 11

Standardization of Uniform Pin Bundle Pressure Drop Calculational Procedure

The rather wide differences in pressure drop correlations require standardization for the pressure loss calculations. The pin region consists of the lower pin entrance contraction from 15.4 in.^{2} to 4.62 in.^{2}, wire wrapped pins to duct transition, 42 inches; transition region from a 4.22 in. hexagonal (flat ID) duct to a round pipe whose ID is 4.925 in.; wire wrapped pins in round section, 23.5 in.; and the upper pin exit expansion from 8.35 in.^{2} to 19.1 inches^2.

Two basic equations were used to describe most of the pressure losses. Sudden contractions or expansions in flow area were handled with the following Equation. The next Equation was used to predict the pressure loss in sections of open piping assumed to have constant cross sectional area. The de Stordeur method was used to predict the pressure drop across the lower reflector and pin-containing portion of the flow duct.

$$\Delta P_c = \frac{K \rho V^2}{2g \times 144}$$

$$\Delta P_L = f \frac{L}{D_{eq}} \frac{\rho V^2}{2g} \times 144$$

where ΔP_c = Contraction or expansion pressure loss, psi
ΔP_L = Linear pressure drop, psi
K = Dimensionless resistance coefficient
f = Dimensionless friction factor
L = Length of pipe, in.
D_{eq} = Equivalent diameter of pipe, in.
ρ = Coolant density, lb/ft^3
V = Coolant velocity, ft/sec
g = Gravitational constant, 32.2 ft-lb-mass/sec^2-lb force

Because there are 19 changes in configuration throughout the fuel assembly, there are 19 corresponding changes in coolant velocity (see Figure 9 and Table IV). The coolant density also changes in the core. Thus the application of 19 equations to determine the pressure drop of the assembly appears somewhat complex. The velocity dependence is eliminated by the use of the following equations:

$M = \rho VA$

M = Mass flow rate in lb/sec
A = Cross sectional flow area in ft^2

$$\Delta P_c = \frac{K}{288 \rho g_c A^2} M^2$$

$$\Delta P_L = \frac{L}{288 \rho g_c A^2 Deq} fM^2$$

For each change in configuration involving the sudden contraction or expansion, the K is known. So is each cross sectional flow area, A. (For contractions and expansions, the applicable A always refers to the smaller area involved.) Also, the ratio L/D can be computed for each change in configuration. By observing that the change in density throughout the core is

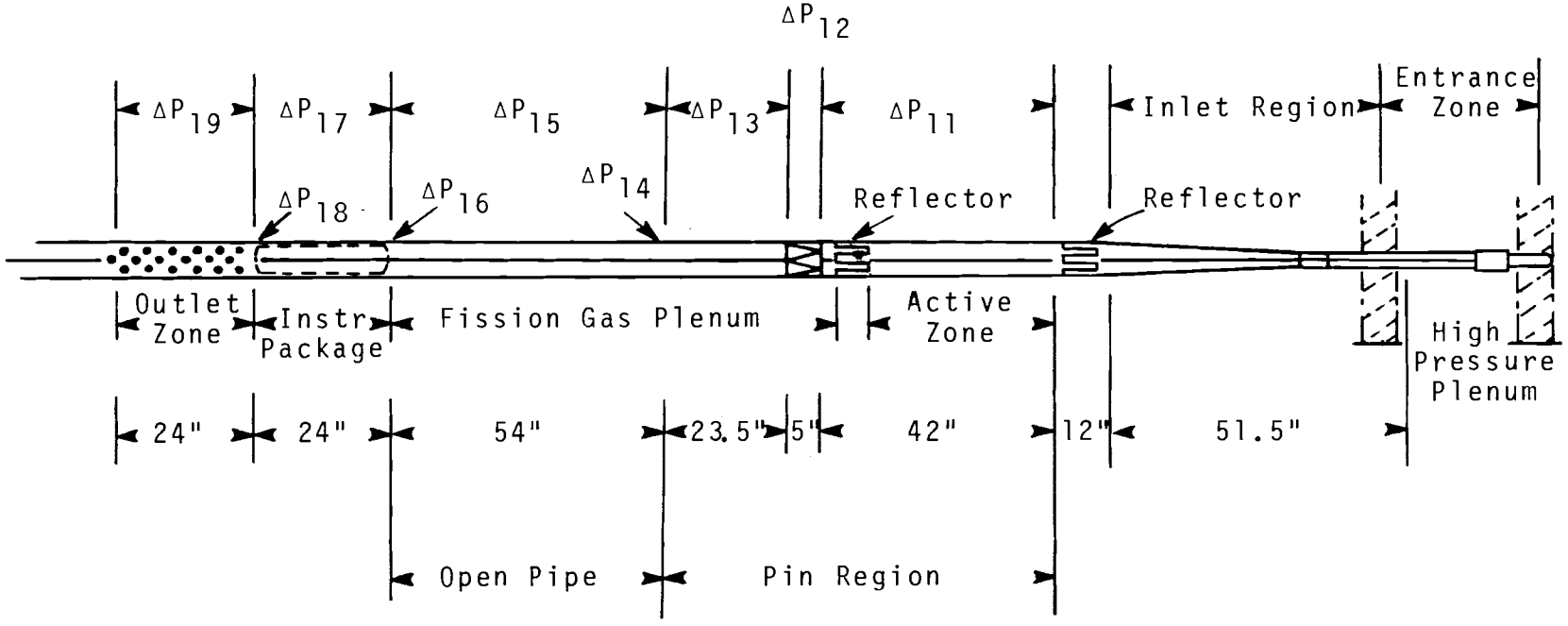

FIGURE 9. Lower Portion of FFTF Assembly

TABLE IV. Fuel Assembly Zones for Pressure Drop Calculations

A. Entrance Zone

1. Oblong entrance slits (see Figure 9)

B. Inlet Region

2. Pipe, 5.375 in. long with ID of 2.5 in.
3. ID increase from 2.5 to 2.735 in. over 1/2 in. of length
4. Pipe, 8.375 in. long with ID of 2.725 in.
5. Transition from 2.725 in. ID round pipe to hexagonal duct with inside flat ID of 3.125 in.
6. Tapered hexagonal duct, ID from 3.125 to 3.97 in. across flats over a length of 32 3/4 in.

C. Lower Reflector Region

7. Lower reflector entrance contraction in area from 13.6 in. to 6.7 in.^{2}
8. Lower reflector itself - 7 in. of length
9. Lower reflector exit expansion from 7.75 to 15 in.^{2}

D. Pin Region

10. Lower pin entrance contraction from 15.4 to 4.62 in.^{2}
11. Wire wrapped pins to duct transition, 42 in.
12. Transition region from a 4.22 in. hexagonal (flat ID) duct to a round pipe whose ID is 4.925 in.
13. Wire wrapped pins in round section, 23.5 in.
14. Upper pin exit expansion from 8.35 to 19.1 in.^{2}

E. Open Pipe

15. Open pipe, 54 in. in length, 4.925 in. in ID

F. Instrument Package

16. Contraction into instrument package from 19.1 to 15 in.^{2}
17. Instrument package, 24 in. long with an assumed equivalent diameter of 2.36 in.
18. Expansion into open pipe from 15 to 19.1 in.^{2}

G. Outlet Pipe

19. Perforated outlet pipe, 24 in. long

relatively small, the following average regional densities may be used: pre-core, 54.8 lb/ft^3; core, 53.4 lb/ft^3; and post-core, 52 lb/ft^3.

For smooth tubes, the friction factor f is a function of Reynolds number:

$$\frac{1}{\sqrt{f}} = 2 \log \left(\frac{R_e \sqrt{f}}{2} \right) - 0.20$$

However, the following equation agrees fairly well with the preceding equation for Reynolds numbers in the range from 1×10^4 to 2×10^6:

$$f = \frac{0.184}{R_e^{0.2}}$$

The Reynolds number can be expressed by:

$$R_e = \frac{\rho V D_{eq}}{\mu} \quad \text{or}$$

$$R_e = \frac{M D_{eq}}{\mu A} \times \frac{3600}{12}$$

where

R_e = Dimensionless
M = Mass flow rate in lb/sec
D_{eq} = Equivalent diam in in.
A = Flow area in ft^2
μ = Viscosity in lb/ft-hr

The pin region pressure drop becomes:

$$\Delta P = 48.21 \frac{M^{1.8}}{10^3} + 1.595 \frac{M^2}{10^3}$$

Figure 10 shows the distribution of pressure losses across the fuel assembly.

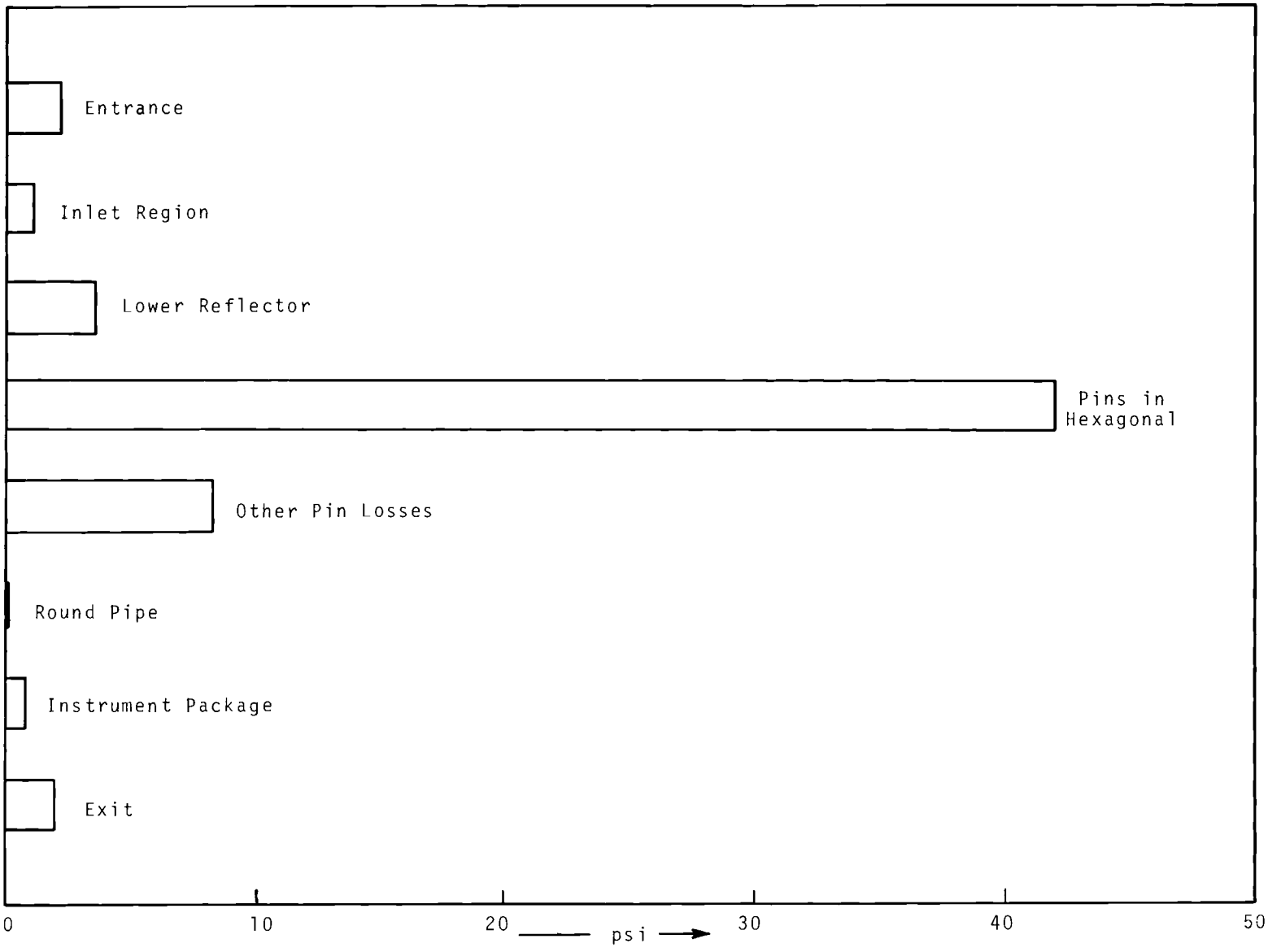

FIGURE 10. Pressure Drop Distribution in Assembly (For M = 46.5 lb/sec, or a core velocity of 27.2 ft/sec.)

CONCLUSION

For a core coolant velocity of 27 ft/sec, the assembly pressure drop is predicted to be 60 ± 9 psi. This and other estimates will be corroborated by the CCTL experiments at Argonne National Laboratories in the near future.

Additional Core Pressure Drop Due to Pin Diametral Growth

In conjunction with the mechanics swelling analyses appearing later in this report, a study was performed to determine the effect of diametral expansion on core pressure drop.

The pin chosen to represent the worst case was pin V 171, a single pin used in the early fast irradiation studies[10] reported by the British in 1965. The expansion characteristics of this pin are greater by a factor of three than those for similar pins. It should be pointed out that this high value of expansion is not necessarily typical of the results currently obtained, but was chosen to represent an extreme case. The U.K. experts consider its growth an anomaly.

When the pin expands diametrally, the increased cross sectional area of the fuel pin results in a decreased flow area for the coolant to traverse. Decreased flow area means increased coolant velocities and increased wetted perimeters resulting in smaller equivalent diameters and larger Reynolds numbers. All of these factors come to play in the MIDAS code correlation for core pressure drop.

$$\Delta P = \frac{(0.307)\ (H_1)\ (\rho)\ (V^2)}{(144)\ (2g)\ (d_{eq})\ (Re.^2)}$$

With no swelling, the equation gives a pressure drop of

50 psi in the fuel pin region when

$H_1 = 32$ in. $\quad g = 32.2$ ft/sec^2
$\rho = 53.4$ lb/ft^3 $\quad d_{eq} = 0.093$ in.
$V = 27$ ft/sec $\quad R_e = 5.7 \times 10^4$
$\mu = 0.7$ lb/ft-hr $\quad R_e{}^2 = 8.9$

The preceding ΔP equation may be used to determine the pressure drop through a swollen flow channel by breaking the expansion curve for pin V 171 down into small segments of uniform diameter (see Figure 11), computing the factors of the pressure drop equation for each unit segment, and then calculating the pressure drop across each segment. In order to make this series of calculations applicable to an FTR fuel pin, the shape of the expansion curve for pin V 171 was applied to a 32-in. FTR pin of the following room temperature characteristics:

Pin Diameter, P = 0.250 in.
Wire Wrap Diameter, W = 0.030 in.
Pin Length, H_1 = 32 in.
Coolant Flow Area, A_F = 0.0214 in.^{2}

In determining the effect of swelling on flow area, a relationship between the two was developed. Assuming (as a worst case) that the wire wraps experience the same expansion as the fuel pins, and that this swelling results in decreasing the flow area of the coolant channel, one derives the following:

$$\frac{dA_p}{A_F} = \frac{\text{(Increased Pin, Wire Wrap Area)}}{\text{Original Flow Area}}$$

Since $A_p = \frac{\pi}{4}(D^2 + W^2)$, simple differentiation gives

$$dA_p = \frac{\pi}{2}(DdD + WdW)$$

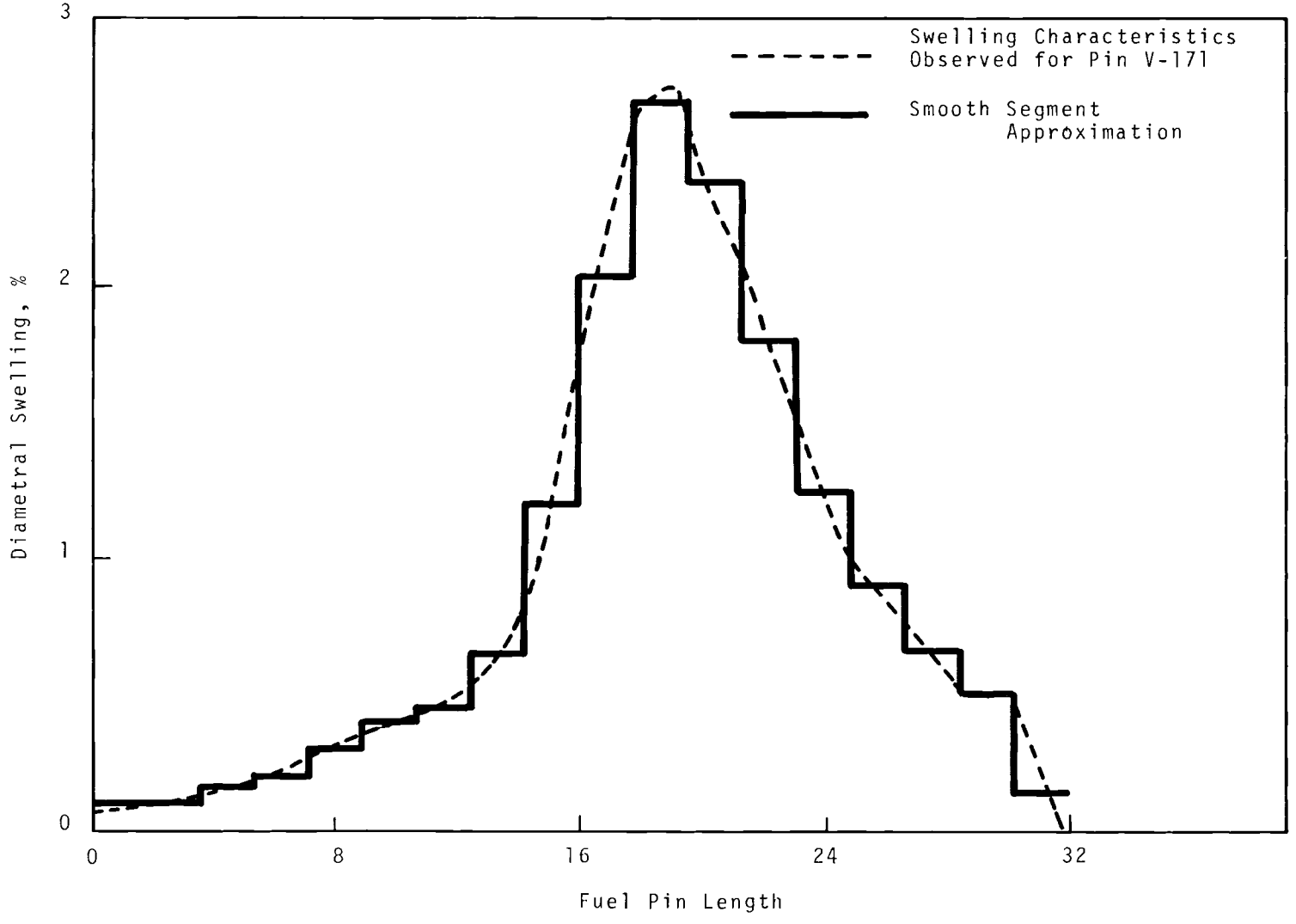

FIGURE 11. Smooth Segment Approximation

By expressing the expansions as percents of the original diameters, dW = xW, and dD = xD, where x is the percent expansion:

$$\frac{dAp}{A_F} = \frac{-\pi\ (D^2 + W^2)}{2\ (0.0214)}\ \frac{x}{100} = -0.0464x$$

This equation gives the relationship between diametral expansion and flow area reduction and the variable factors of the equation are set up in the following manner with the primed subscripts denoting the expanded relationship:

$$d_{eq}' = d_{eq}\left(\frac{A_c'}{A_c}\right)\left(\frac{P}{P'}\right)$$

$$R_e' = R_e\left(\frac{V'}{V}\right)\left(\frac{d_{eq}'}{d_{eq}}\right)$$

For the preceding equations, the expanded or swelled quantities are related to the cold values by the following:

$$P' = P\left(1 + \frac{x}{100}\right)$$

$$A_c' = A_c\left(1 - \frac{4.64x}{100}\right)$$

$$V' = \frac{V}{1 - \frac{4.64x}{100}}$$

$$\Delta P_{increase} = \Delta P' - \Delta P$$

where

$$\Delta P' = \frac{0.307\rho}{288g} \sum_{i=1}^{n} \frac{(V_i')^2\ H_{1i}'}{(d_{eq}')_i\ (R_e')_i^{0.2}}$$

Substitution yields the relationship between the percentage of diametral expansion, x, and the increased reactor pressure drop as follows:

$$\Delta P_{increase} = \frac{\Delta P}{H_1}\left[\sum_i \frac{(1 + 0.01x_i)^{1.2}}{(1 - 0.0464x_i)^3} H_{1i} - H_1\right]$$

Before applying the swelling characteristics of the Dounreay pin to an FFTF pin, a comparison of the similarities and differences between the two should be made. These are shown in the following tabulation.

Item	Dounreay	FFTF (expected)
Coolant flow direction	Down	Up
Axial peaking factor	1.27	1.24
Approximate inlet temperature	450 °F	550 °F
Approximate outlet temperature	1220 °F	1030 °F
Approximate peak flux	2×10^{15} n/cm^2-sec	6×10^{15} n/cm^2-sec
Approximate peak fluence	7×10^{22} n/cm^2	2×10^{23} n/cm^2

The above equation, when applied to an FTR pin assumed to have experienced the same percentage of swelling as Pin V 171, yields an 8 psi pressure drop increase. The resultant reduced flow rate is within the allowed hot channel flow variation for the subassembly. This 8 psi increase was calculated using the series of smooth pin segments shown in Figure 11. Although the calculation was performed for one pin occupying 1/217 of the flow area in a hexagonal flow duct, the pressure drop increases for all 217 pins (assuming all experience equal swelling profiles) and hence the core portion of a flow duct will also be 8 psi. The profiles of two adjacent pins in such a cluster would assume a configuration similar to that shown in Figure 12.

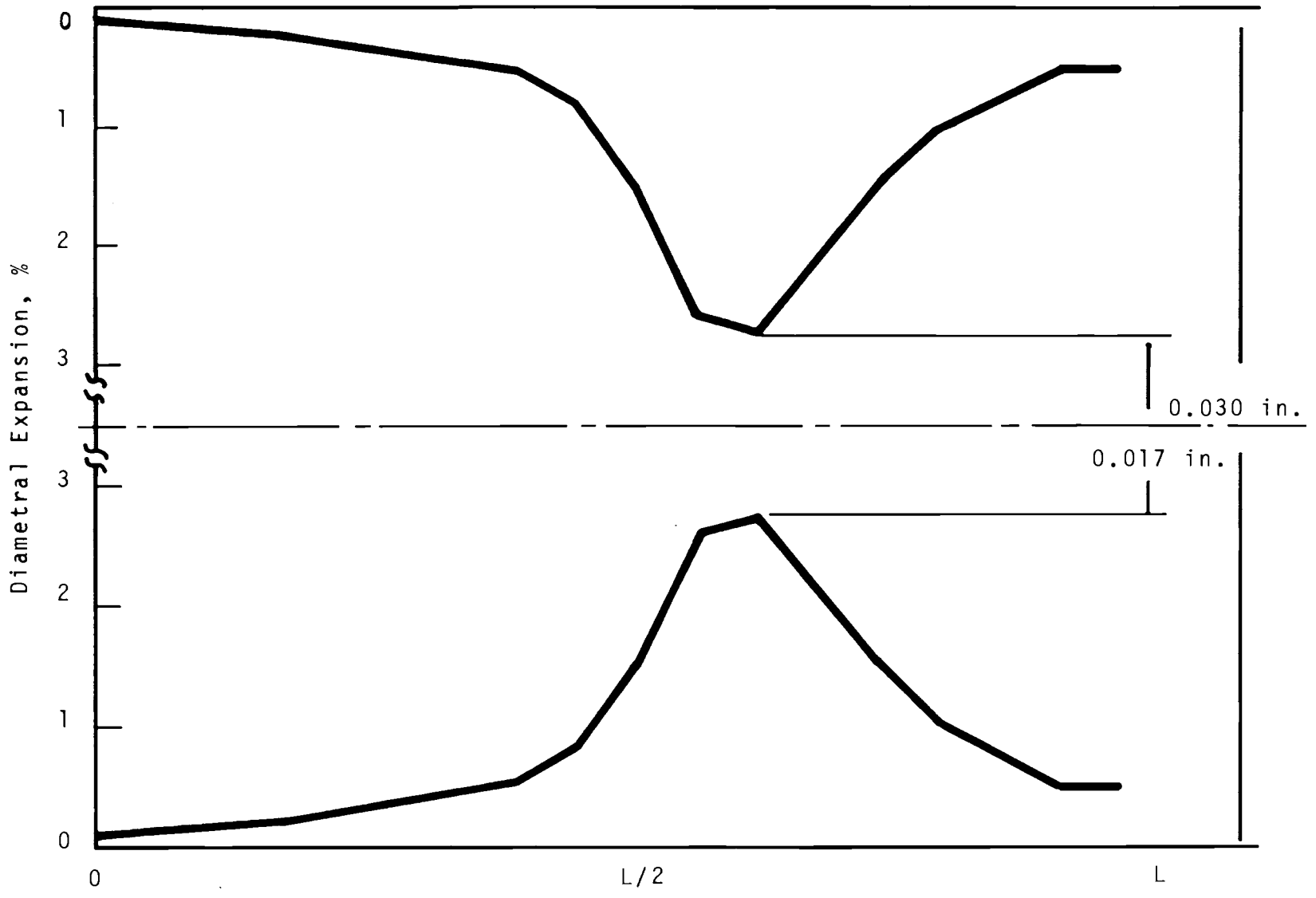

FIGURE 12. Swelling in Two Adjacent Pins

It is interesting to perform a Venturi calculation to compare the "smooth-segment" approach to one accounting for the constantly changing diameter shown in Figure 12 (the Venturi equation).

In the following equation, the Venturi equation,

$$\Delta P = \frac{\rho (V')^2 \left(1 - \left[\frac{D_i}{D_o}\right]^4\right)}{(0.975)^2 \ (2g_c) \ (144)}$$

where

$$V' = \frac{V}{1 - 4.64x/100}$$

X = maximum % of diametral growth
D_i = minimum pin separation
D_o = nominal pin

or

$$\Delta P = \frac{(53.4) \ (31) \ (31) \left(1 - \left[\frac{17.2}{30}\right]^4\right)}{(0.975) \ (0.975) \ (2) \ (32.2)(144)} = 5.2 \text{ psi}$$

Thus the "smooth-segment" approach is observed to be more pessimistic than the Venturi approximation.

A pin experiencing a uniform expansion of 3% over 1 ft of its length with the rest of it remaining at normal size would increase the pressure drop by 11.6 psi. If it suffered a 3% expansion over half of its length, the resulting pressure drop increase would be 13 psi.

By assuming half of the pins in a cluster to expand an amount equivalent to a uniform swelling of 2%, and the other half to expand 1%, the resulting additional pressure drop of the subassembly will be 14 psi.

Since swelling is thought to be a function of both flux and burnup, one might anticipate more expansion in the FFTF pin since the fluence of pin V 171 is only one-third that of the FFTF pin. The effect of burnup is further discussed in the following.

Pin V 171 achieved 7.3 at.% burnup, corresponding to 64,000 MWd/T. The average FTR pin will absorb an exposure of 45,000 MWd/T, corresponding to a burnup of 4.6 at.%. By multiplying the average exposure by the radial, axial, and engineering factors, the maximum exposure will be 83,000 MWd/T, or an atom burnup of 8.4%. Assuming the diametral expansion and exposure relationship to be linear (more expansion resulting from higher exposures), a maximum expansion of 3.2% will be observed. This figure corresponds to an additional pressure drop of 9.3 psi. These various conditions are condensed in the following tabulation. Figure 13 shows the effect of uniform swelling versus additional pressure drop.

Condition	Atom Burnup, %	Exposure, MWd/T	Max Diametral Expansion, %	Equivalent Uniform Diametral Expansion, %	Predicted Additional Core Pressure Drop, psi
FFTF-Design	4.6	40,000	∿1.00	∿0.35	∿2.5
DFR-V-171	7.3	64,000	2.75	0.95	8.0
FFTF-Hot Spot Hot Channel Radial Peaking 1.30 Axial Peaking 1.24 } 1.84 Engr. Factor 1.14	8.4	83,000	∿3.2	∿1.1	∿9
3% expansion over 1 ft of core	-	-	3.0	1.36	11.6
3% expansion over half the core	-	-	3.0	1.50	13.0
Half of the core expands a uniform 1%, other half, 2%	-	-	2.0	1.58	14

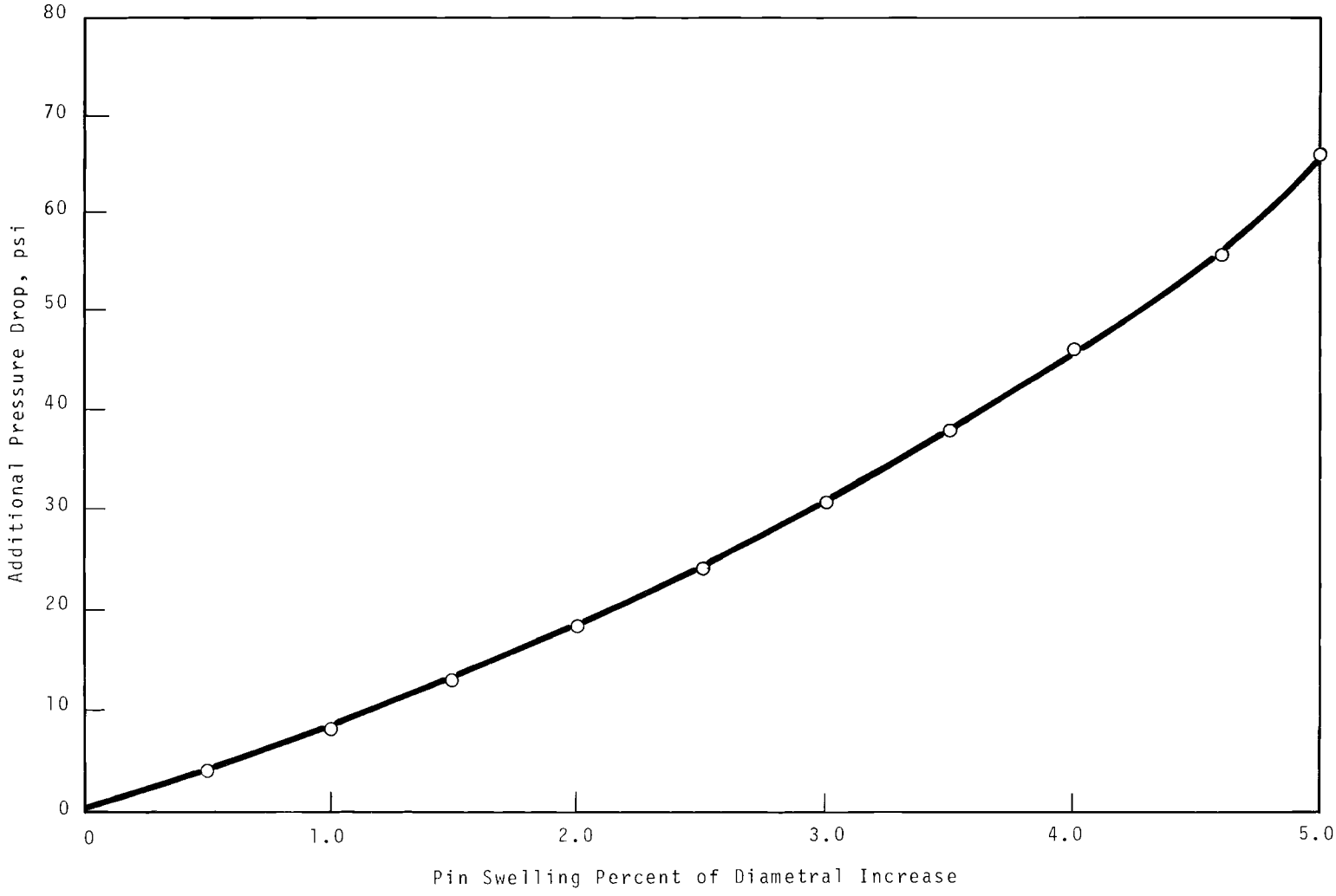

FIGURE 13. Additional Pressure Drop Versus Uniform Pin Swelling

GRID SPACER HYDRAULICS

Figure 14[2] presents total core pressure drop data for fuel assemblies using wire wrap and grid spacers. It may be seen that the pressure drop for the grid spacers is about 30% greater than the pressure drop for the wire wrap at the FTR design conditions for P/D = 1.12. These data are also corroborated by data presented in Reference 3. The additional supporting analyses for grid spacer performance such as temperature peaking under the grid spacer, flow performance with pin diametral growth, etc. will be completed in FY 1969.

THERMAL HYDRAULIC ANALYSES

FLOW AND COOLANT TEMPERATURE DISTRIBUTION ANALYSIS

D. C. Kolesar

Analyses for "Nominal Dimensions" for 30, 40, and 50-mil Wire Wrap

The coolant temperature and velocity distributions across a narrow strip of a 217-pin subassembly for various wire wrap dimensions have been determined by means of the COBRA[11] computer program.

The hottest subassembly was chosen for analysis. The computed and given characteristics of the systems used nominal clearance between the outer row of pins and the duct wall (wire wrap diameter + 19 mils). The hot channel power distribution was employed. An average temperature drop of 350 °F was required through the core regardless of wire wrap dimension.

One-in. axial increments were used by COBRA. Conservative and optimistic values of the turbulent mixing parameter β were estimated from a correlation of Rowe and Angle[12] as a function of pin spacing and average Reynolds number. The value of β

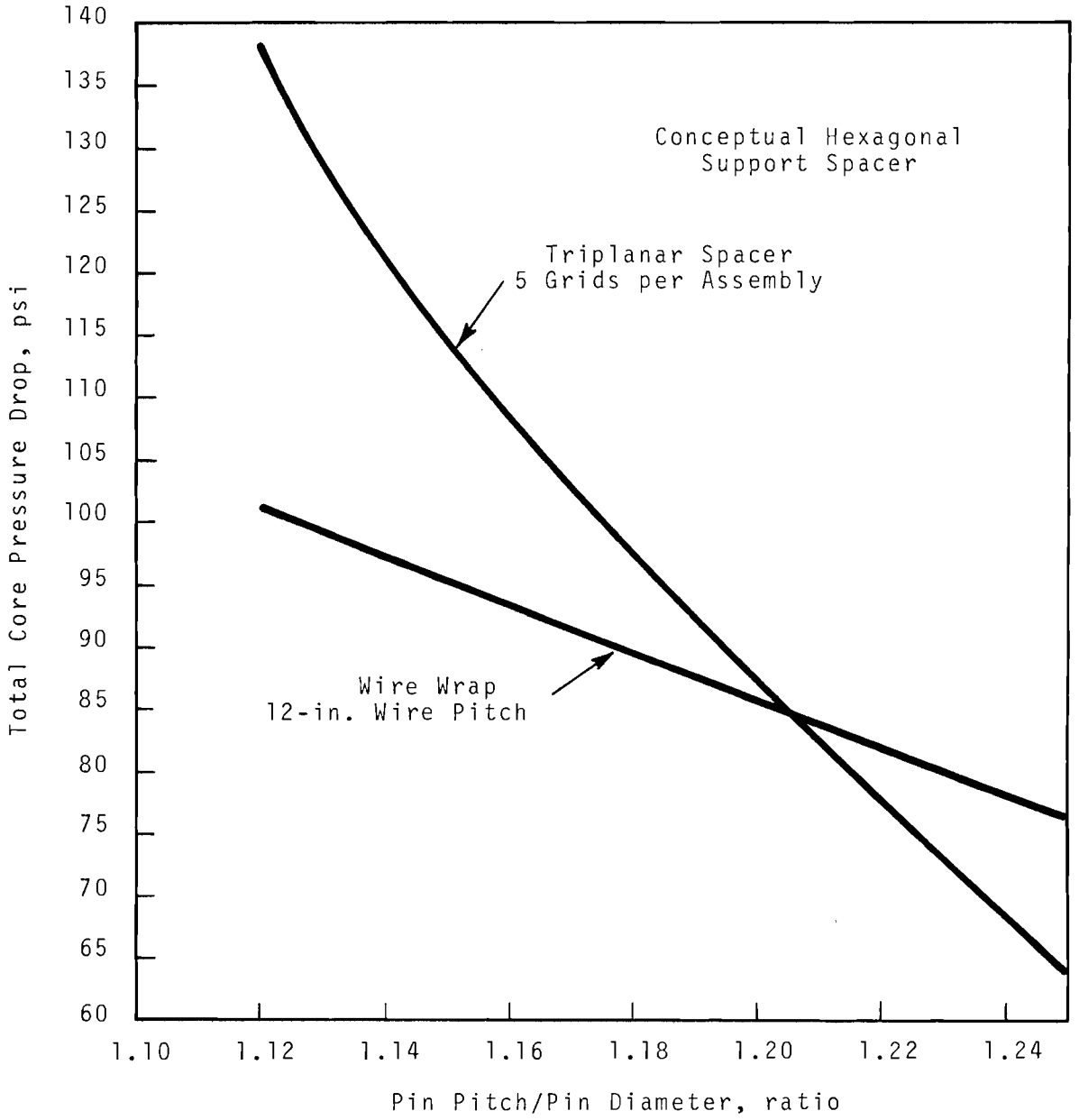

FIGURE 14. Total Core Pressure Drop Versus Pin Pitch-To-Diameter Ratio

reflects turbulent mixing only. The mixing imparted by the wire wrap will probably reduce the subassembly radial temperature gradients below those shown for the "optimistic" β. The friction factor employed was justified by an analysis using the de Stordeur[6] wire wrap correction technique (Figure 15). The same friction factor computed for the 30-mil case was employed for wraps of 40 and 50 mils.

It is observed that the change in wire wrap dimension does not significantly alter the temperature distribution (Figures 16 and 17). Figure 18 shows the temperature distribution of the coolant at the pin bundle outlet. However, the velocity profile is observed to be significantly altered for different size spacers (Figure 19). For the 30-mil wire wrap, a 21% change in the velocity (66% change in volumetric flow rate) is predicted across the subassembly with "channeling" very much in evidence near the duct walls. The channeling is less evident for the larger wire wrap (16% velocity change for 50 mil wire wrap) but its effect on the overall temperature profile (Figure 16) and maximum temperature gradient (Figure 18) is minimal.

Effect of Fabrication Tolerances and Selective Assembly on Coolant Temperature Distribution

The range of the coolant temperature profile within the subassembly for various bundle-duct geometries consistent with fabrication and assembly tolerances is found to be small though not negligible. The limiting character of the coolant temperature profile at the end of the fuel region within the subassembly imposed by fabrication and assembly tolerances was established using the COBRA[11] computer program. This includes symmetric arrangements as well as various asymmetric bundle packings and/or component arrangements.

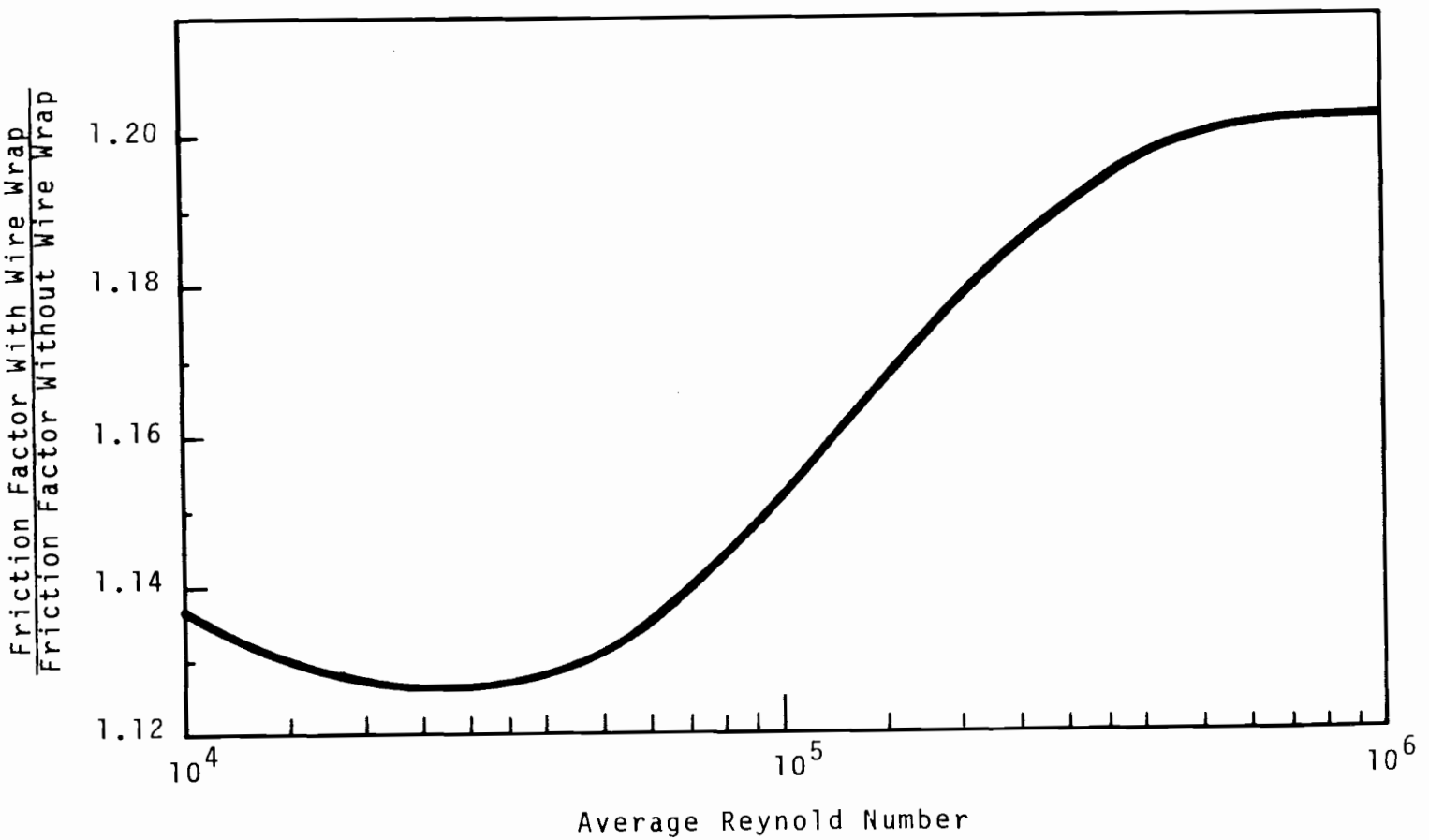

FIGURE 15. Effect of 30 Mil Wire Wrap on Friction Factor As a Function of Average Reynolds Number (Wire Wrap Based Upon Nominal Clearances)

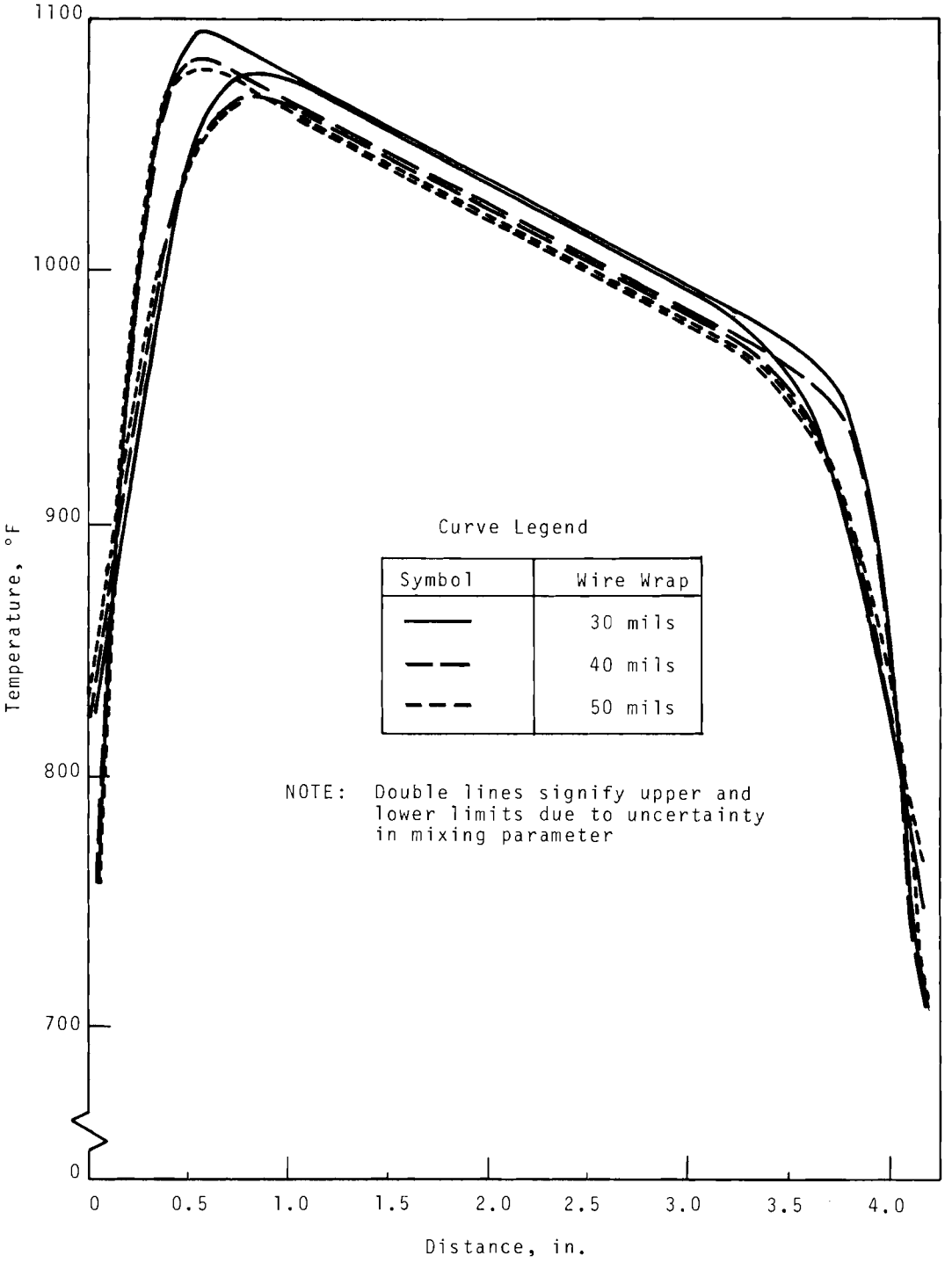

FIGURE 16. Coolant Temperature Distribution Across 217 Pin Subassembly at Upper Fuel-Insulator Boundary for Various Sizes of Wire Wrap Using the COBRA Computer Program

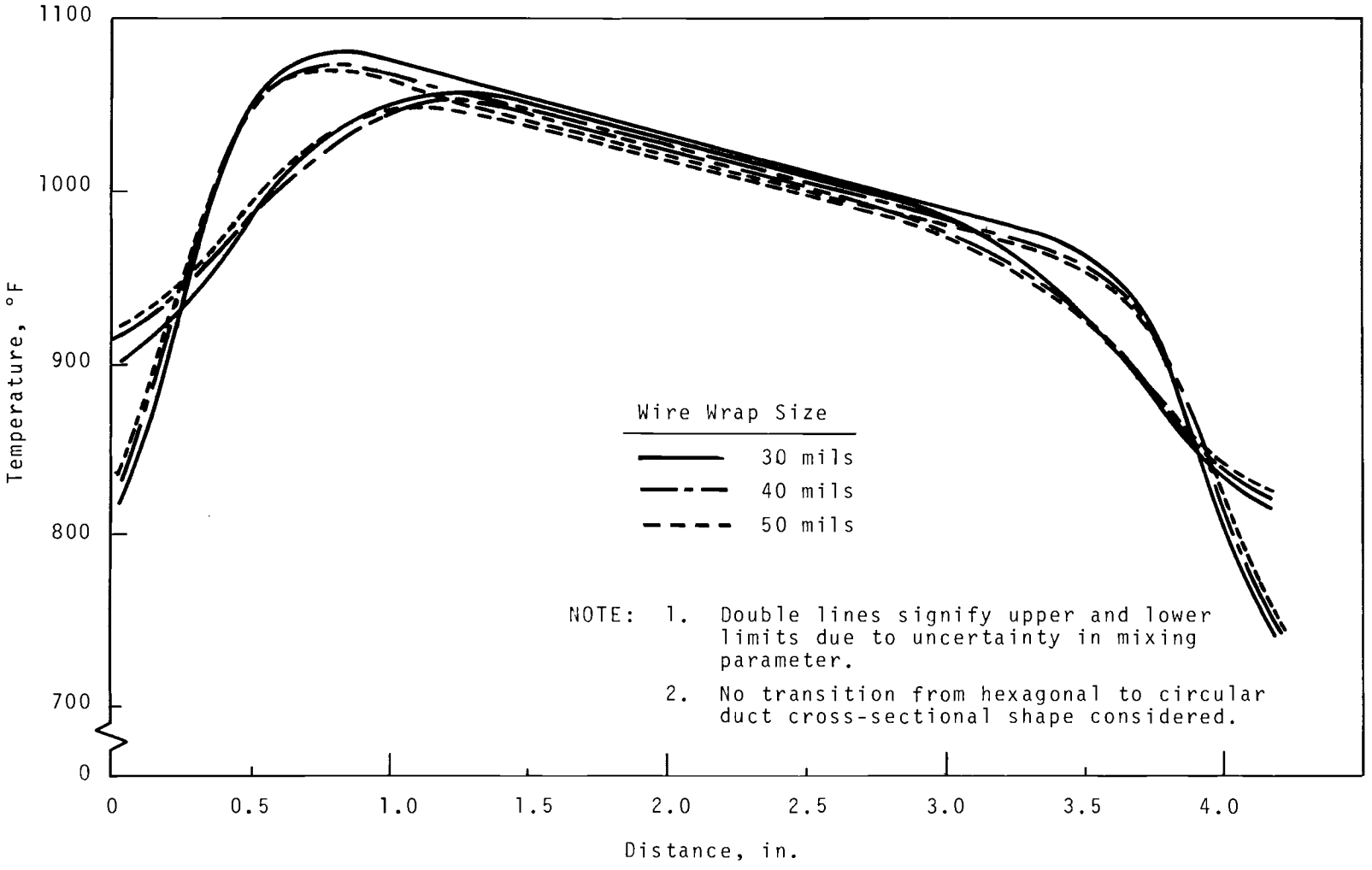

FIGURE 17. Coolant Temperature Distribution Across 217 Pin Subassembly at End of Pin Bundle for Various Sizes of Wire Wrap Using the COBRA Computer Program

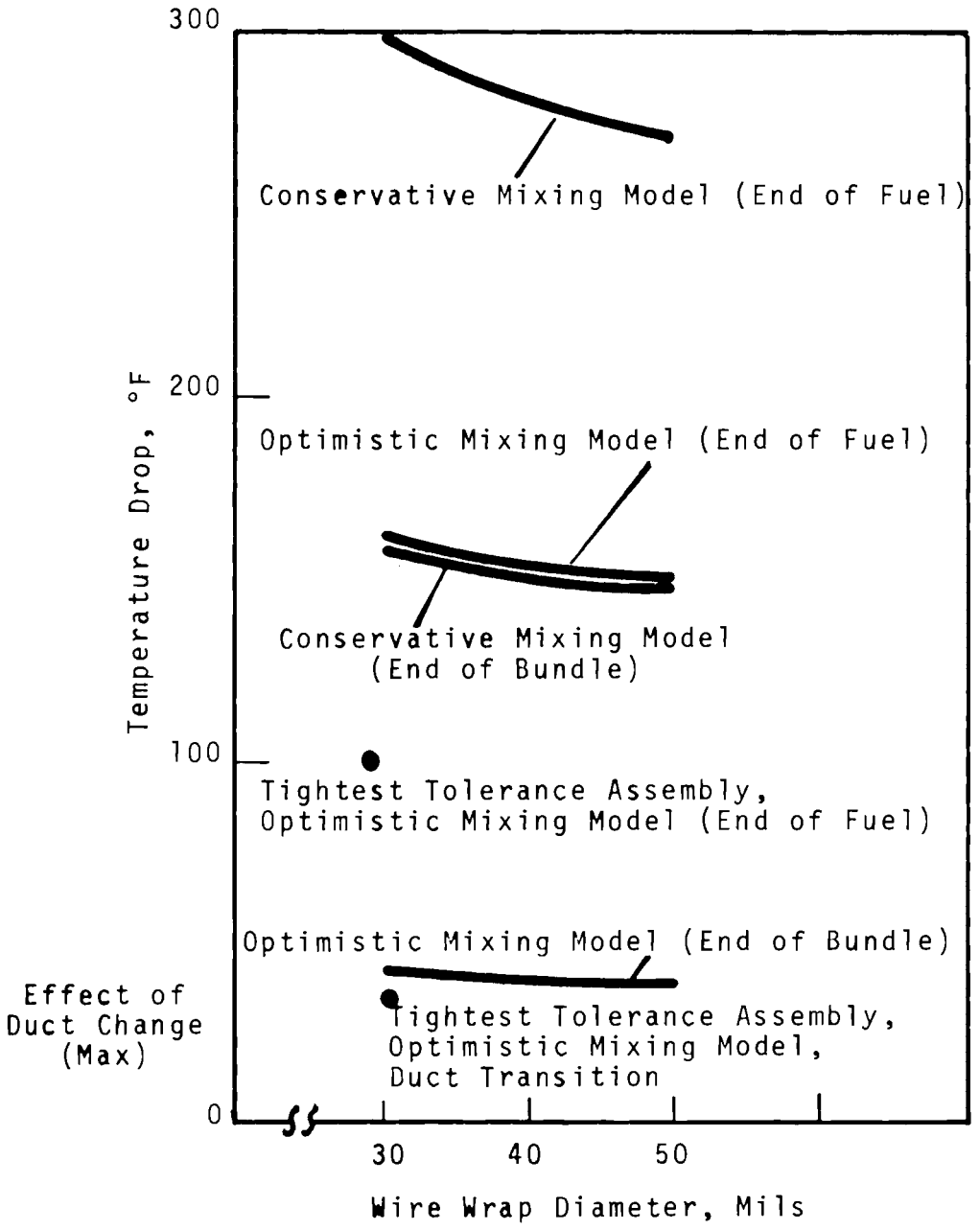

FIGURE 18. *Temperature Drop Across Pin in Subassembly Possessing the Largest Power and Power Gradient Versus Wire Wrap Diameter Based on the COBRA Computer Program*

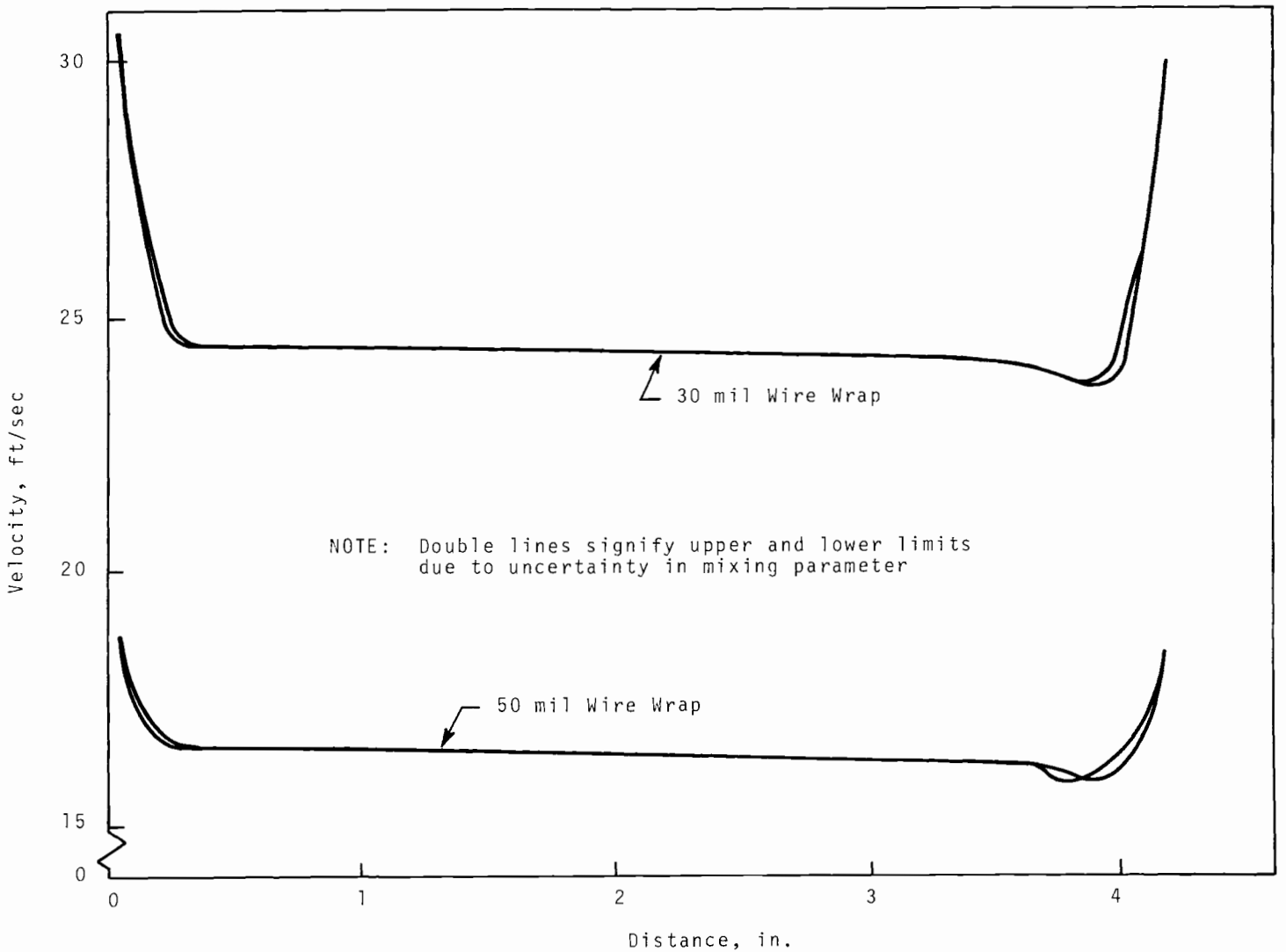

FIGURE 19. Coolant Velocity Distribution Across 217 Pin Subassembly at Upper Fuel-Insulator Boundary for Two Wire Wrap Sizes Using COBRA Computer Program

Due to COBRA limitations, it was necessary to approximate the three-dimensional character of the subassembly by a "somewhat two-dimensional" model--a narrow strip of coolant and fuel pins located between the flats of the subassembly. Sketches and a discussion of this model can be found in FTR Monthly Progress Reports.[13, 14, 15] The narrow strip model is not especially suited for the study of local geometric asymmetries since the coolant flow patterns would be decidedly three-dimensional. However, predictions based on this model should be conservative, viz., overemphasize the effect.

The hottest subassembly was chosen for analysis. Except for the bundle geometry and the related coolant mass flux, the parameters and constants are identical to those employed earlier. It should be noted particularly that the design is based on the reference 30-mil wire wrap. The following seven cases were considered:

Case 1 - Tightest bundle in largest duct with assembly tolerances met

Case 2 - Loosest bundle in smallest duct with no interference and with assembly tolerances met

Case 3 - Nominal bundle in nominal duct

Case 4 - Four large pins asymmetrically located in as nearly nominal a bundle-duct configuration (see sketch) as possible

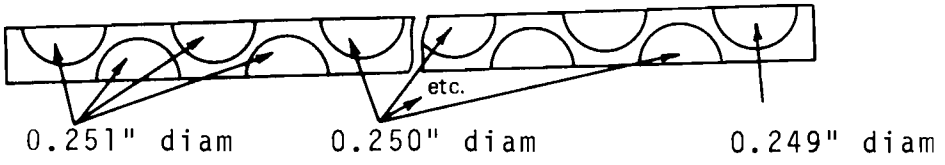

Case 5 - Tightest bundle in largest duct without regard to assembly tolerances

Case 6 - Same as Case 1 but with bundle shifted to coolest side of duct wall

Case 7 - Same as Case 4 but with bundle shifted to coolest side of duct wall.

Details pertaining to the foregoing cases are shown in Table V.

TABLE V.

Case Number	Fuel Rod Diam, in.	Spacer Wire Diam, in.	Flow Duct Width, in. (flat-to-flat)	Bundle-* Duct Spacing, in.	Pin-to-Pin** distance, in.
1	0.2504	0.029	4.1798	0.0226	0.2420
2	0.2496	0.031	4.1998	0.0076	0.2430
3	0.2500	0.030	4.1898	0.0151	0.2425
4	-	-	4.1898	0.0151	-

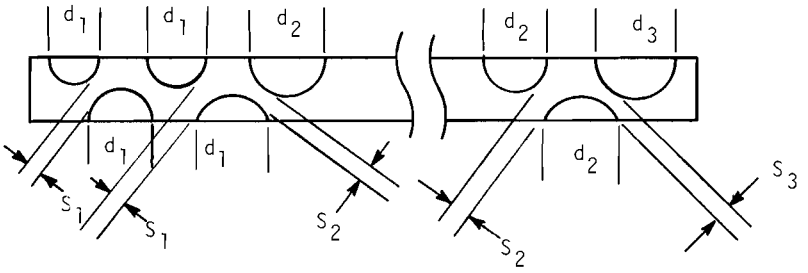

$S_1 = 0.029$ $d_1 = 0.251$

$S_2 = 0.030$ $d_2 = 0.250$

$S_3 = 0.03055$ $d_3 = 0.24945$

5	0.2490	0.029	4.1591	0.033	0.24075
6	0.2504	0.029	4.1798	and 0 / 0.0452	0.2420
7	***	***	4.1898	and 0 / 0.0302	***

* 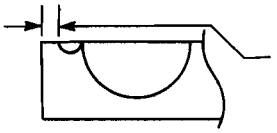 Bundle-duct spacing

** 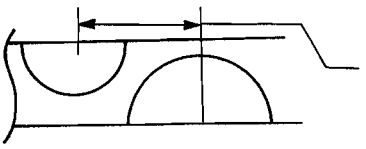 Pin-to-pin distance

*** See figure in Case 4

Figure 20 displays the temperature distribution limits employing conservative and optimistic turbulent mixing parameters (β) for configurations possessing the extreme tolerance limits (Cases 1 and 2), as well as the nominal values (Case 3).

Figure 21 illustrates the possible effect when a bundle is assembled from pins possessing nonuniform sizes. Here, four "large" pins are introduced at the worst location (steepest temperature gradient) into an otherwise nearly nominal bundle-duct arrangement. For comparison, Figure 21 includes the distribution characteristic of a nominal configuration. It is observed that only a relatively minor peaking is produced by the presence of the large pins. This effect vanishes for enhanced mixing.

Shifting a bundle within the duct, Cases 6 and 7 only, noticeably alters the temperature gradients at the outer periphery of the bundles.

Figure 22 summarizes the expected temperature drops across the hottest pin for the various cases studied. The limits are established by the uncertainty in the turbulent mixing parameter.

It may be concluded that bundle asymmetries lead to changes that are not negligible. The results presented illustrate, from the standpoint of thermal-hydraulic considerations, the need for adequate assembly tolerances in addition to the usual component tolerances. The mechanical problems (thermal stress) resulting from the asymmetries will be evaluated to determine the need for tighter tolerances, peripheral flow suppression, etc.

Effect of Duct Wall Roughening on Coolant Channeling

The presence of wire wrap (or other spacers) in the fuel subassembly, creating larger coolant channel areas (120-170%)

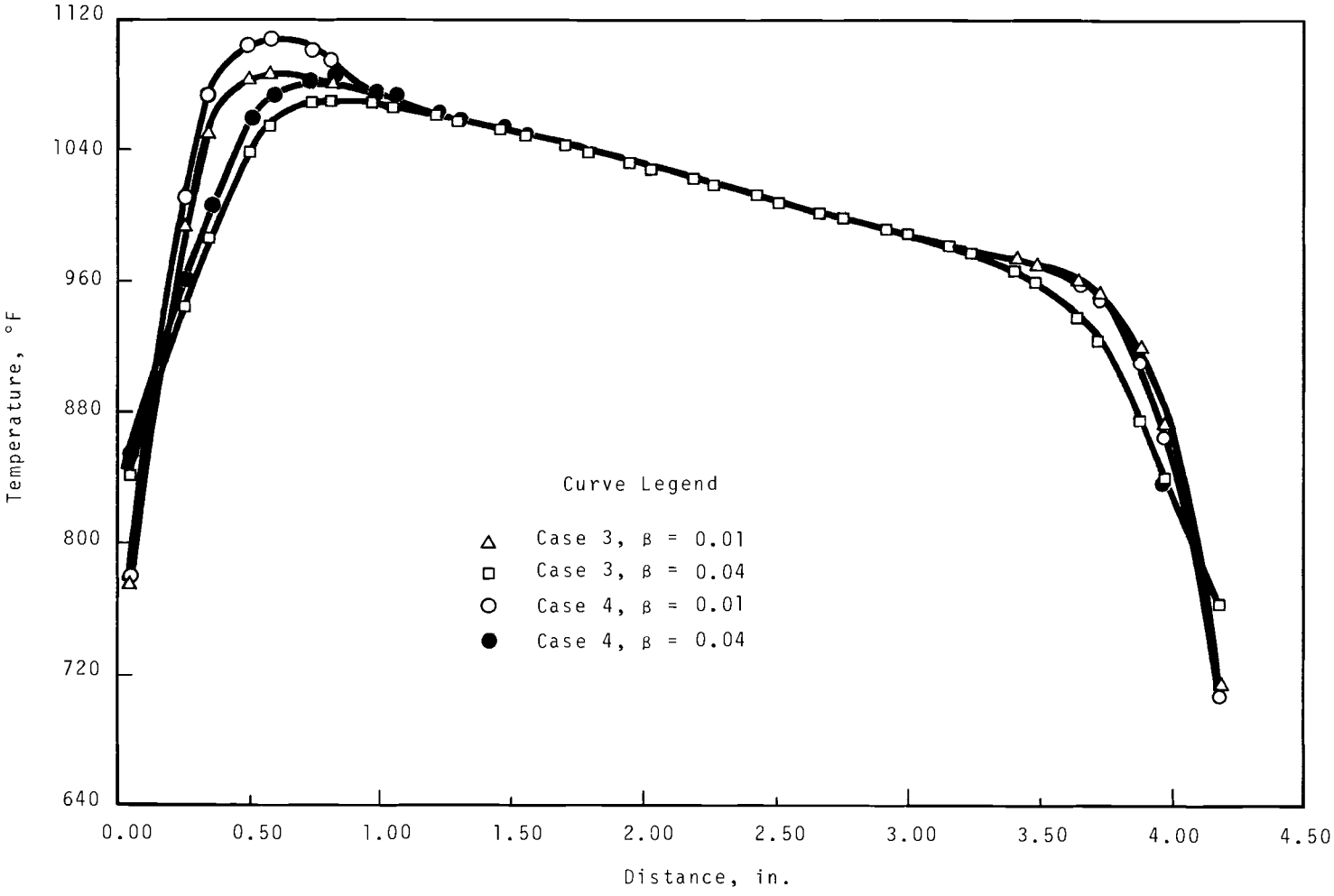

FIGURE 20. Coolant Temperature Distribution Across 217 Pin Subassembly at Upper Fuel-Insulator Boundary for Designs Employing Extreme Limits of Tolerance and Nominal Dimensions - Cases 1, 2, and 3

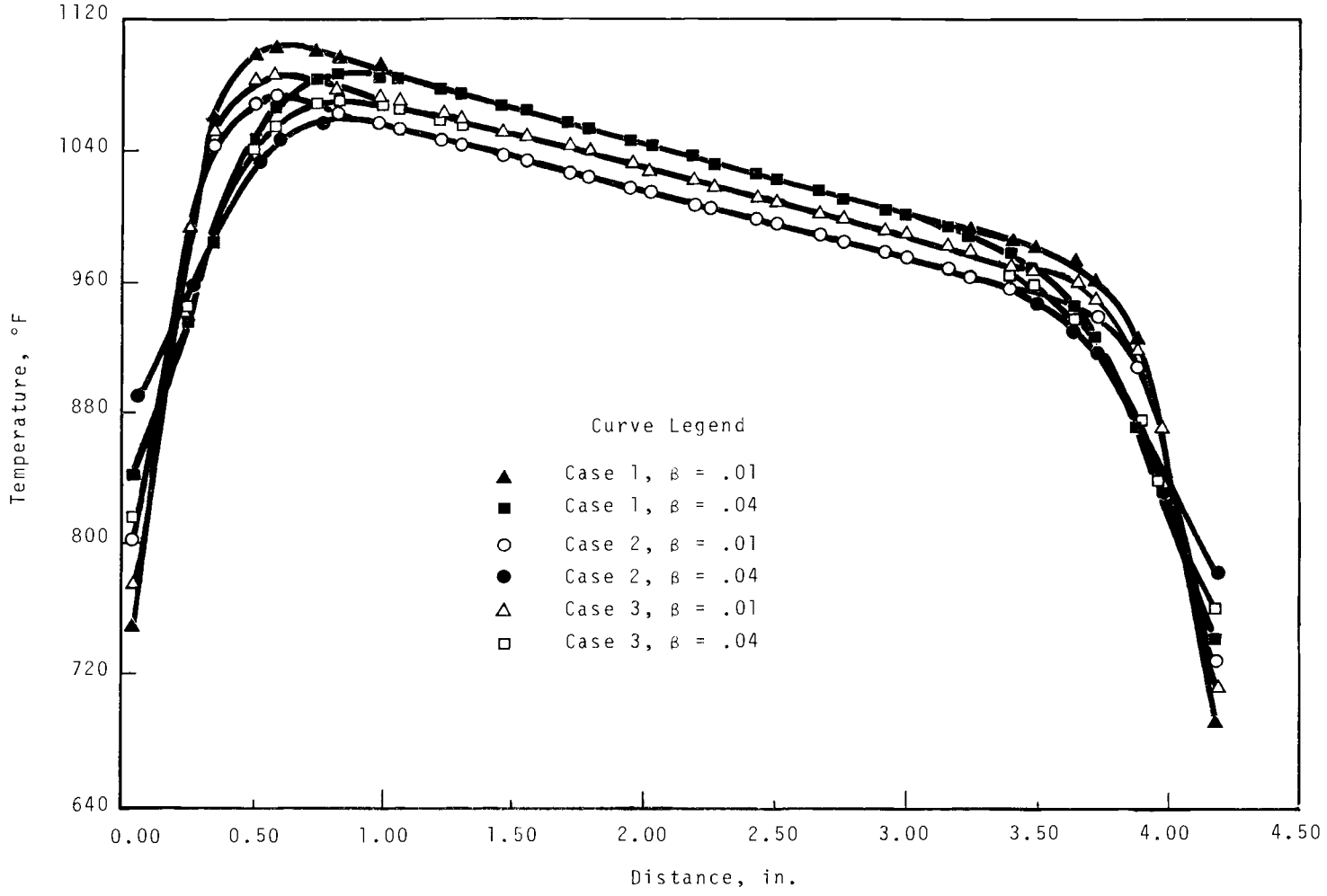

FIGURE 21. Coolant Temperature Distribution Across 217 Pin Subassembly at Upper Fuel-Insulator Boundary for Bundle Possessing Four Large Pins in a Nearly Nominal Subassembly - Case 4

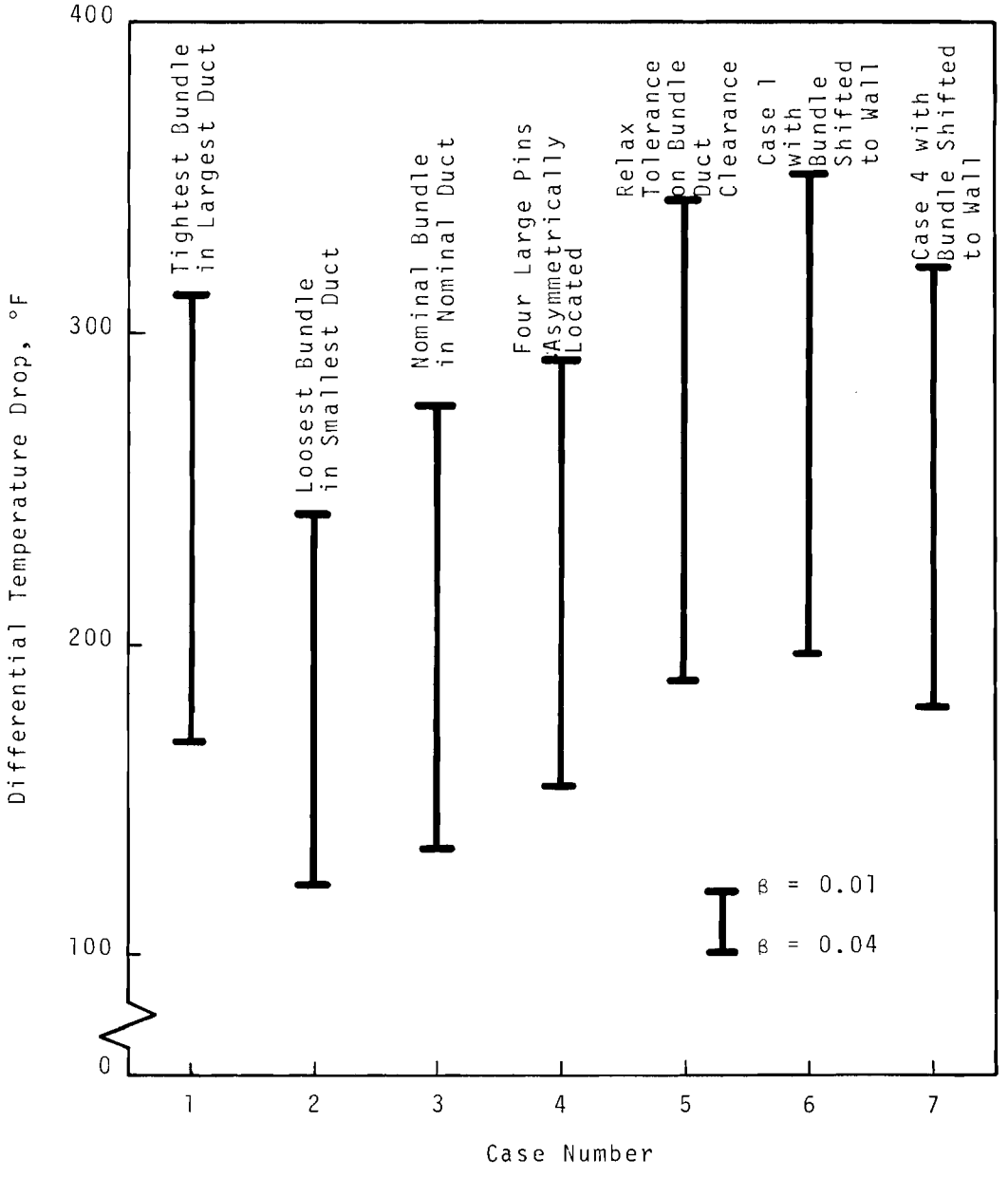

FIGURE 22. Coolant Temperature Drop Across Highest Gradient Pin in Hottest Subassembly at Upper Fuel Insulator Boundary for Various Bundle-Duct Configuration

beyond the outer row of fuel pins than within, results in flow channeling around the pin bundle. The extent to which these temperature gradients can be reduced by simple roughening of the interior duct walls is explored here.

Duct wall roughening is calculated to be helpful in minimizing severe coolant temperature gradients in the fuel subassembly, and the effect is very sensitive to bundle arrangement within the tolerance limits. However, the amount of roughening required to produce significant effects is infeasible.

In order to simulate the thermal-hydraulic processes operating in the fuel subassembly, the COBRA digital computer code (modified version) was employed. Due to the nodal limitations of COBRA, it was necessary to approximate the three-dimensional character of the subassembly. The computational matrix consisting of a thin strip model between the flats parallel to the steepest power gradient was employed (Figure 23). Justification and use of this model is reported in the preceding sections beginning on pages 39 and 41.

The hottest subassembly chosen for analysis possesses the particularly significant characteristic of very nearly the maximum power gradient in the core.

The parameters employed in this analysis were:

Pin OD, in.	0.250
Wire wrap OD, in.	0.030
Inlet coolant temperature, °F	550
Average core ΔT, °F	350
Average pin linear power, kW/ft	7.85
Active fuel length, in.	32
Axial power peaking factor	1.24
Subassembly tube dimension (flat-to-flat), in.	4.22

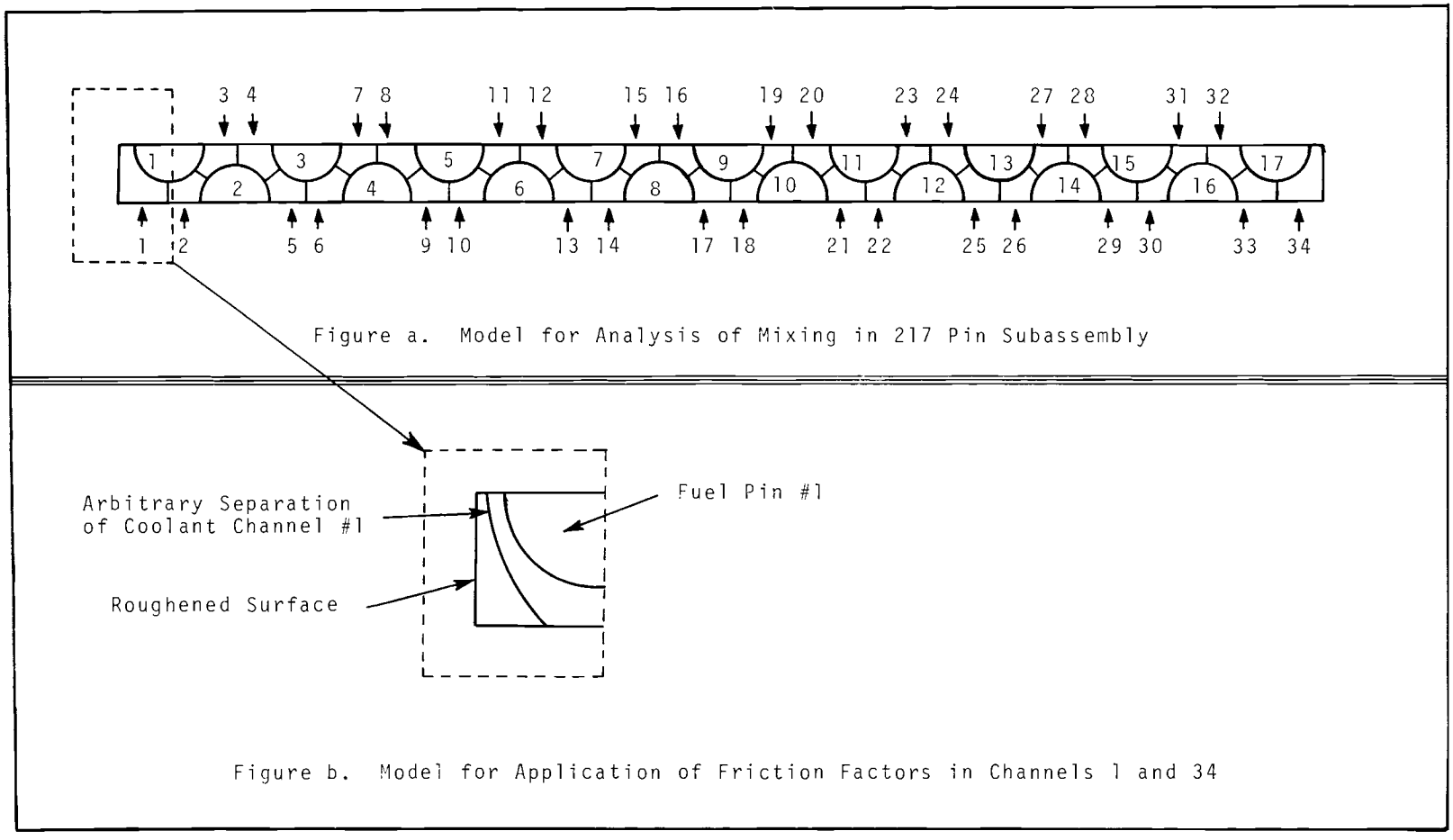

FIGURE 23. Geometric Model for COBRA Analysis

Other parameters used were:[13]

$$\frac{\text{Average power of hottest subassembly in outer zone}}{\text{Average power of average core subassembly}} = 1.137$$

$$\frac{\text{Peak heat generation rate in hottest subassembly in outer zone}}{\text{Average heat generation rate in hottest subassembly in outer zone}} = 1.17$$

Pin bundle clearances of 0 and 19 mils between bundle and duct wall were considered. Design tolerances presently range between 7.5 and 22.5 mils for the reference design, with a nominal value of 15 mils. Uncertainty in the degree of mixing necessitated consideration of two values of the lumped mixing parameter, β. As was assumed elsewhere, β should possess a value of about 0.01 in the absence of spacers for this geometry.[12] If spacers are introduced, β could possess a value as large as 0.04. The latter value is substantiated by an experiment[16] as yet unreported.

The frictional forces on all interior channels (2 through 33 in Figure 23) were presumed to be characterized by an equivalent circular channel and by the Koo correlation for the Moody Friction Factor for long smooth tubes, where

$$f = 0.6/Re^{.32} + 0.0056, \text{ and}$$

Re is the Reynolds number. The coefficient of the first term is about 20% higher than given in the literature. This correction provides a conservative estimate of the effect of wire wrap. According to results employing the de Stordeur method, a correction on the entire expression should range from about +14 to +20%, depending upon the choice of the representative coolant flow rate.

The friction factor characteristic of channels bounded by the smooth fuel pins and the roughened duct wall (channels 1 and 34 in Figure 23) are not obvious for a given degree of roughness. Derivation of the friction factor requires a detailed knowledge of the velocity distribution in this complicated geometry. Though this information is not impossible to obtain, it appears to be most time-consuming. Another, though less sophisticated, tack assumes the defining of a mean friction factor in this combination roughened-smooth walled region and that it be constant. Justification for this assumption is provided later.

Based upon the assumption of a constant mean friction factor in the exterior channels (1 and 34), COBRA provides the results shown in Figures 24 through 26. Figure 24 displays the coolant temperature profile for the case where the duct wall is 30 mils from the closest pin (30 mils of wire wrap) - the minimum possible clearance. Figure 25 illustrates the case where the pin-duct wall separation is 49 mils (30 mils of wire wrap plus 19 mils of clearance)--a value somewhat larger than nominal clearance. Both Figures 24 and 25 show, for comparison purposes, the results for a smooth duct and a rather rough duct. Figure 26 shows the velocity distributions corresponding to the same cases. Figure 26 illustrates that, by roughening the duct wall, the flow at the periphery of the bundle is transformed from a channeling state to a retarded state. However, the effect is not sufficient to completely alleviate the adverse temperature gradient as shown in the preceding figures.

A unique interpretation of Figures 24, 25, 26, and 20 is not possible due to the uncertainty in the interpretation of the mean friction factor in the exterior (of the bundle) channels. To this end it is further assumed that:

1. The exterior channels can be subdivided into two parts or subchannels (Figure 23). Each subchannel is then

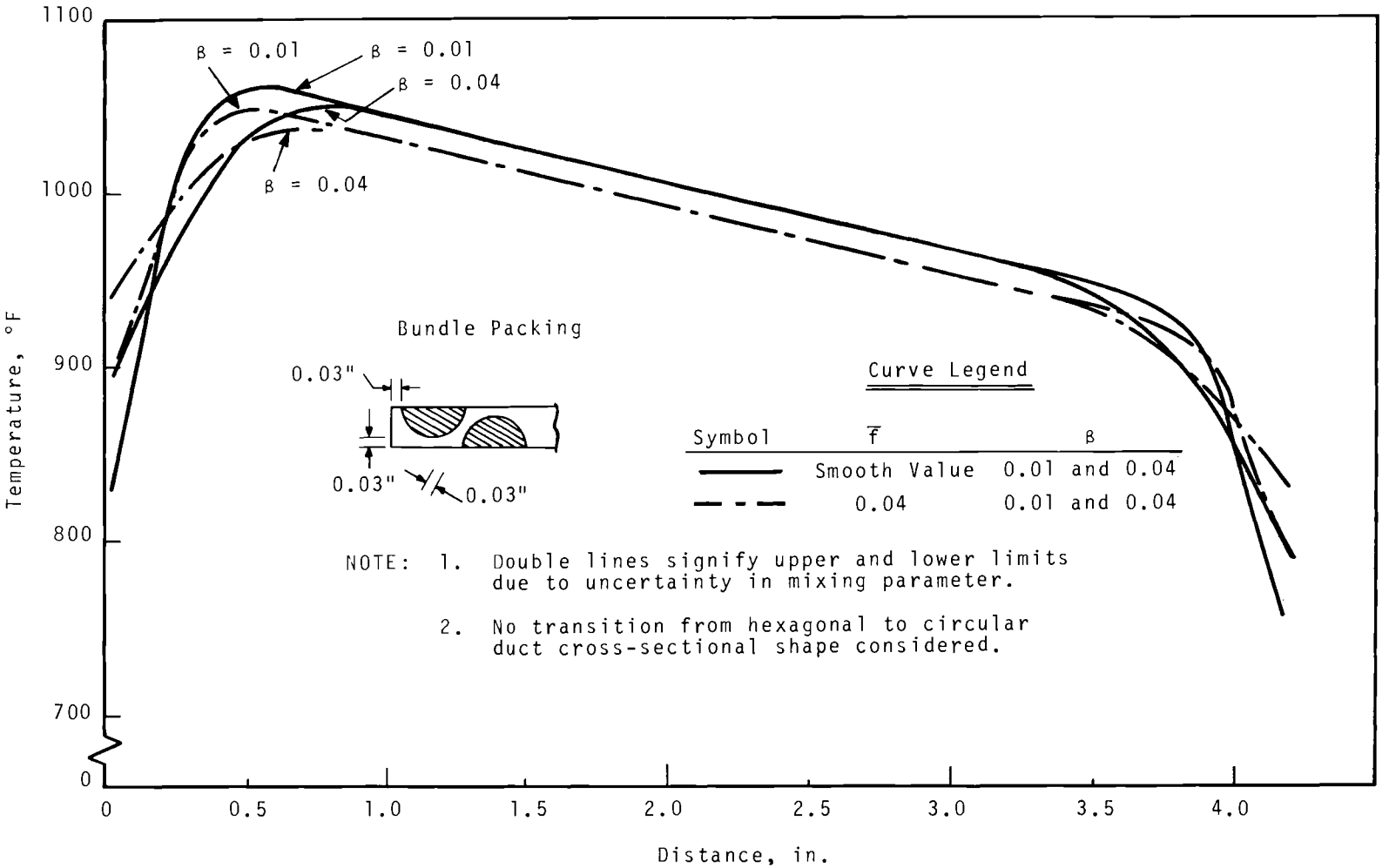

FIGURE 24. Coolant Temperature Distribution Across 217 Pin Subassembly at Upper Fuel-Insulator Boundary for Tight Bundle Packing

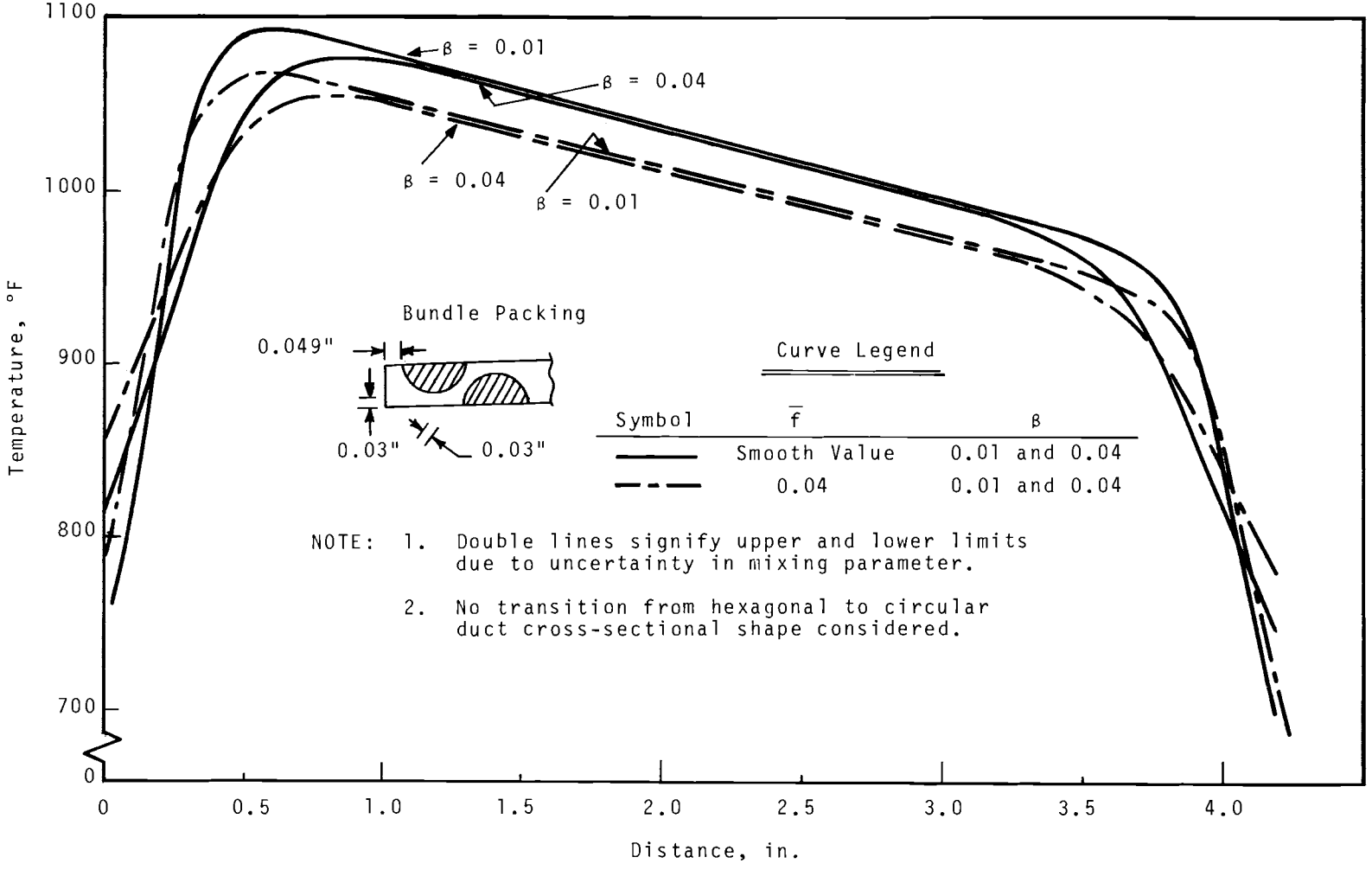

FIGURE 25. Coolant Temperature Distribution Across 217 Pin Subassembly at Upper Fuel-Insulator Boundary for Nominal Bundle Packing

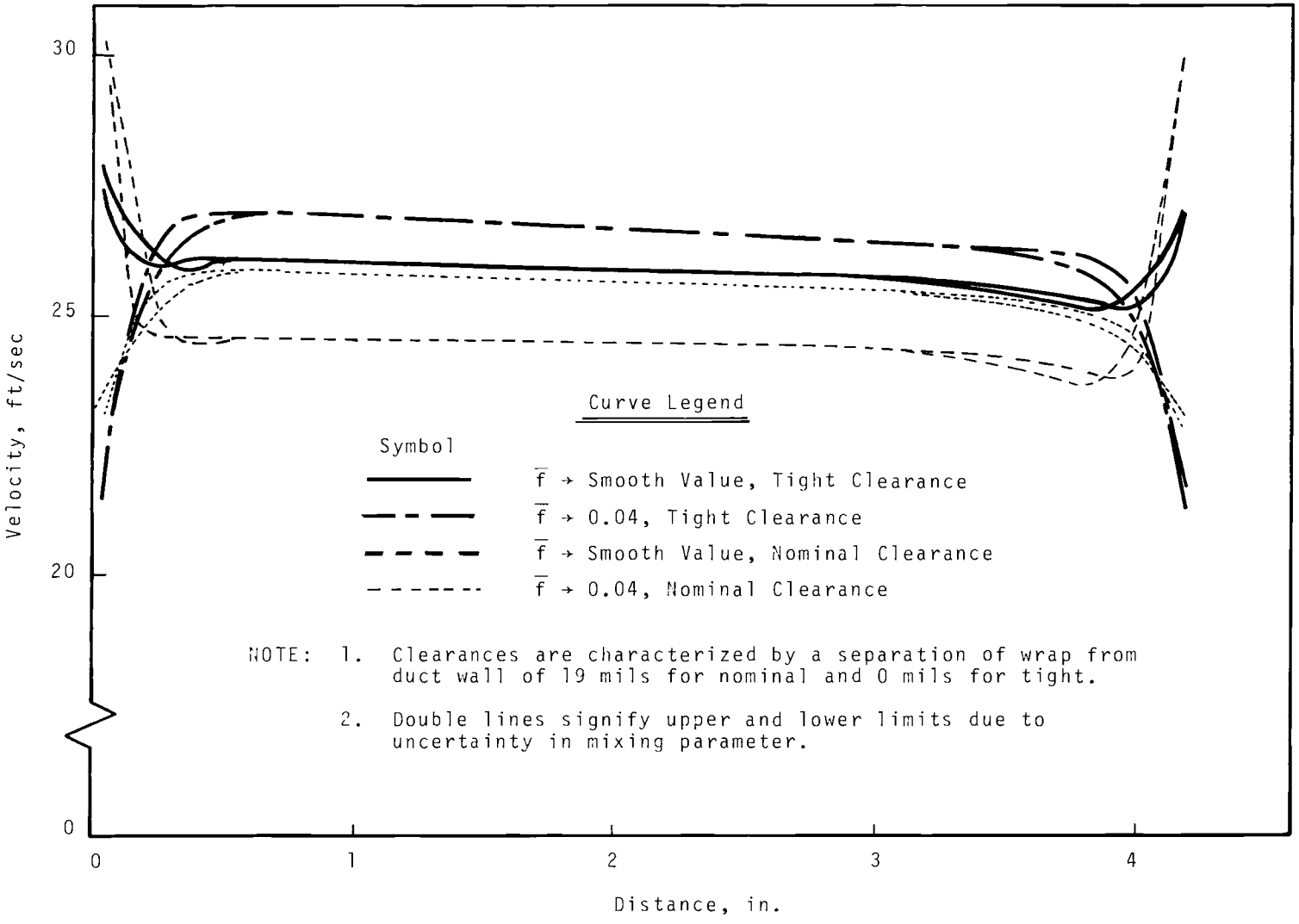

FIGURE 26. Coolant Velocity Distribution Across 217 Pin Subassembly at Upper Fuel-Insulator Boundary Using COBRA Computer Program

treated as a channel with an equivalent diameter for each. However, the choice of the subdivision is not arbitrary.

2. The division of flow between the two subchannels in each of the exterior channels follows from Darcy's formula and the requirement of equal pressure drops. After equating kinetic energies there results

$$\bar{f} = \frac{1}{\frac{a_R^2}{f_R C_R} + \frac{a_s^2}{f_s C_s}} \qquad (2)$$

where a_R and a_s are the area fractions, f_R and f_s are the Moody friction factors, and C_R and C_s are the wetted perimeter fractions of the rough and smooth walled subchannels, respectively. The area fractions are selected such that $\bar{f} = f_s$ when $f_R = f_s$. The mean friction factor approaches the smooth tube value when all surfaces are smooth. Fixing the area fraction is the process of subdivision just noted. A consequence of this selection of the area fractions is the establishment of an asymptotic upper limit of $\bar{f} = 0.056$. This upper limit of $\bar{f}$ is probably artificial and reflects the departure of the approximation from the more rigorous theory; the area fraction in the more rigorous theory would probably be a function of roughness and might force the limit on $\bar{f}$ upward.

For the mean friction factor to be constant, the Reynolds number must be large and nearly constant along the channel axis, and the duct wall must be sufficiently rough so that its contribution to the friction factor may be described by the asymptotic value. The former requirement is justified by COBRA output. The latter requirement follows from the degree of roughening of the duct wall.

If various degrees of roughness are ascribed to the duct wall while retaining smooth pins, Equation (2) may be employed

along with COBRA results to estimate the "bulk" coolant temperature distribution about the outer hottest pin. Figure 27 displays these results. Interpretation of the roughness by way of f_R was accomplished by means of Moody's experimental results.[17] It can be observed in Figure 27 that even with the roughest of natural surfaces, tightest subassembly packing, and with the most optimistic yet reasonable mixing model, a 50° temperature increase in the coolant can be expected about the pin closest to the core axis. This temperature rise is sensitive to packing. Severe roughening of the duct wall could reduce the coolant temperature drop about the hottest pin in the most tightly packed subassembly by about 50%. However, this reduction would drop to less than 30% for the loosest packing.

Several weaknesses of these calculations should be emphasized. First, the temperatures reported are bulk average temperatures and do not consider the local peaking possibly resulting from the presence of the wire wrap, etc. The version of COBRA employed did not incorporate a conduction mode. Where the temperature gradient is large, viz., low "f" region shown in Figure 27, the conduction mode will favor reduction of the gradient. Uncertainty in the selection of mixing intensity exists because of insufficient experimental data. However, this deficiency is reflected in the figures presented here. The pins are presumed to stand parallel to the duct wall. The effects of bundle bulging due to external forces, of pin swelling, of vibration, etc. are neglected. Finally, the interpretation of the mean friction factor depends upon the validity of the equivalent diameter concept, and also involves the extrapolation to very large roughnesses combined with small flow areas.

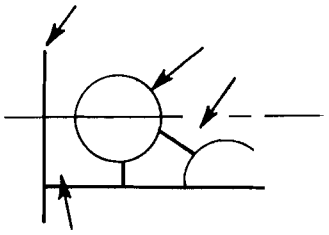

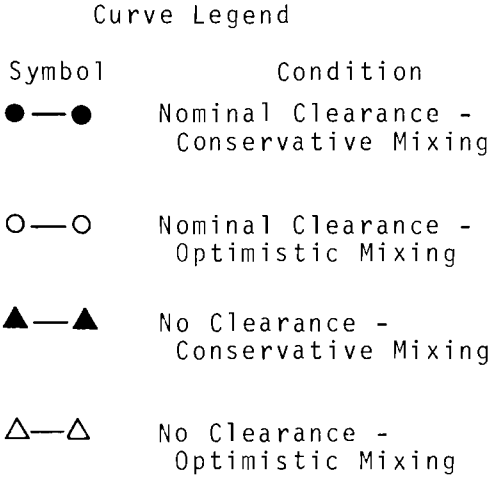

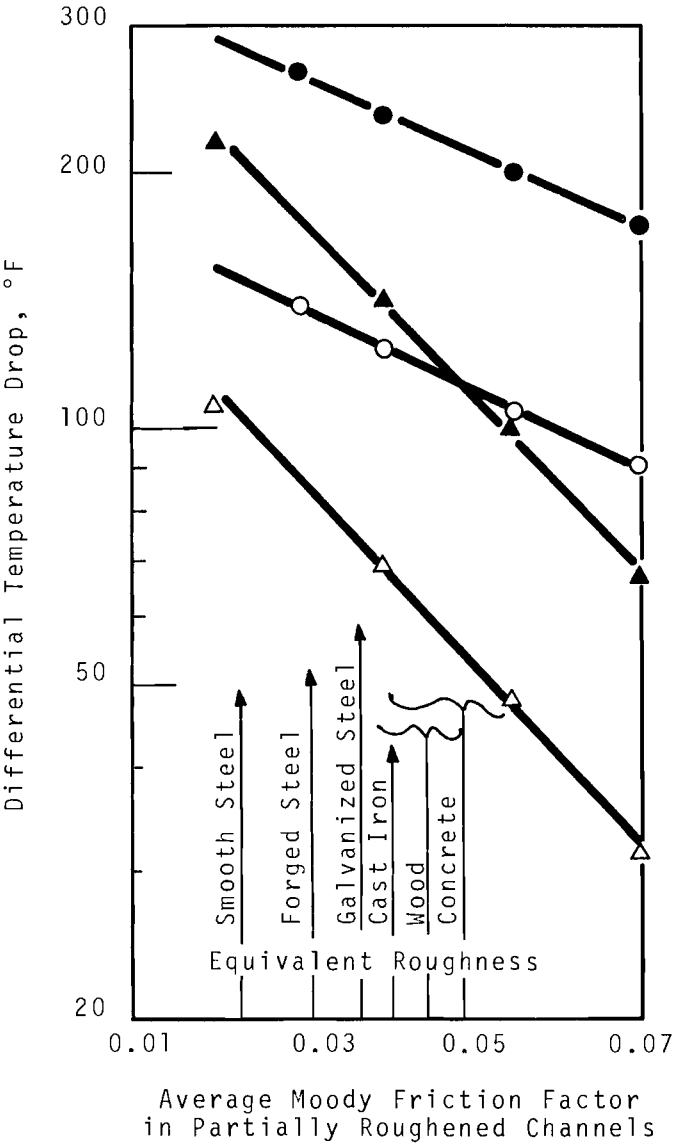

FIGURE 27. Coolant Temperature Drop Across Hottest Pin Resulting from Various Degrees of Duct Wall Roughening

TEMPERATURE EFFECTS OF PIN-TO-PIN CONTACT

T. J. Bennett

The TIGER-V code was used to determine the radial temperature distribution for touching fuel pins. The model assumed a linear heat generation rate of 14 kW/ft, with a fuel radius of 0.11 in., and an outer cladding radius of 0.125 inches. The pins are assumed to be tangent at the mid-point between 30-mil supports, with a 6-in. (in line) support span.

The following tabulation shows the circumferential variation of temperature away from the point of contact. These temperatures represent the difference between a pin in contact with another pin and a normal or untouching pin. Figure 28 details the temperature distribution data.

	Contact Point ΔT (°F)	0.01 Inches from Contact Point ΔT (°F)	0.02 Inches from Contact Point ΔT (°F)
Outer Fuel Surface	36	19	9
Inner Cladding Surface	47	24	7
Cladding Interior	54	29	11
Outer Cladding Surface	101	37	8
Coolant	55	0	0

TEMPERATURE EFFECTS OF TOUCHING PIN TO DUCT

T. J. Bennett

Data in Flow and Coolant Temperature Distribution Analysis has shown the coolant associated with the peripheral pins (those adjacent to the duct wall) to be a minimum of 100 °F cooler than the hottest pin of a 217 bundle. Thus the peaking and temperature level of a pin touching the duct is expected to be less than that for a pin in contact with another pin. The effect is further diluted by the fact that the duct wall is not a heat source, and that its mass represents a potential heat sink. These considerations have precluded further analysis of the pin-to-duct wall contact problem.

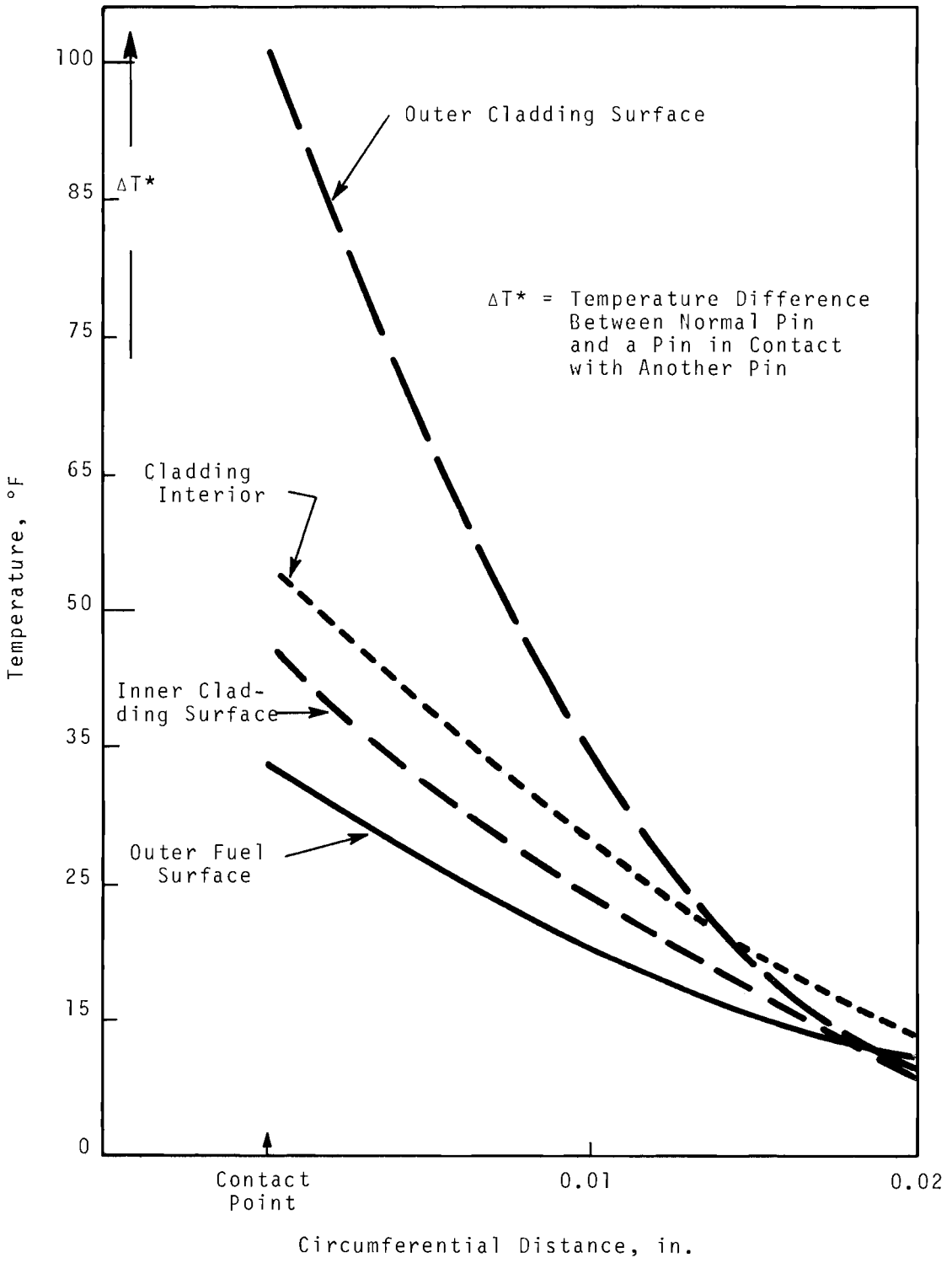

FIGURE 28. Pin Touching Circumferential Temperature Distribution

TEMPERATURE PEAKING UNDER THE WIRE WRAP

D. C. Kolesar and D. L. Koreis

Introduction

Temperature peaking in the proximity of the wire wrap of the hottest FFTF fuel pin was investigated using MANTA,[18] a code written at General Electric (APED). The peaking phenomenon is a consequence of lower coolant flow rates in relatively confined spaces. The lower local heat transfer coefficients cause temperature peaking. Calculations in three dimensions for a single pin and neighboring coolant were subject to assumptions making the problem tractable and bracketed the solution. Results from a not yet complete analysis disclose only a modest circumferential variation of temperature. The seriousness of this temperature peaking would depend upon the particular related phenomenon to be investigated, e.g. thermal stress, reactor safety analysis, pin life, etc.

Specification of the Problem

Attention was confined to the hottest fuel pin and adjacent coolant in the FFTF core. The parameters employed in this analysis were[19]

Pin OD, in.	0.250
Wire wrap OD, in.	0.030
Inlet coolant temperature, °F	550
Average core ΔT, °F	350
Peak pin linear power, kW/ft	14.4
Active fuel length, in.	32
Axial power peaking factor	1.24
Radial power peaking factor	1.30

The "Engineering, Hot Spot-Hot Channel Power Peaking Factor," not used as the results of this analysis, will be employed in the evaluation of that number.

The composition and the resulting power distribution of the fuel pins were predicted by the SINTER Code.[20] Prior to sintering, the fuel pin was assumed to possess a cosine power distribution with an extrapolation distance obtained from the latest physics estimates.[21]

Model for Analysis

The physical problem was approximated by a model consisting of 1/12 of a unit cell (see typically Figure 29). The "cell" is composed of a single fuel pin and a fraction of the coolant established by symmetry based upon geometric considerations. One-twelfth of a unit cell is the smallest part that can be isolated for analysis due to its nearly adiabatic "boundaries". The gradient of the core power profile and bundle coolant velocity are assumed to be small in the neighborhood of the hottest pin.

Both MANTA restrictions and limitations imposed by the film coefficient libraries require the assumption that the wire wrap is oriented parallel to the pin. Two configurations have been previously studied for the purpose of establishing the velocity field and, thereby, the circumferential variation of the film coefficient. Koreis[22] placed the wire equidistant and between the neighboring tri-cusp channels while Dwyer[23] considered the same region without spacers. The actual wire spacer pitch is one complete revolution about the pin per foot of length. However, results for the case consisting of the wire in the channel gap and for that of no wire should bracket the actual solution. For the upper limit, the error due to the longer path traveled by fluid "trapped" by the wire (thereby increasing exposure to a higher energy flux), as compared to fluid channeling down the center of the tri-cusp region, is disregarded. Neglect of this effect should be more than neutralized by confining the wire wrap to the region where its influence is the greatest. The common basis for the two configurations was an identical mass flow rate (lb/hr).

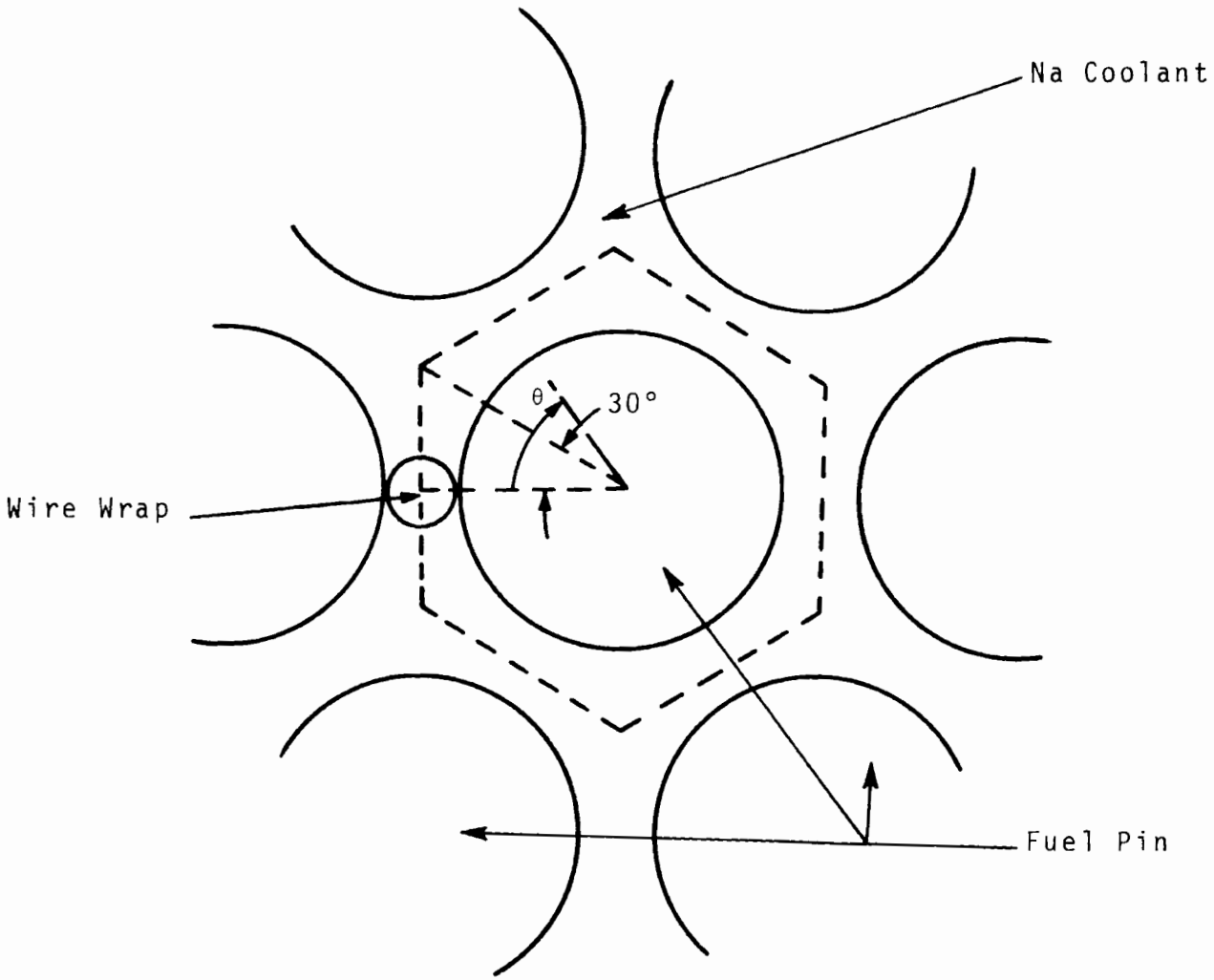

FIGURE 29. Unit Cell Model Analyzed by MANTA

Only the active fuel region was considered in the analysis. The velocity profile was assumed to remain unchanged along this length. The velocity field was obtained from an intermediate step in establishing the film coefficient (see typically Figure 30). The heat transfer coefficient was assumed to be independent of axial position.

Figure 31 illustrates the nodal mesh employed in the geometric model characterizing the Koreis configuration. The Dwyer configuration would replace the wire with three coolant channels. Three material regions, mixed oxide fuel, 316 SS, and flowing sodium, are considered. The region in and around the wire wrap has been divided for the convenience of the computer code. The active fuel was divided into sixteen equal lengths each possessing the nodal arrangement displayed in Figure 31.

Method of Calculation

The MANTA code employs mass, momentum, and energy balances in conjunction with the equivalent diameter concept. However, the equivalent diameter concept, while not strictly valid for coolant channels of the type displayed in Figure 31, did not introduce any conceptual difficulty since the velocity profile was to be fixed and therefore only the energy balance in MANTA was needed (independent of equivalent diameter). Use of only the energy balance could not be accomplished directly, so an iterative process was employed as follows:

1. The pressure drop was estimated from experimental data.
2. The friction factors were adjusted to give this pressure drop in each channel, as well as to approximate the coolant flow distribution.
3. The friction factor obtained in Step 2 based upon MANTA results, viz input velocity profile, were corrected to identical to the output velocity profile and repeated until velocity profiles converged sufficiently.

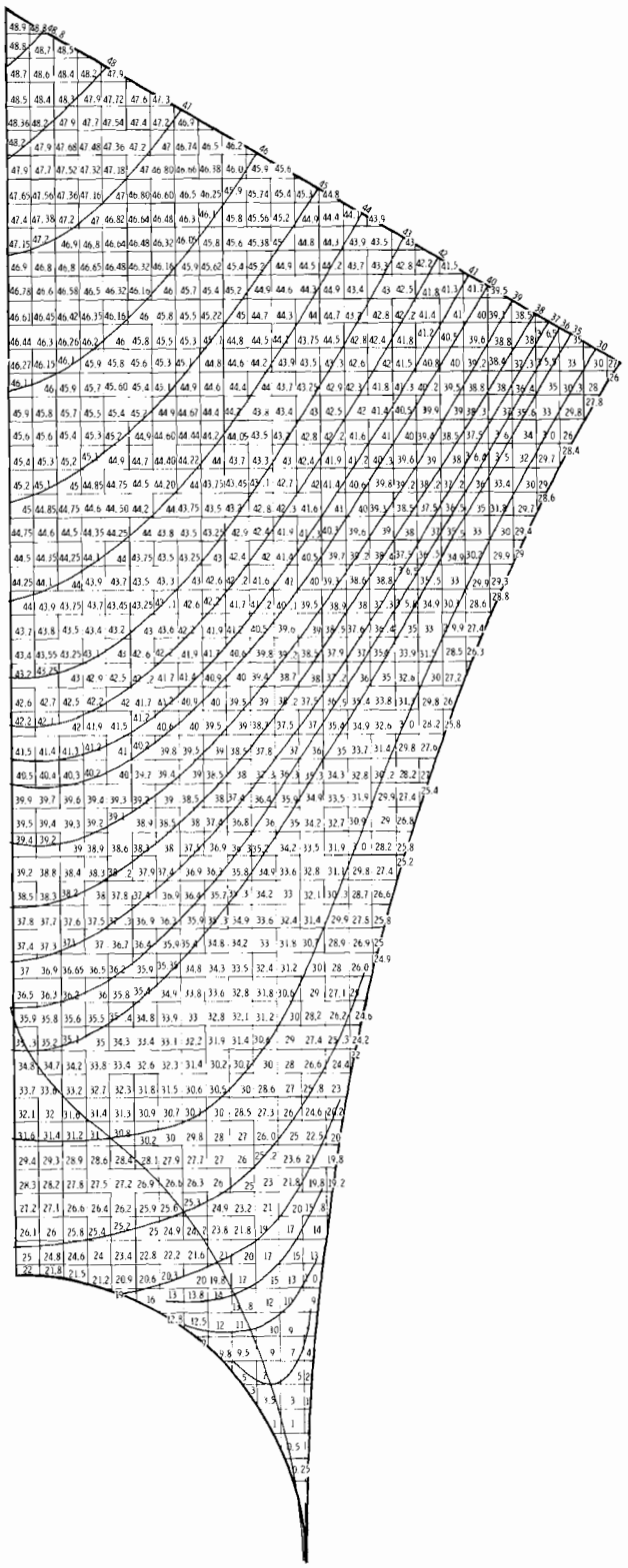

FIGURE 30. Velocity Grid

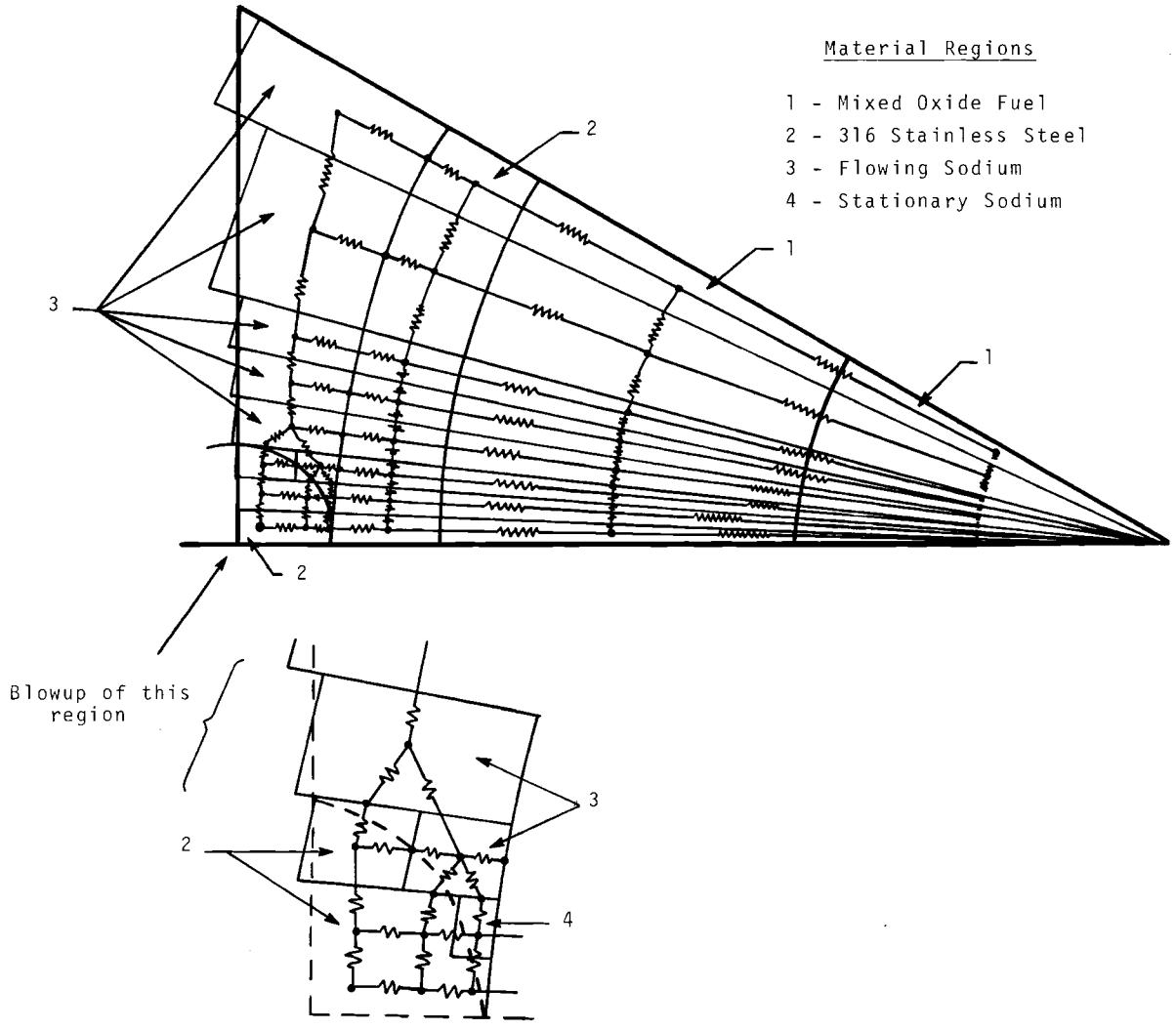

FIGURE 31. Subdivision and Nodal Network for 30° Slice of Cell Model

Steps 1 and 2 were based upon relative incompressibility of the fluid and the inability of turbulence to lead to net interchannel mass transfer. Step 3 is required because of natural computer inaccuracies as well as the temperature dependence of some properties, e.g. viscosity. The iteration in Step 3 was considered complete when errors in the mass flow in each channel were of the order of 0.5% or smaller (0% for critical channels).

Material Constants and Heat Transfer Coefficient

Most transport and thermodynamic property inputs were somewhat similar to those employed in like calculations at PNL. A significant exception was the film coefficient. Predicting the temperature variation about the pin circumference requires use of a local heat transfer coefficient dependent upon polar angle, with origin at the center of the fuel pin. Dwyer[23] has accomplished this for some typical cases in the absence of spacers. PNL employed the same technique but introduced a wire wrap at the point of closest separation between pins. To assist in the analysis, a refinement originally employed by Deissler and Taylor[24] was incorporated to handle the perturbation of the velocity field caused by the wire wrap. Dwyer's method is a graphical determination achieved by a complicated series of related plots of various field quantities and transport constants. Thereby the necessary heat transfer coefficient (a function of polar angle) is deduced from the computer temperature field.

The basic assumptions used in the analysis were (1) fully developed turbulent flow, (2) uniform heat flux from the surface of the fuel pin, and (3) fully developed velocity and temperature profiles.

Values Used in Calculations

D_{pin} = 0.25 in.

$D_{wire\ wrap}$ = 0.03 in.

ρ = 53.4 lbm/ft^3

μ = 0.725 lbm/ft-hr

k = 41.6 Btu/hr-ft °F

$C\rho$ = 0.307 Btu/lbm °F

ΔT_{core} = 350 °F

$\mathring{m}$ = 790 lb/hr/pin

q/A = 0.446 x 10^6 Bru/hr-ft^2

The calculational procedure may be summarized as follows:

1. Determine the velocity field by first arbitrarily subdividing the coolant by coolant flow lines carefully selected to represent the velocity gradient lines. This subdivision is accomplished for two cases, one with velocity gradient lines emanating from the pin, and one from the wire wrap. Solutions for each case will be sought separately and will be matched at a common line. This line, the line of maximum velocity between the fuel pin and the wire wrap, was positioned by assumption. Dimensionless velocity versus position were hypothesized for each subdivision based upon its shape, and upon experimental data pertinent to that shape. These data were then used to establish the wall shear stress in each division and, thereby, the velocity versus position. Connection of points of common velocity yields constant velocity lines. With coolant flow lines perpendicular to the velocity lines, and the velocities at all points on the line of maximum velocity between pin and wire equal when calculated independently from both pin and wrap, the original subdivision must be correct. Otherwise the process would be repeated. Figure 32 gives the correct flow and velocity lines. The final result is the velocity grid displayed in Figure 30.

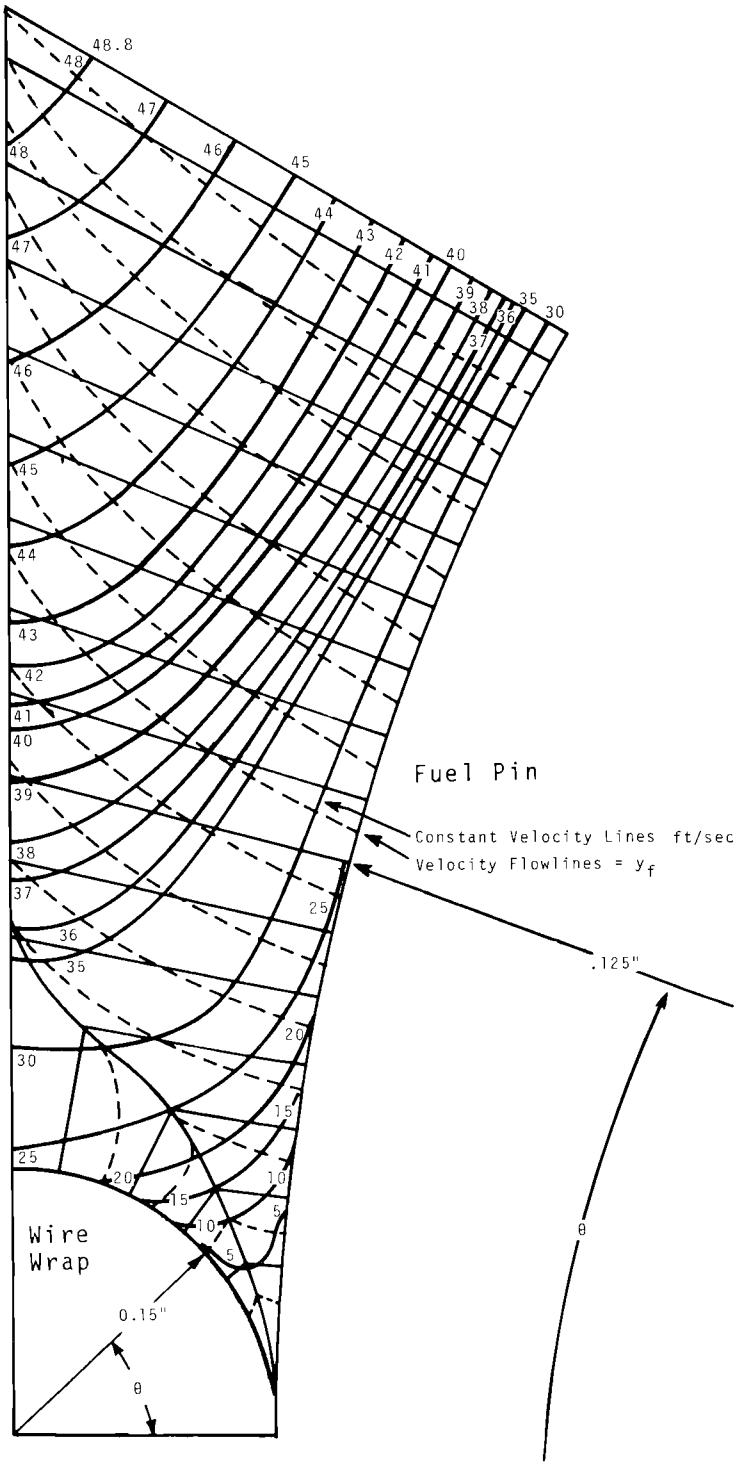

FIGURE 32. Coolant Flow Lines and Constant Velocity Lines

2. Determine the paths of Energy Transfer in the Coolant. The cross sectional flow area above the line of maximum velocity is divided arbitrarily into segments such that each segment has the same amount of coolant flowing through it. The latter, established by trial and error, is displayed in Figure 33. It is assumed that the heat flux is uniform and thus each of these segments removes the same amount of heat from the fuel pin.

3. Determine the eddy thermal conductivity. If one assumes the eddy diffusivities of momentum and heat transfer are equal, the eddy thermal conductivity may be computed from the expression $k_e = C_p \mu_e$ where the eddy viscosity may be obtained directly from a knowledge of τ and velocity gradients previously calculated. Figure 34 provides the resultant eddy thermal conductivity.

4. Determine the Temperature Distribution. After superimposing previously determined plots appropriately, the solution of an energy balance on a heat-flow segment yields the temperature field.

5. Determine the local heat transfer coefficient. To determine the variation of the local heat transfer coefficients, it was necessary to obtain the bulk temperature of the coolant above the line of maximum velocity. Once the bulk temperature was determined, the following formula was used to obtain the local film coefficients:

$$h_l = (q/A)/(T_{wl} - T_b)$$

h_l = local coefficient, Btu/hr ft^2 °F

q/A = heat transferred, Btu/hr ft^2

T_{wl} = local wall temperature, °F

T_b = bulk temperature of the coolant, °F

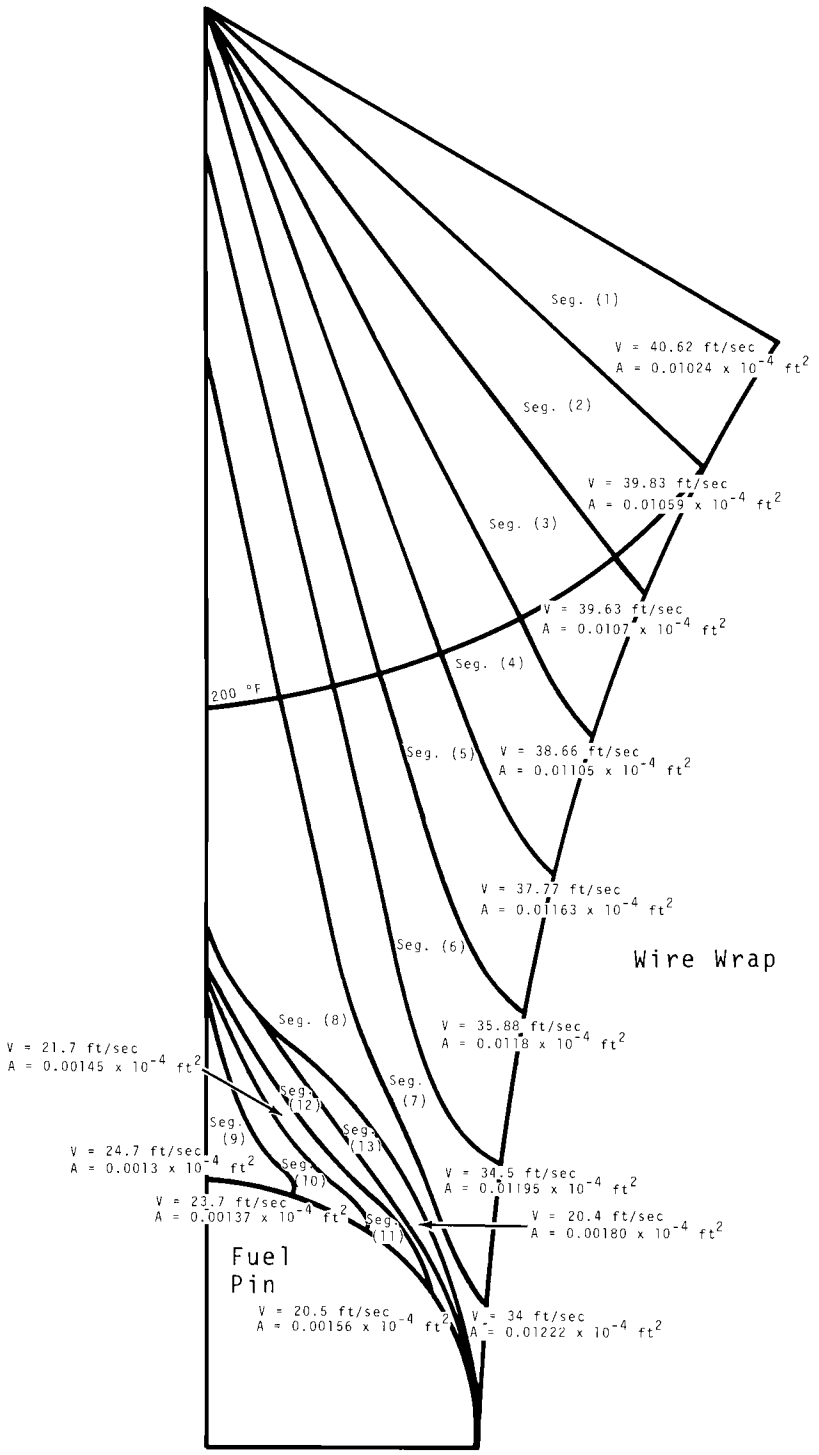

FIGURE 33. Paths of Energy Transfer

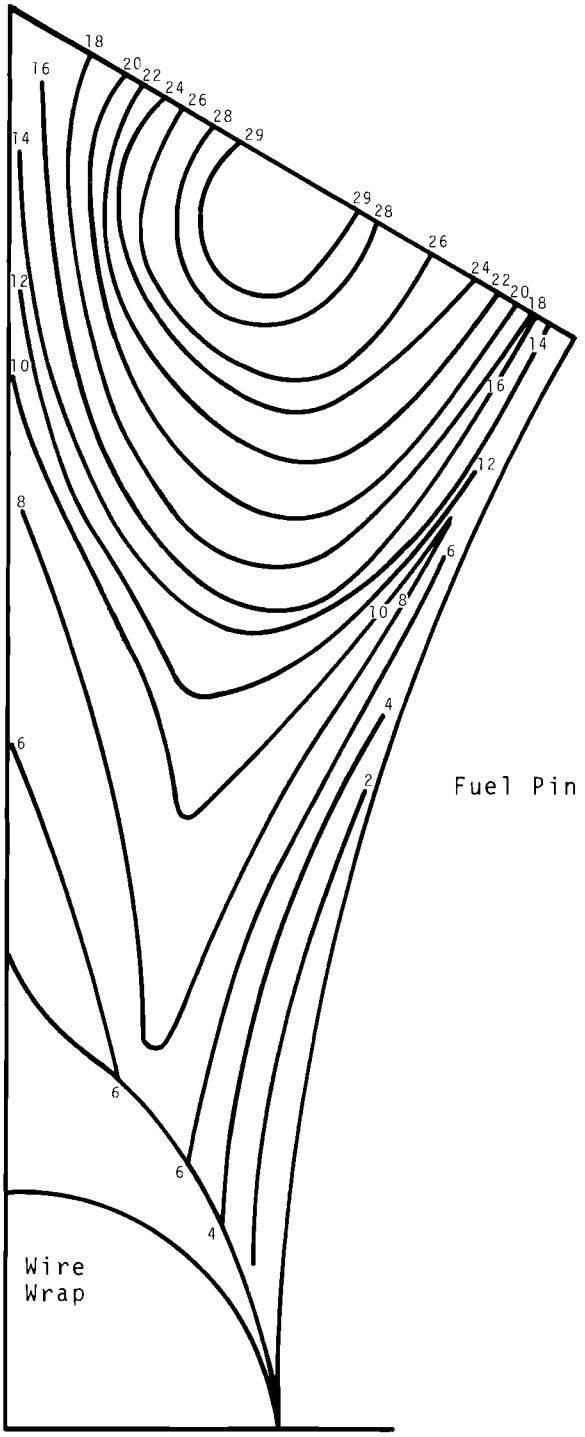

FIGURE 34. Eddy Thermal Conductivity

Variations of the local film coefficients with the polar angle θ (see Figure 29 for definition of θ) are shown in the following tabulations.

θ	h
1.88	5.12×10^3
5.62	8.13×10^3
9.38	1.465×10^4
13.12	2.42×10^4
16.88	3.85×10^4
20.62	1.145×10^5
24.38	3.19×10^5
28.12	1.112×10^6

The film coefficients for a rod bundle with a wire wrap spacer, when compared to a rod bundle without the wire wrap spacer, is seen to have a higher variation in film coefficients.

Nonspacer (Dwyer) Rod Bundle	Wire Wrap Spacer
P:D = 1.1	P:D = 1.12
P_e = 206	P_e = 319
$\bar{h}$ = 20,520	$\bar{h}$ = 14,350
$q/A = 2 \times 10^5$	$q/A = 4.46 \times 10^5$

θ	h/$\bar{h}$	h	h/$\bar{h}$	h
1.88	0.497	10,200	0.357	5,120
5.62	0.520	10,650	0.565	8,130
9.38	0.590	12,100	1.002	14,650
13.12	0.804	16,500	1.685	24,200
16.88	1.431	29,400	2.69	38,500
20.62	3.295	67,500	7.90	114,500
24.38	9.71	199,000	22.3	319,000
28.12	32	657,000	77.5	1,112,000

The heat transfer coefficients at $\theta = 28°$ contain some error because, at this location, the wall temperature is very close to the bulk temperature. Small changes in this temperature difference lead to large variations in the heat transfer coefficient. Also the heat transfer coefficients at $\theta = 2°$ contain some error because of difficulty in obtaining an accurate evaluation of the wall temperature at this position.

MANTA employs a diffusional mixing model with a multiplying factor, k, inserted to permit correlation with experimental data. Here, results are reported for no mixing (k = 0), molecular diffusion (k = 1), and mixing characteristic of the conservative mixing parameter ($\beta = 0.01$) employed in earlier COBRA code calculations[15] (k = 5). The COBRA calculations attempted to duplicate, through this value β, tightly packed bundle phenomena based upon experimental data obtained in the absence of wire wrap. Indeed, the presence of wire wrap could require a β four times larger.[16] The use of a k greater than unity implies eddy diffusion in the absence of diversion cross flow and forced mixing. The turbulent mixing parameter β, used in COBRA, is predicted from experimental results based upon full interchannel mixing and not for transfer between arbitrarily defined subchannels as illustrated in Figure 31 (intrachannel mixing). Whether a gross parameter such as β can be employed for the local effects investigated here is not certain. Bader and O'Neill[25] have analyzed intrachannel effects using MANTA where "complete mixing" was thought to exist, and which they simulated with k = 150.

RESULTS

The expected temperature peaking in the coolant near the center and at the upper end of the fuel region is bracketed in Figures 35 and 36. These locations are characteristic of the maximum circumferential temperature peaking and the maximum bulk mean temperature of the coolant, respectively. It is observed that the wire wrap produces only a very localized effect.

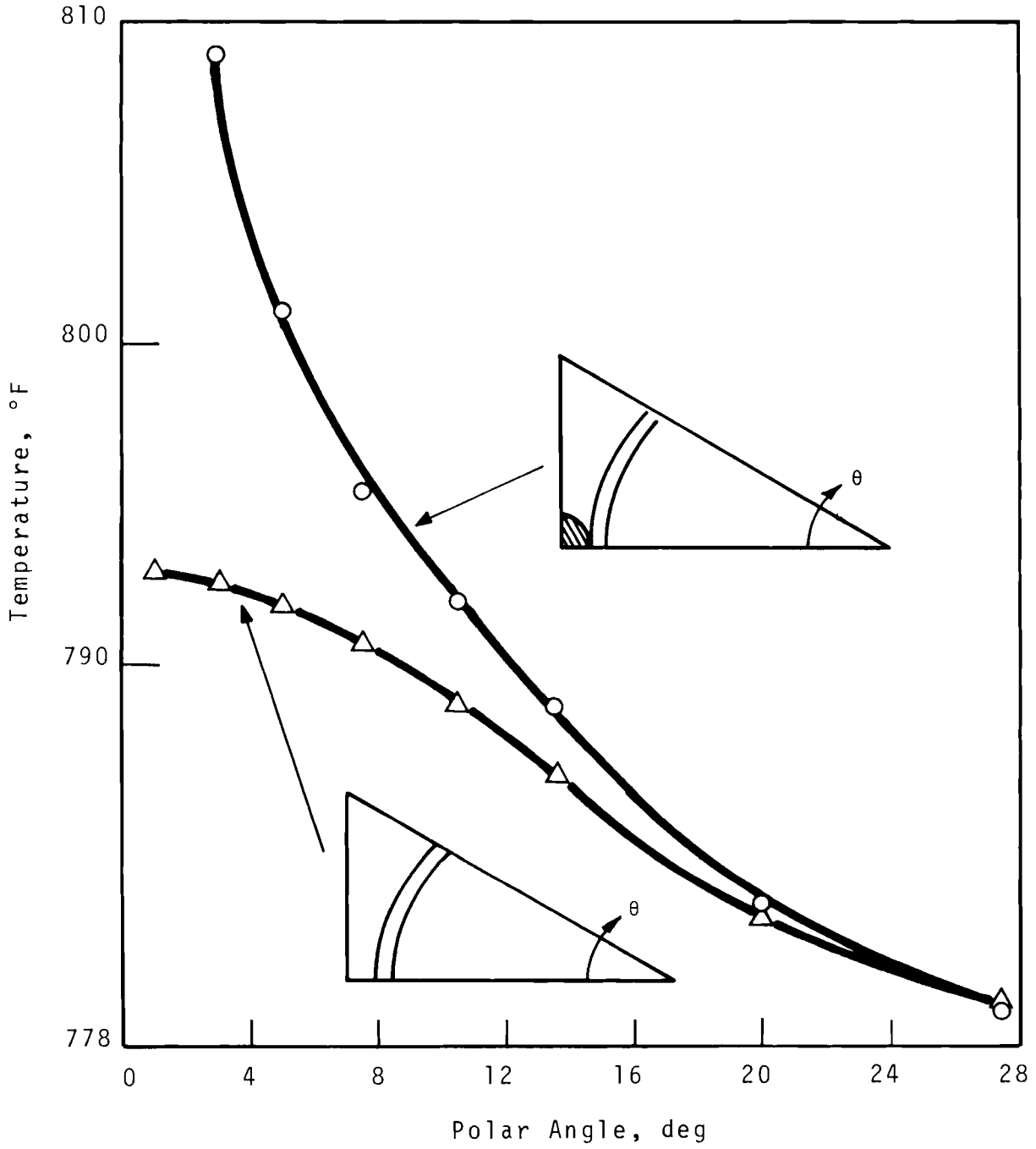

FIGURE 35. Circumferential Temperature Distribution in the Coolant Near the Center of the Fuel Region for the Wire Wrap in and far From the Gap Using the Molecular Diffusion Mixing Model

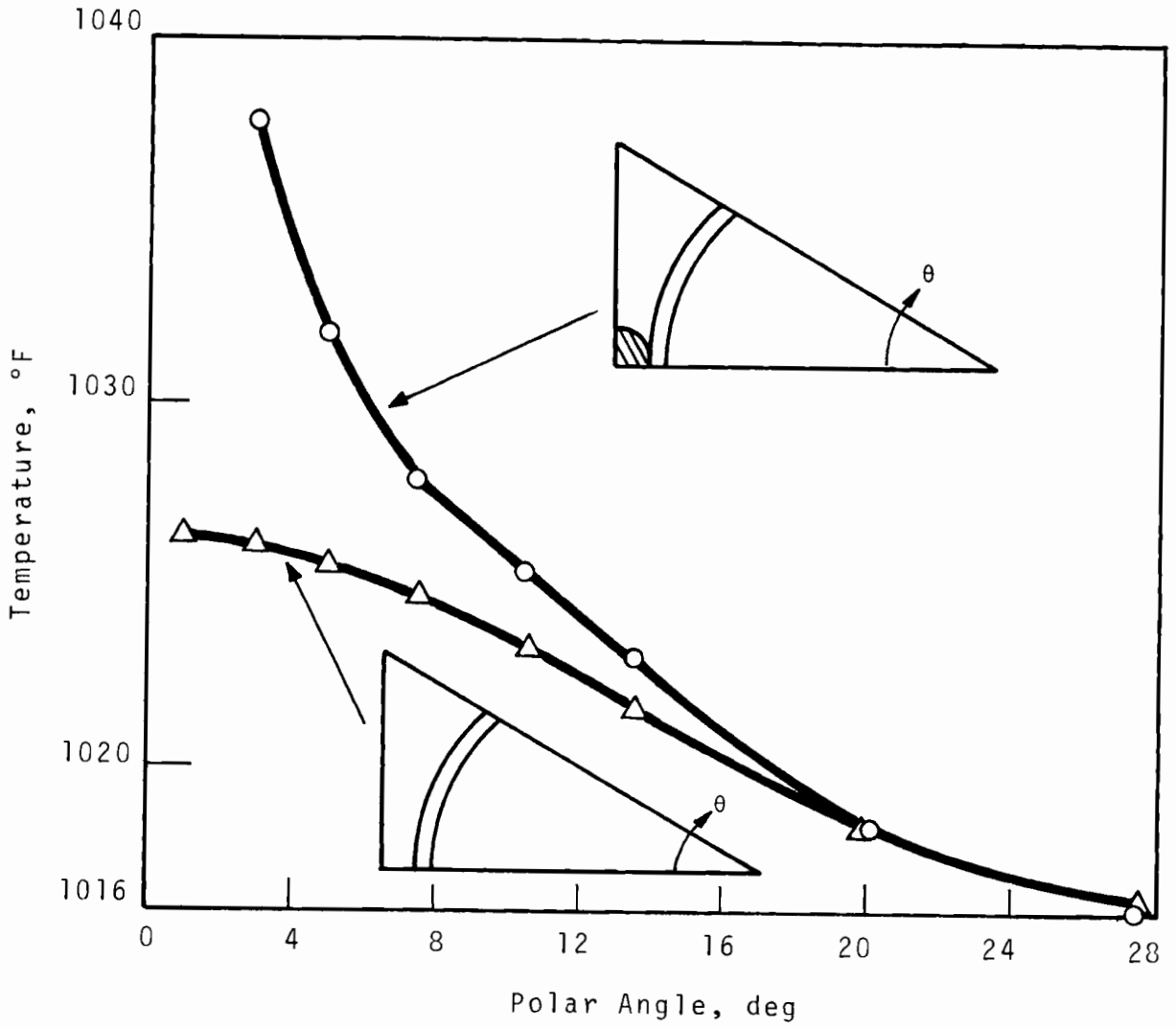

FIGURE 36. Circumferential Temperature Distribution in the Coolant Near the Upper End of the Fuel Region for the Wire Wrap in and far from the Gap Using the Molecular Diffusion Mixing Model

Figures 37 through 40 display features of the case involving the wire wrap. Each figure presents results with the mixing multiplying factor, k, as a parameter. It can be concluded that the degree of mixing, thus far unknown, is a significant factor. Indeed, even the value of k = 5 may prove excessively conservative. An experimental program now in progress at PNL should prove definitive on this matter.

Figures 41 through 43 are representative of the case without the wire wrap.

MECHANICAL DESIGN

FUEL SUBASSEMBLY ASSEMBLY PROCESS AND TOLERANCE CONTROL, WITH EMPHASIS ON WIRE WRAP APPLICATION

Assembly

M. K. Millhollen

The initial step in the FTR Driver Fuel Element Subassembly assembly process[26] is the assembly of the fuel pins (Figure 2). The bottom end cap is TIG welded to the cladding tube after pin components have been fabricated, accepted and cleaned. The weld is inspected. Internal components are placed within the tube. These are, in order of insertion, a 1/2-in. length of depleted UO_2 pellets, a 32-in. length of UO_2-PuO_2 pellets, a 1/2-in. length of depleted UO_2 pellets, a 6-in. long nickel rod, an Inconel-x compression spring, and a spacer tube. The top end cap is positioned in the top of the tube by pusing it down on the spacer rod which, in turn, compresses the spring. The slot in the end cap is carefully oriented parallel to the slot in the bottom end cap. The top end cap is TIG welded in place.

An appropriate length of 0.030-in. spacer wire, inserted through the hole provided in the top end cap and welded in place, is accomplished with the fuel pin placed in the wire wrap machine. The machine is turned on and the wire is wrapped spirally the length of the pin on a 12-in. pitch. The wire is applied to the pin under a constant load of 7 lb to avoid stressing the wire beyond its yield point. The wire is pulled through the welding hold at the bottom end cap and welded in place.

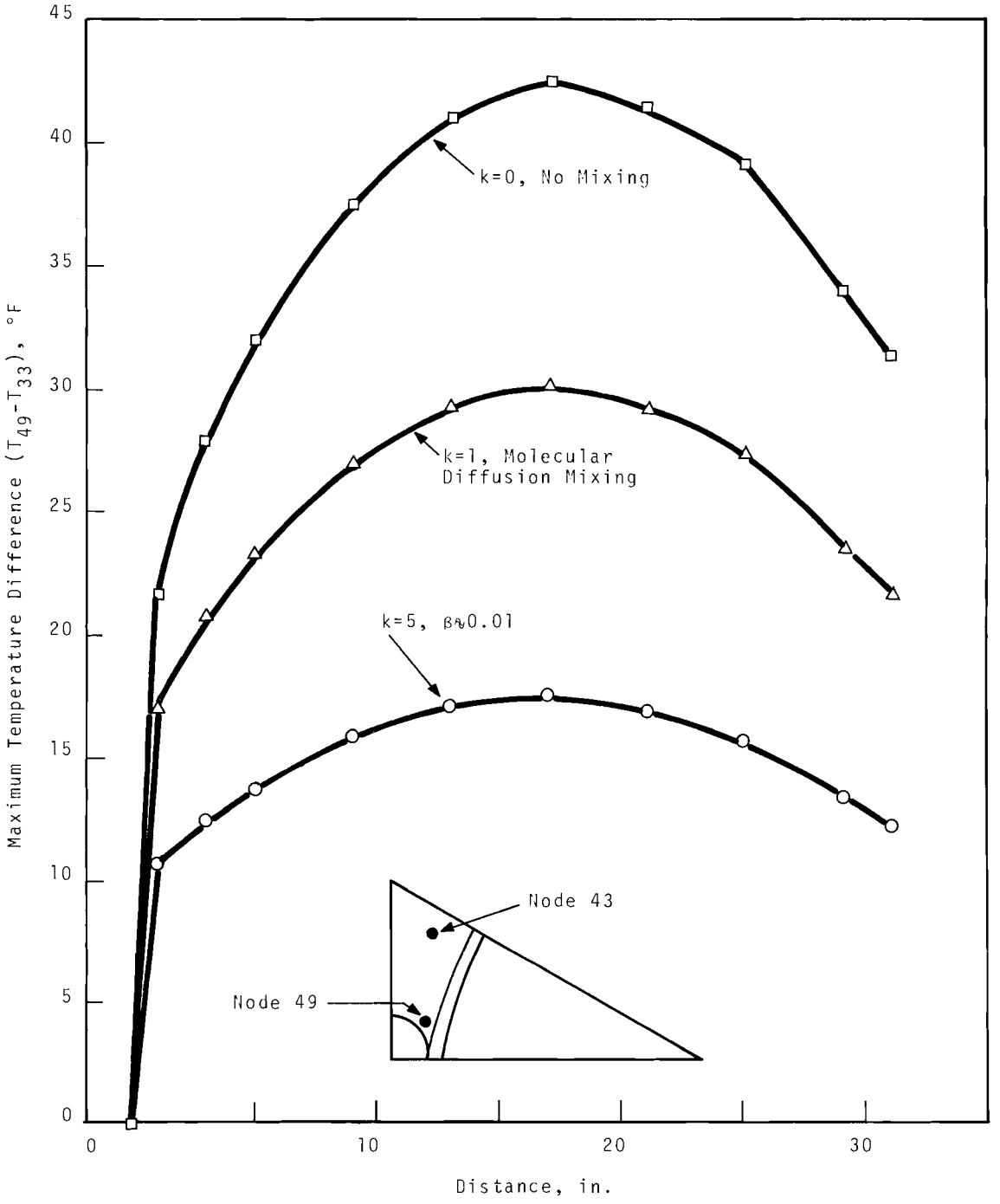

FIGURE 37. Temperature Peaking as Represented by the Maximum Circumferential Temperature Difference of the Coolant as a Function of Axial Distance Along the Fueled Portion of the Hottest Pin with the Wire Wrap Located in the Gap

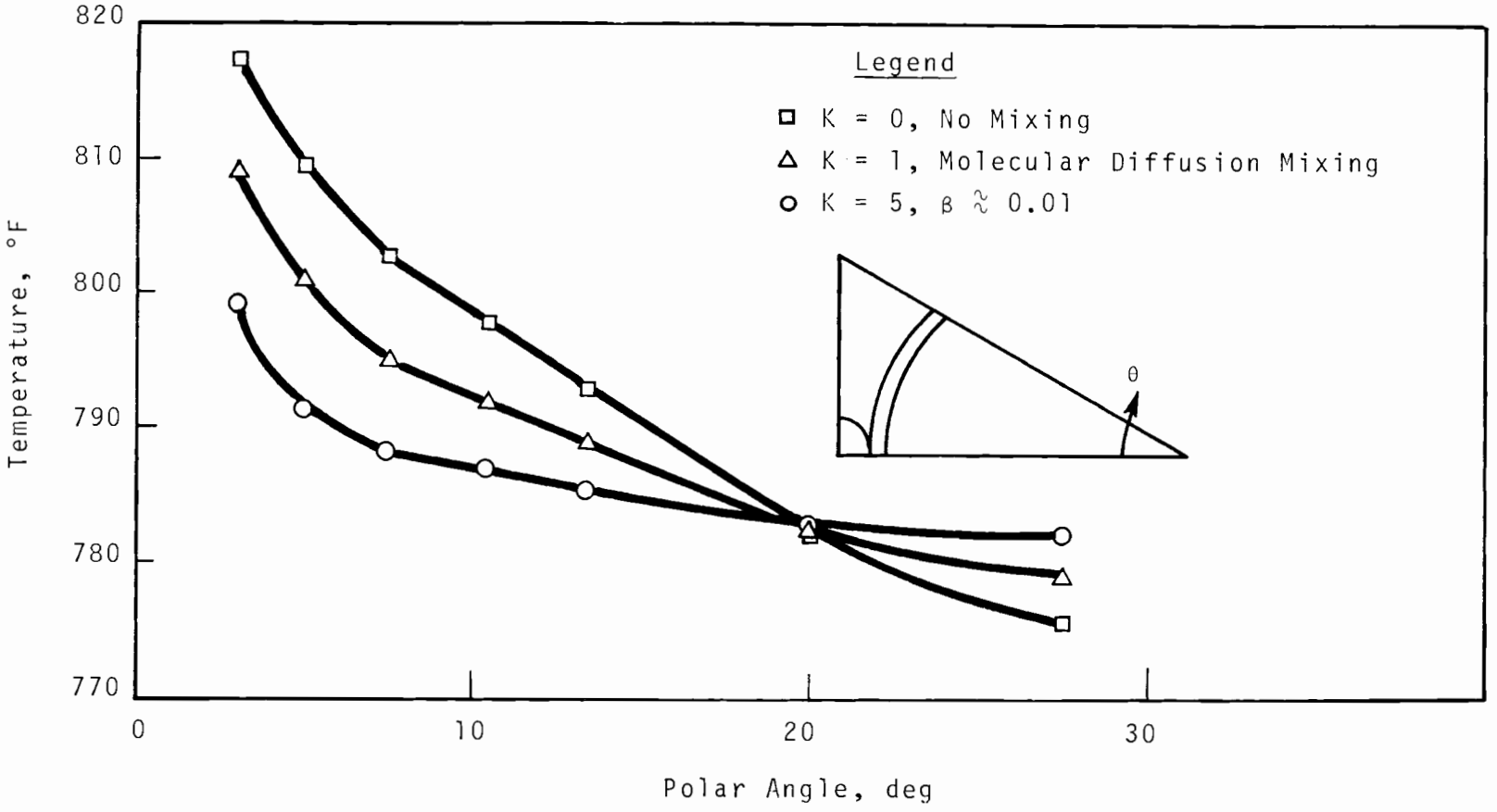

FIGURE 38. *Circumferential Temperature Distribution in the Coolant Near the Center of the Fuel Region for Various Degrees of Mixing with the Wire Wrap Located in the Gap*

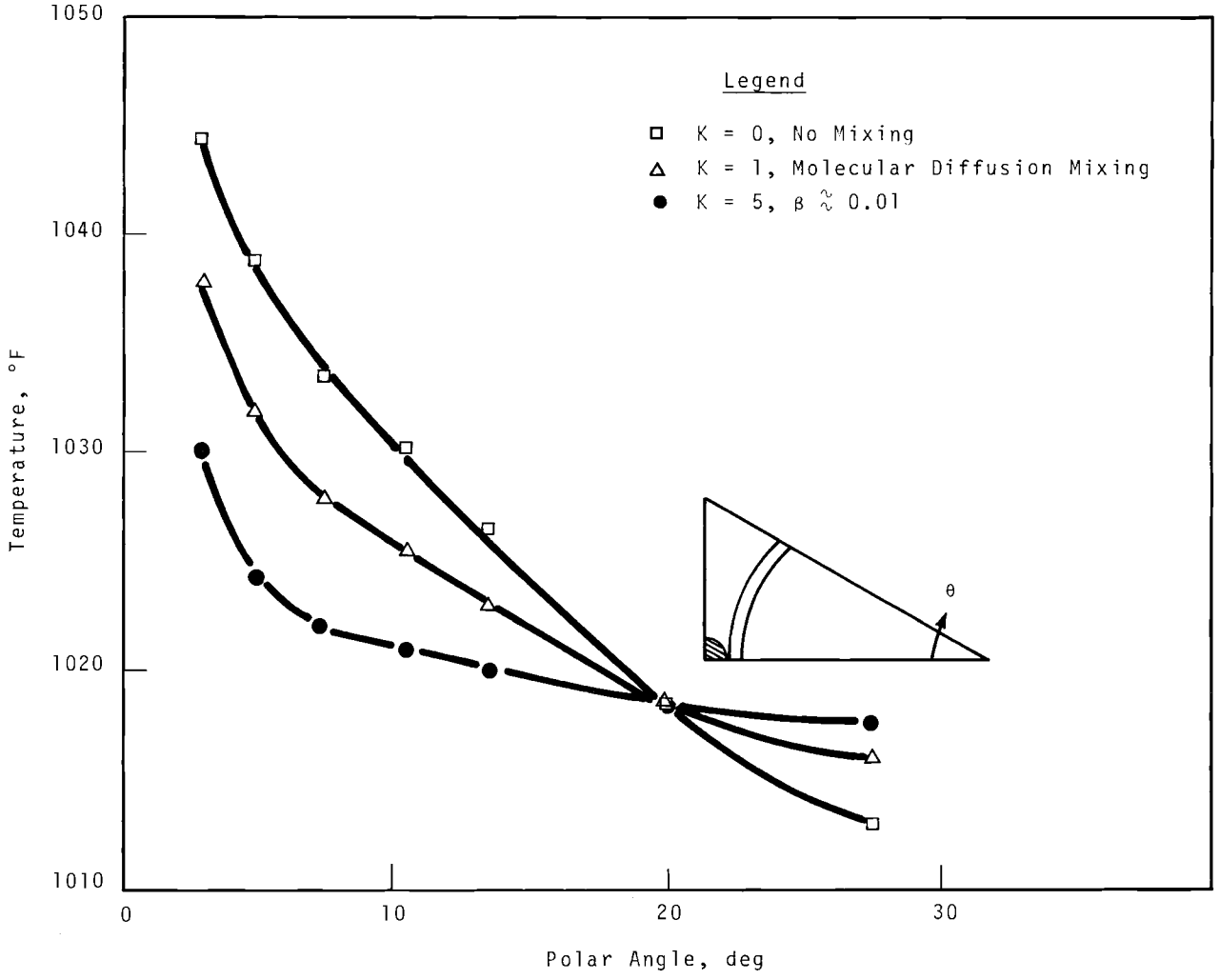

FIGURE 39. Circumferential Temperature Distribution in the Coolant Near the Upper End of the Fuel Region for Various Degrees of Mixing with the Wire Wrap Located in the Gap

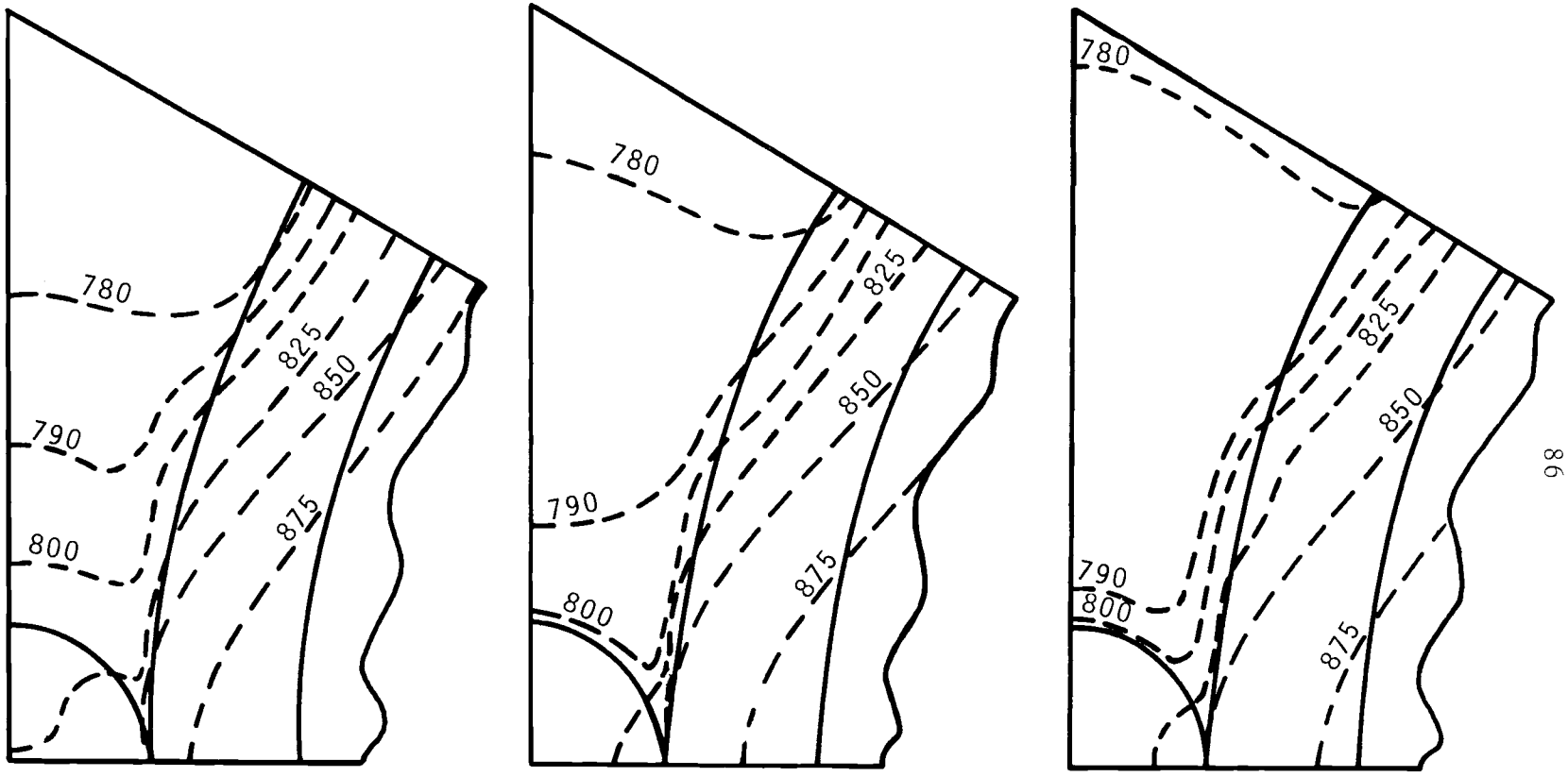

(a) Mixing Constant K = 5

(b) Mixing Constant K = 1

(c) Mixing Constant K = 0

FIGURE 40. Temperature Field Near the Center of the Fuel Region for Various Degrees of Mixing

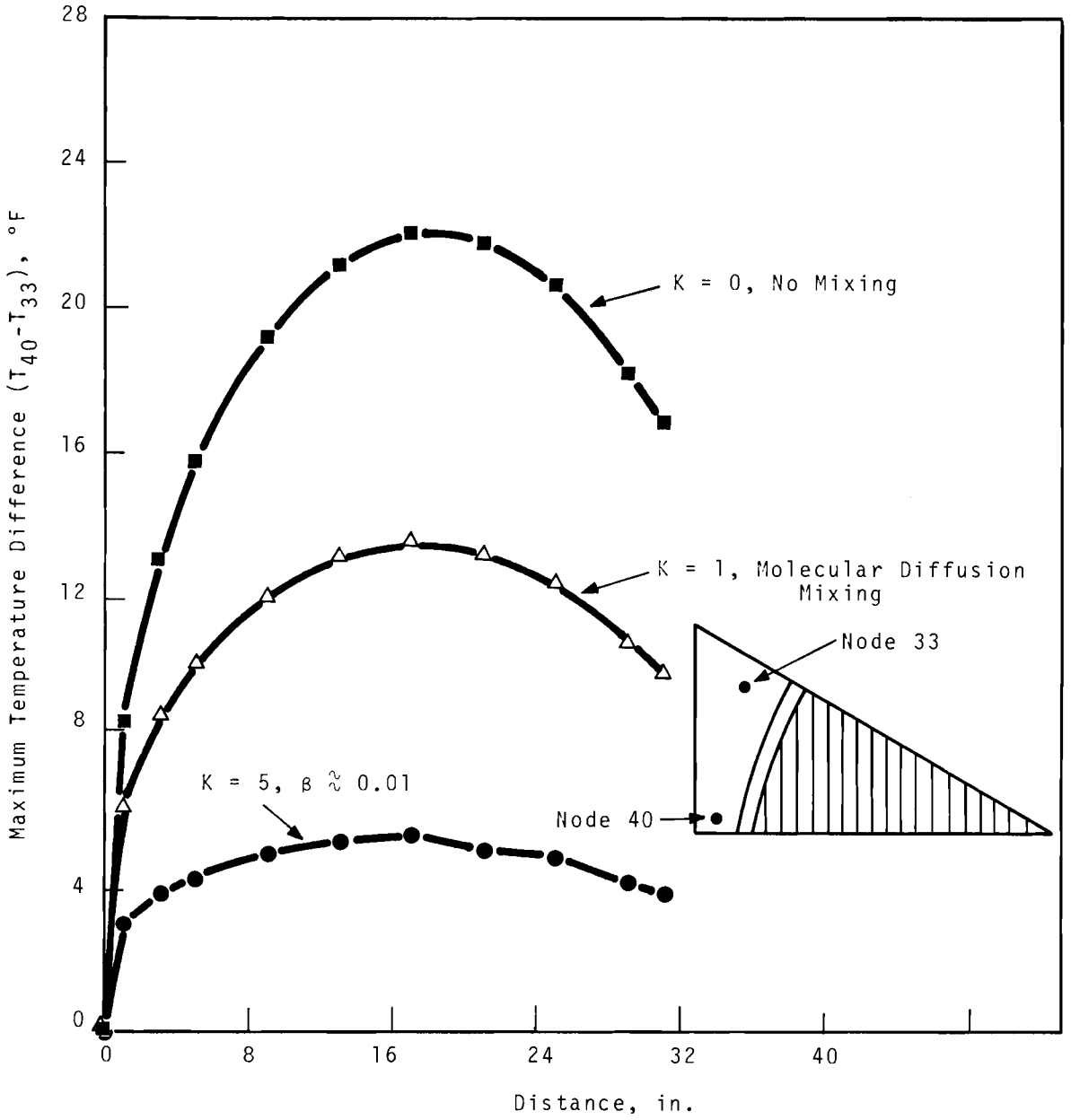

FIGURE 41. Temperature Peaking as Represented by the Maximum Circumferential Temperature Difference of the Coolant as a Function of Axial Distance Along the Fueled Portion of the Hottest Pin With the Wire Wrap Located far from the Domain of this Problem

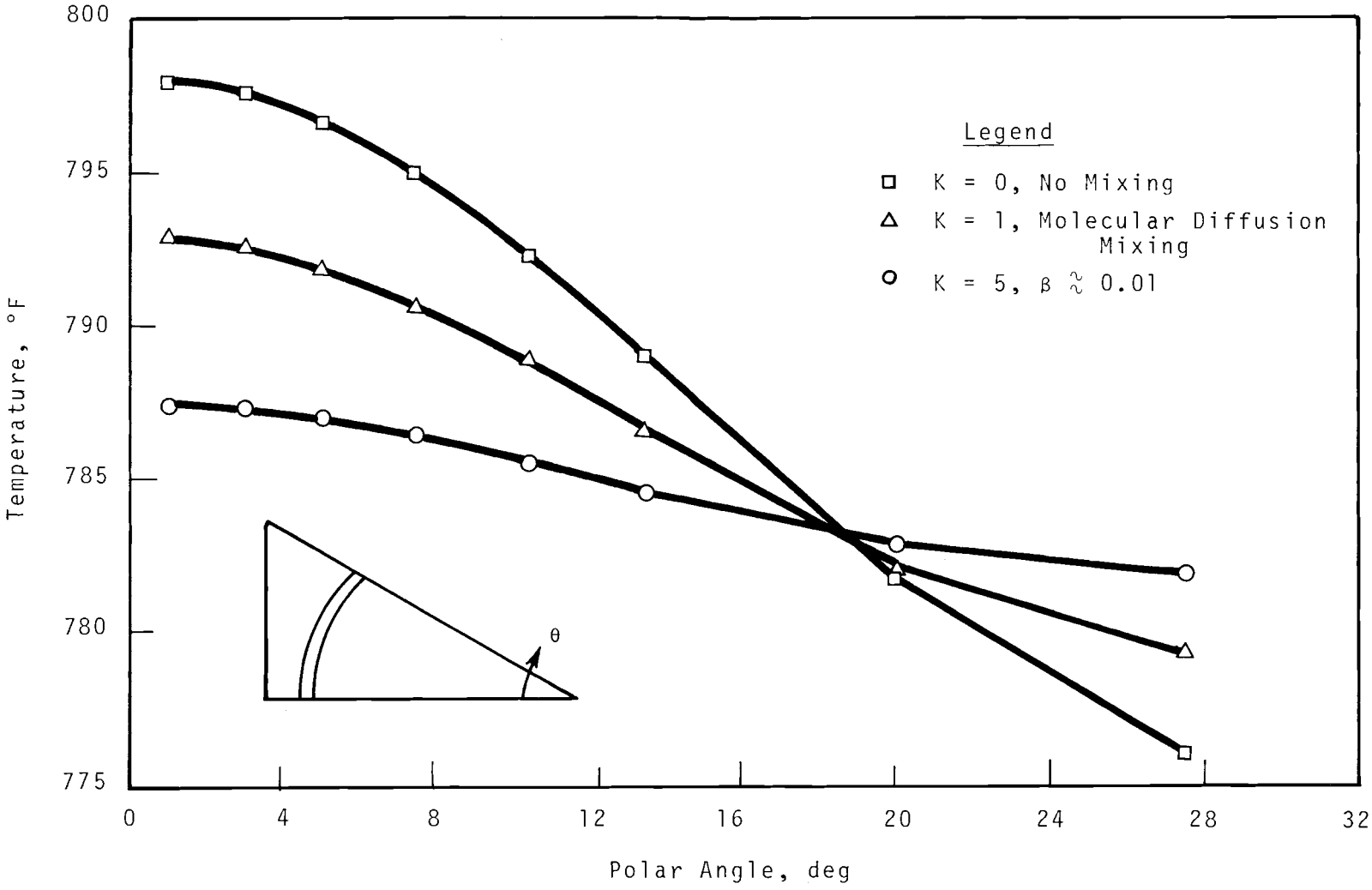

FIGURE 42. Circumferential Temperature Distribution in the Coolant Near the Center of the Fuel Region for Various Degrees of Mixing with the Wire Wrap Located far from the Domain of the Problem

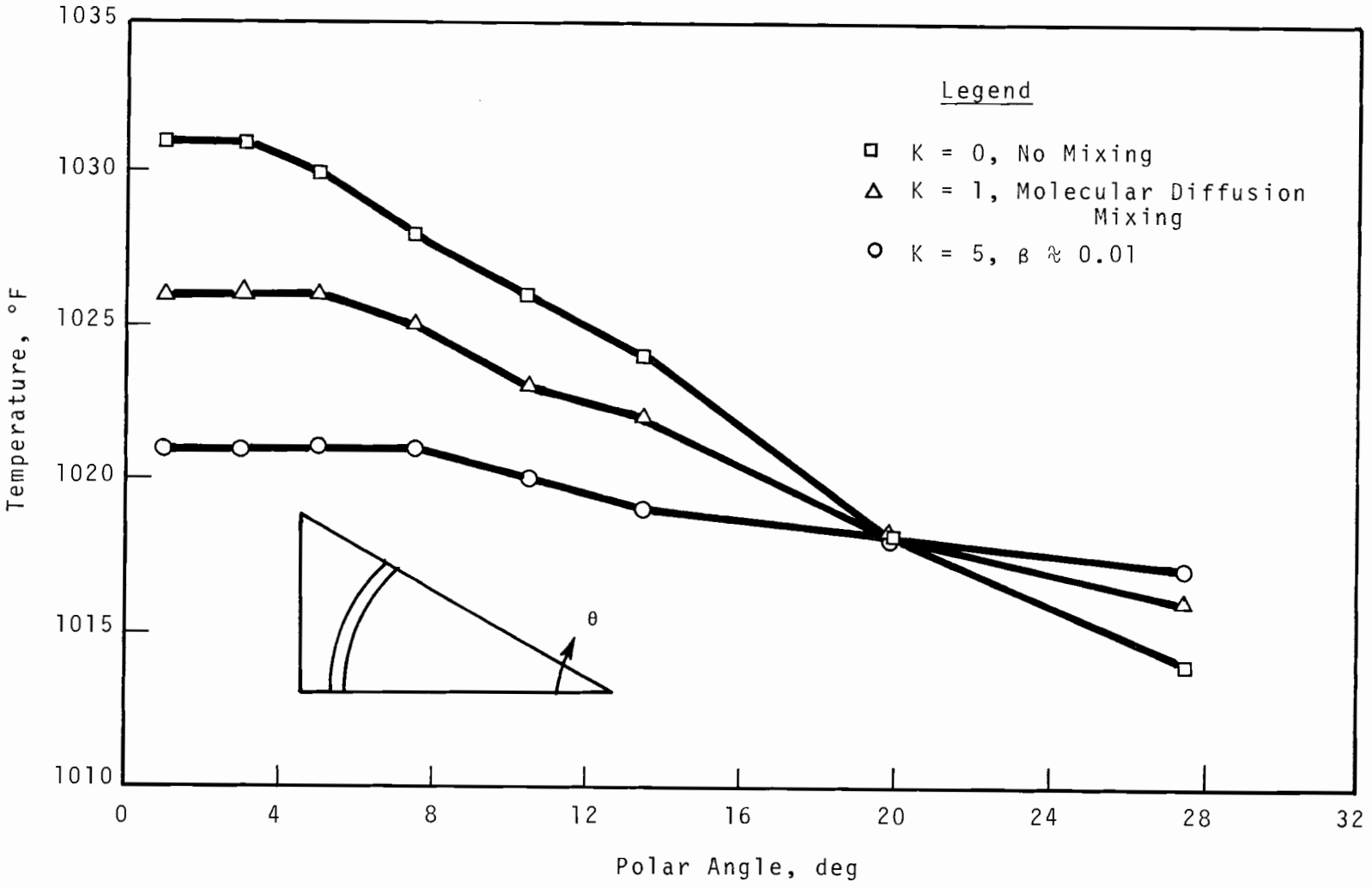

FIGURE 43. Circumferential Temperature Distribution in the Coolant Near the Upper End of the Fuel Region for Various Degrees of Mixing with the Wire Wrap Located far from the Domain of the Problem

The next step in the assembly process is fastening the fuel pins to the grid strips in rows (SK-3-13188). The maximum number of pins in a row is 17 and the minimum is 9. A complete hexagonal array (a 217-pin cluster) contains 17 rows of pins fastened to the grid strips. Individual pins are pinned to a grid strip with 0.050-in. diam pins which are then welded on both sides of the end cap (Figure 44). In order to control the fuel pin-to-fuel pin centerline dimension to 0.280 in., the wire wrap diameter is varied. Tubes from a particular mill run will tend to be of the same diameter. Wire is stocked in 0.0005-in. diam increments between 0.0290 and 0.0310-in. diameters. By adapting the correct wire size to the cladding sizes, the 0.280-in. dimension between rods is controlled.

The 217 pin bundle is assembled by placing the grid strips of the fuel pin rows into the bottom grid cross piece hardware and welding them in place (Figure 45). The bottom grid cross piece hardware is located in a die in the fuel assembly equipment. When all the rows have been welded to the bottom grid hardware, a top grid assembly is placed at the top of the bundle (Figure 46). The slot in the top end cap of each pin rides unfastened around a strip in the top grid. The top grid piece merely holds the pins in a bundle and is, itself, fastened only to the tops of three pins located near the center of the cluster.

All the wire wraps are assembled parallel in the bundle to each other and located at the same point on the diameter of the fuel pins at any given cross section through the bundle (Figure 47).

The final assembly step is to draw the flow duct up over the fuel bundle. When the duct is pulled up to the correct location, three locking bars are pushed through the flow duct and bottom grid assembly and welded at the outside surface of the flow duct.

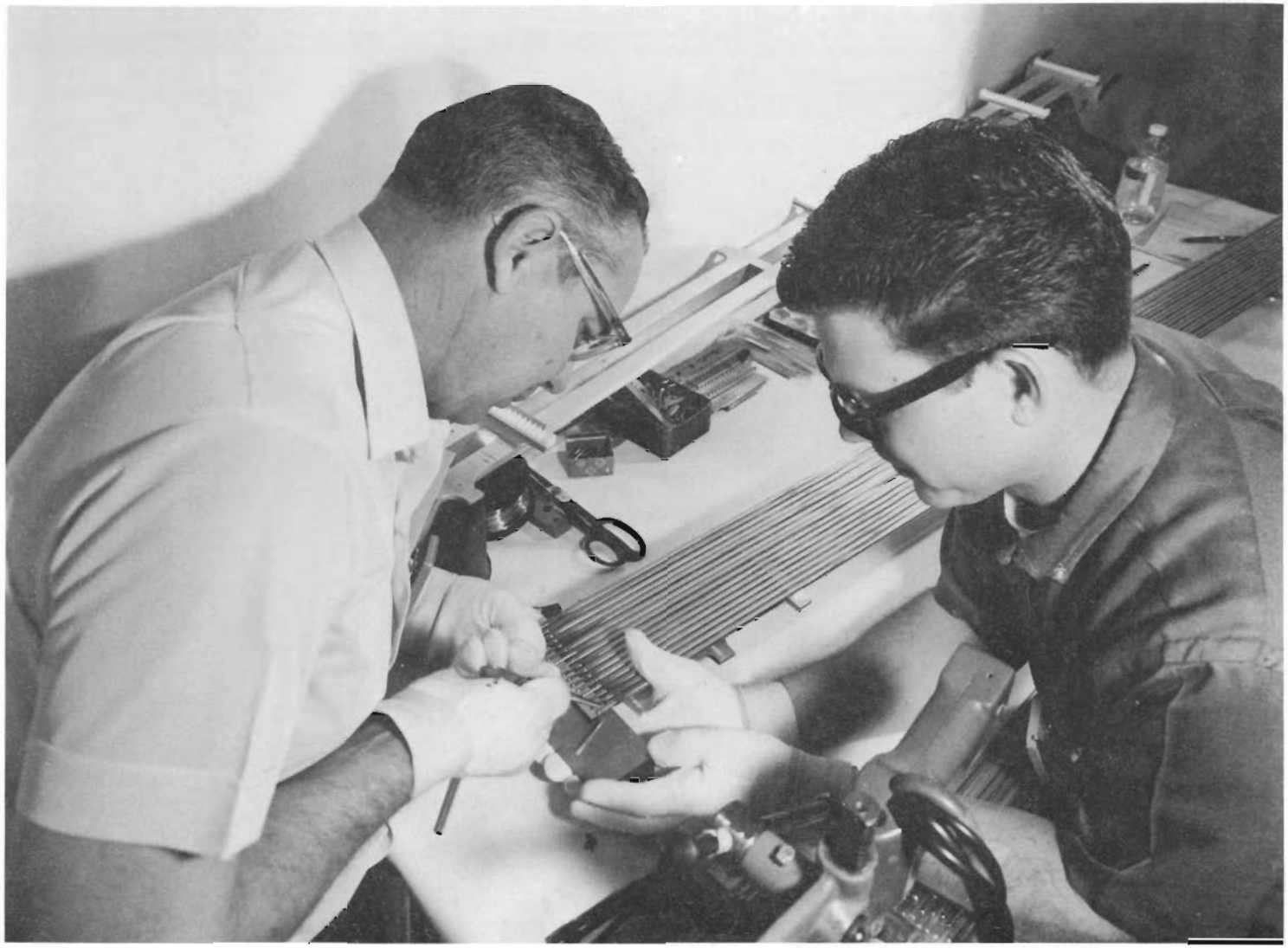

FIGURE 44. Fastening Rows of Fuel Pins to Grid Strips

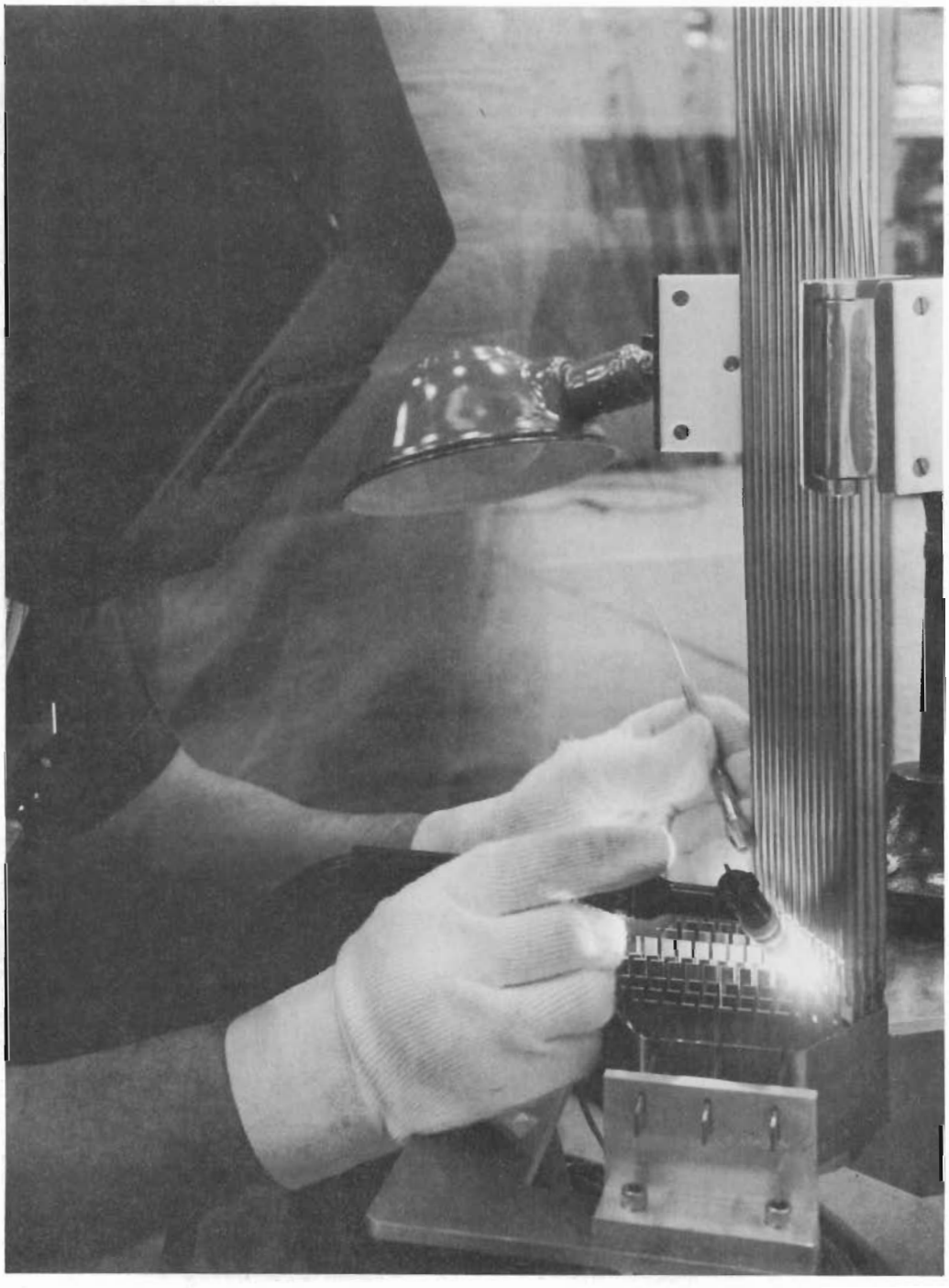

FIGURE 45. Welding Fuel Pin Row Grid Strips in Place

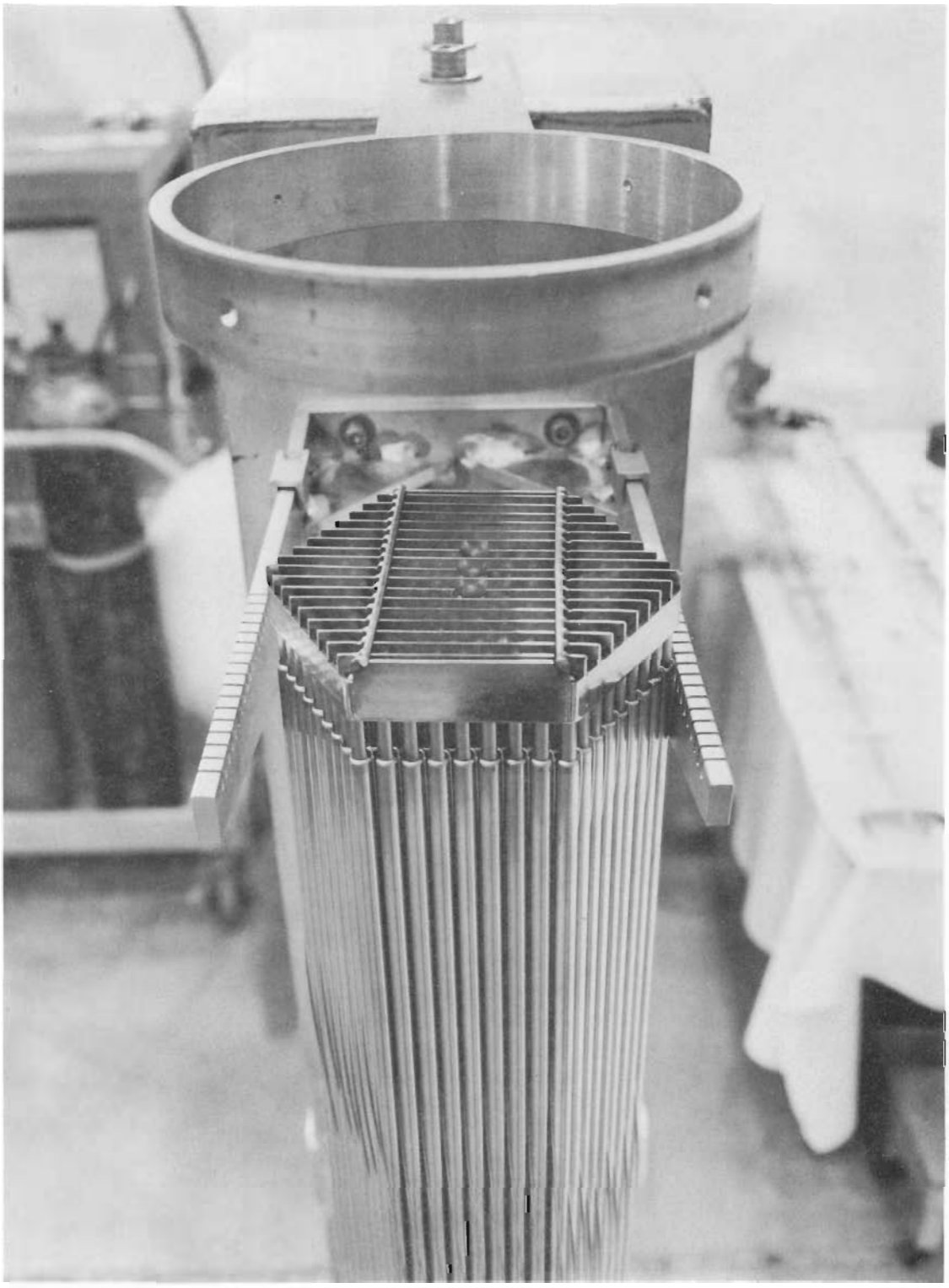

FIGURE 46. Placing Top Grid Assembly on Fuel Pin Bundle

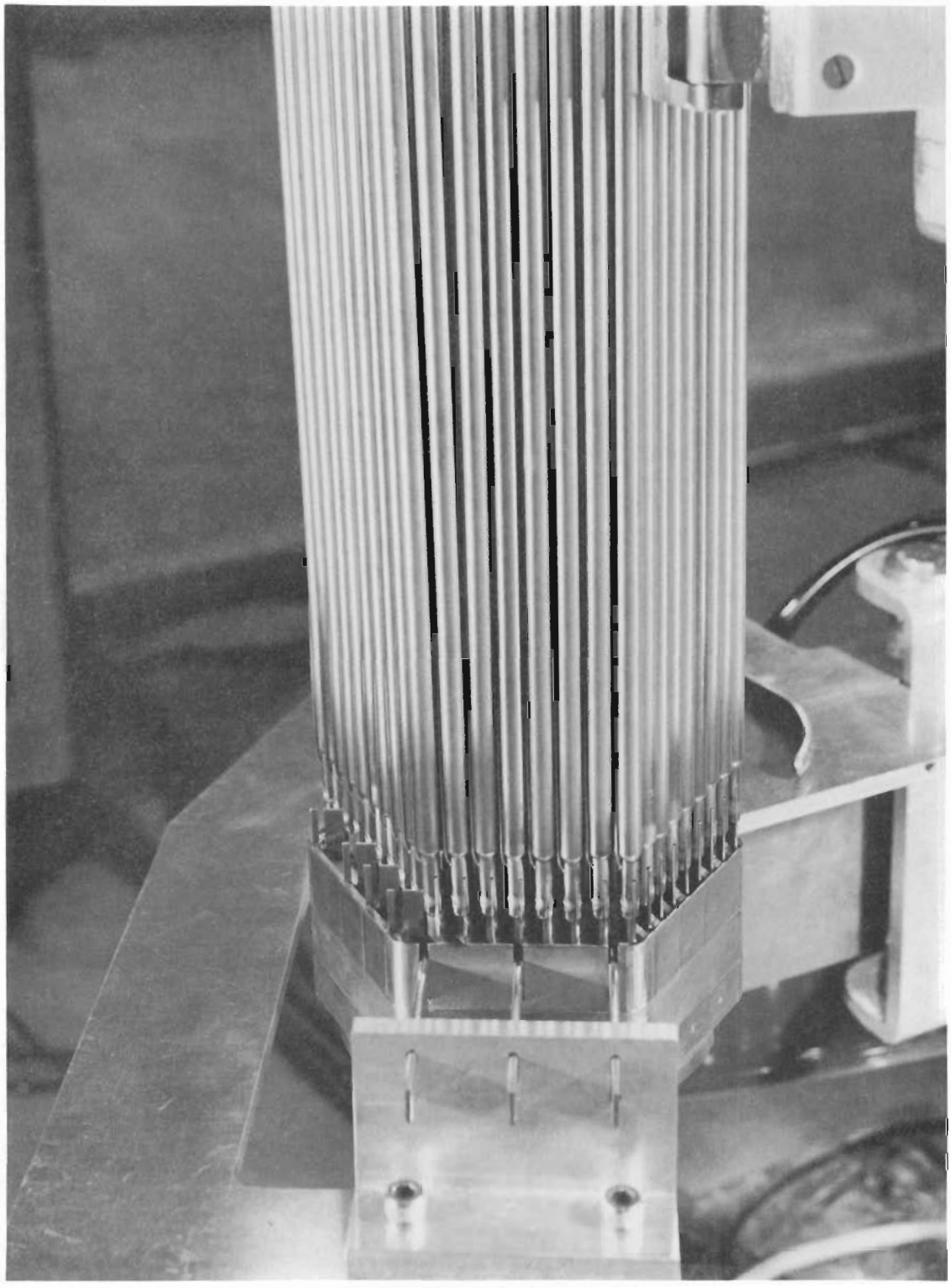

FIGURE 47. View Showing Relative Positions of Wire Wraps

Fuel Bundle Dimensional Tolerances

H. G. Powers

It was considered from an analysis of the fuel pin OD, spacer wire, and flow duct tolerance stack-up that a preferred mode of assembly would be to compensate for any change in lot average clad OD by using a different diameter spacer wire, thereby maintaining a near constant average total (fuel pin/spacer wire) diameter. The total space across flats between outer spacer wire and flow duct wall could be controlled to 0.030 ± 0.010 in., it was concluded, by using this assembly technique based upon the following assumptions:

- Homogeneous lotting (with respect to dimensions) of tubing and wire can be maintained.
- Wire can be stocked in 0.0005-in. average diameter increments.
- The minimum slip fit diametral gap between fuel bundle and flow duct is 0.020 in.
- Standard deviation (inherent)

  σ F Pin OD = 0.0004588

  σ Wire OD = 0.0005/3 = 0.0001667 in.

  σ Flow Duct Inscribed ID = 0.005/3 = 0.001667 in.
- Clad, wire, and duct dimensions vary independently of one another and are normally distributed.

The preceding tolerance is based upon a probability distribution derived in the following manner:

$$\sigma_T^2 = \Sigma\sigma_1^2 + \Sigma\sigma_2^2$$

σ = standard deviation

Subscripts

T - Total diametral

1 - Clad OD

2 - Wire diameter

$$\Sigma\sigma_1^2 = 1\sigma\ (\cos\ 30°)\ (4.588)^2\ 10^{-8} + (4.588)^2\ 10^{-8}$$

$$= (312.71)\ 10^{-8}$$

$$\Sigma\sigma_2^2 = 1\sigma\ (\cos\ 30°)\ (1.667)^2\ 10^{-8} + 2\ (1.667)^2\ 10^{-8}$$

$$= 44.062\ 10^{-8}$$

$$\sigma_T^2 = 356.77\ (10^{-8})$$

$$\sigma_T = 18.89\ 10^{-4} = 0.001889$$

σ_T = the standard deviation of a single pin row

Since spacer wire would be stocked only to the nearest 0.0005 in., the average total diameter (clad OD + wire diam) could, by varying as much as 0.25 mils from the desired nominal, result in an additional variation of 1σ (cos 30°) 0.00025 + 0.0005 = 0.00396 in.

It is assumed that this amount of variation could occur in an uncontrolled manner and therefore must be added to the statistically derived tolerance.

The fuel bundle contains the equivalent of 13 rows of pins. The probability of obtaining one of the thirteen rows beyond a given limit was determined from the Poisson distribution and is given in

$X = X_i + 0.004 + 4.1898$	$Z = \frac{X_i - X}{\sigma T}$	P_1	nP_1	Prob. of Occurrence of 1 or More Rows at Z P^-
4.1947	0.5	0.3085	4.01	0.982
4.1957	1.0	0.1587	2.06	0.870
4.1966	1.5	0.0668	0.868	0.580
4.1976	2.0	0.0228	0.296	0.26
4.1985	2.5	0.0062	0.081	0.077
4.1995	3.0	0.0014	0.018	0.019
	3.5	0.00023	0.003	

Using the foregoing stated standard deviation for the fuel duct, the probability of exceeding given limits was determined from the normal curve.

The probability of a given tolerance between fuel bundle and flow duct is the product of the probabilities of each independent variable exceeding given values. The tolerance distribution shown in Figure 48 shows the probability of occurrence of a space less than 0.020 in. between the fuel duct wall and the outer wire to be less than 1%.

During the early phase of development, the assumptions in this analysis will be tested, and the assembly techniques developed as required to achieve acceptable process capabilities.

FUEL PIN DEFORMATION ANALYSIS

R. J. Jackson

A major aspect of fuel pin - spacer interaction is experienced during fuel pin diametral growth during the fuel lifetime. This subsection presents the pin diametral deformation analysis used for pin - spacer mechanical, hydraulic, and mechanical analysis throughout this report.

Cladding and fuel swelling has been experienced in DFR and in EBR-II. Three published data points from one fuel pin and one published data point from a different fuel pin irradiated in DFR indicate cladding swelling. One interpretation of the available data is illustrated in Figure 49. Obviously, much more data are needed before cladding swelling can be properly included in the fuel pin design. Except for the empirical relationship developed by the U.K. for the solution-treated clad pins in the Mark-I and Mark-IB subassemblies, no fuel-cladding interaction models presently consider cladding swelling. This model relates pin diametral growth to the fuel burnup and the clad temperature by the equation.[27]

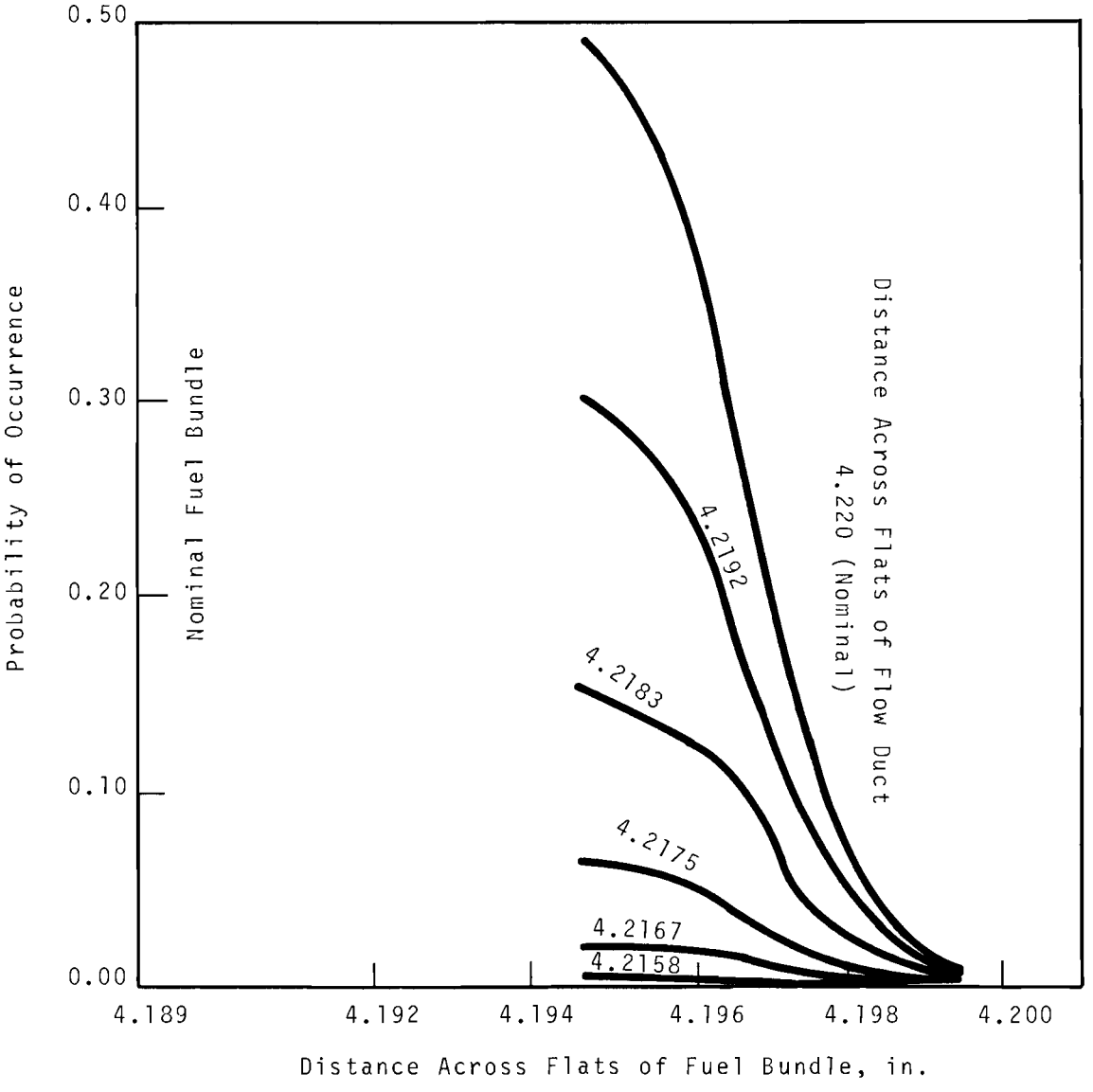

FIGURE 48. Probability Distribution of Tolerances Between Fuel Bundle and Flow Duct

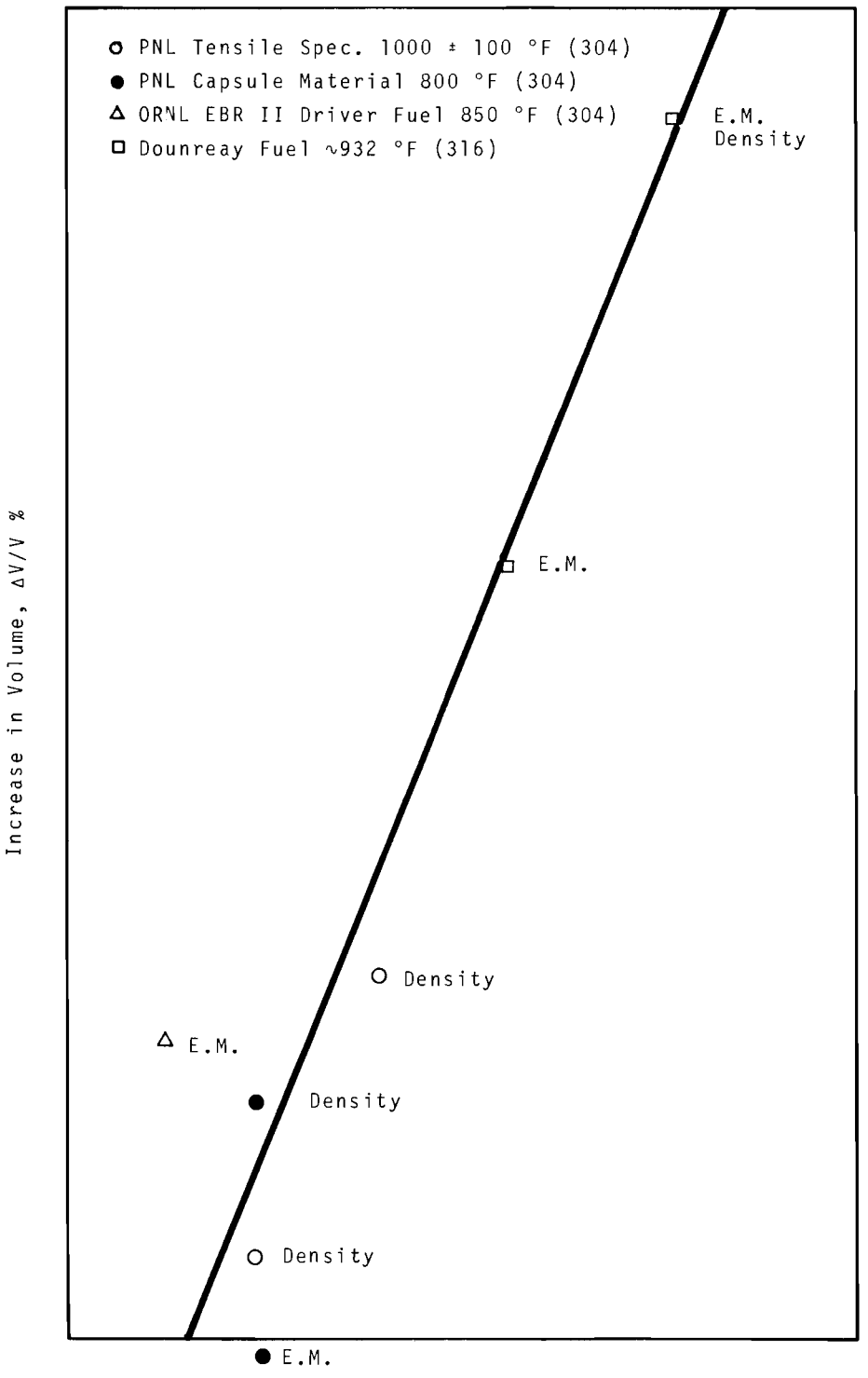

FIGURE 49. Irradiation Swelling of Austenitic Stainless Steel

$$\varepsilon = 8.3 \times 10^{-4} \text{ (Bu) (T)} - 1.51$$

where

$\varepsilon = \Delta D/D$, percent
BU = atom percent burnup of fuel, <8%
T = clad temperature, °C, <650 °C

The equation, because it is empirical, includes the fuel swelling and growth incubation period and the cladding swelling. Thus, it is only directly applicable to the fuel burnup/cladding fluence ratio associated with DFR. The fit of the equation to the data is illustrated in Figure 50.

The equation, when adjusted for the difference in cladding fluence, may give a first-order estimate of FTR fuel pin diametral growth. The validity of this approach is questionable at best. In lieu of any other model, however, the anticipated FTR cladding temperatures and fuel burnups were used to calculate pin diameter increases for the peak and average FTR pins, as shown in Figure 51.

The predicted diametral increase in FTR pins was calculated from

$$\varepsilon_{FTR} = 0.5\ [8.3 \times 10^{-4}(BU)\ (T) - 1.51] + (0.5)(T)\ [8.3 \times 10^{-4}(BU)(T) - 1.51]$$

This assumes that half the DFR diametral growth results from fuel swelling and the remaining growth results from cladding swelling. The cladding swelling contribution is calculated in the second term of the equation which is adjusted for clad fluence by the factor Gamma. Gamma is the ratio of FTR fuel burnup-cladding fluence ratio to the DFR-irradiated mixed-oxide fuel specimen burnup-cladding fluence ratio, and its value was taken as 2.15.

Figure 52 shows the calculated diametral growth for other values of burnup. It was assumed that the average pin could remain in the reactor, by appropriate fuel management techniques, until it reached a peak burnup of 80,000 MWd/tonne.

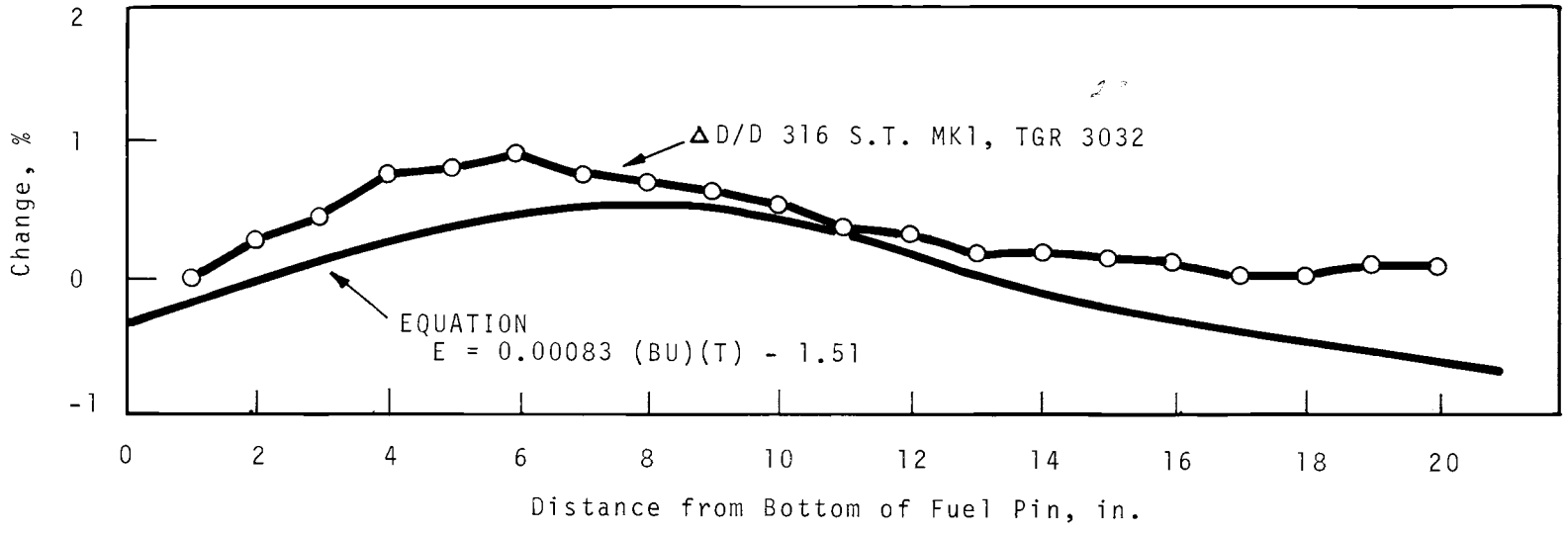

FIGURE 50. Relationship Between Strain Data of MK1 and U.K. Empirical Equations

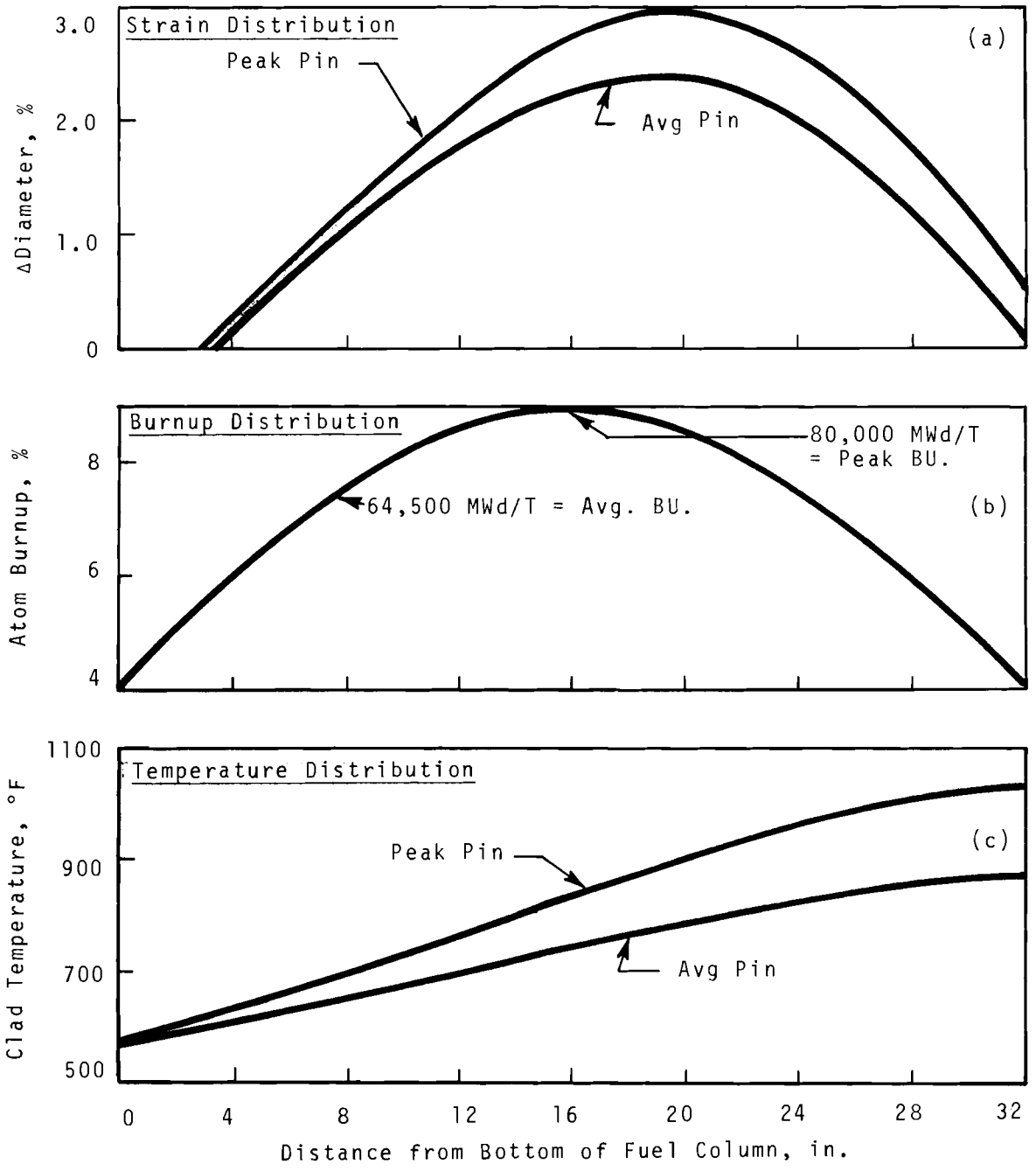

FIGURE 51. FTR Pin Diameter Increase Based Upon Empirical U.K. Relationship Between Temperature and Burnup and then Adjusted for Difference in Clad Fluence

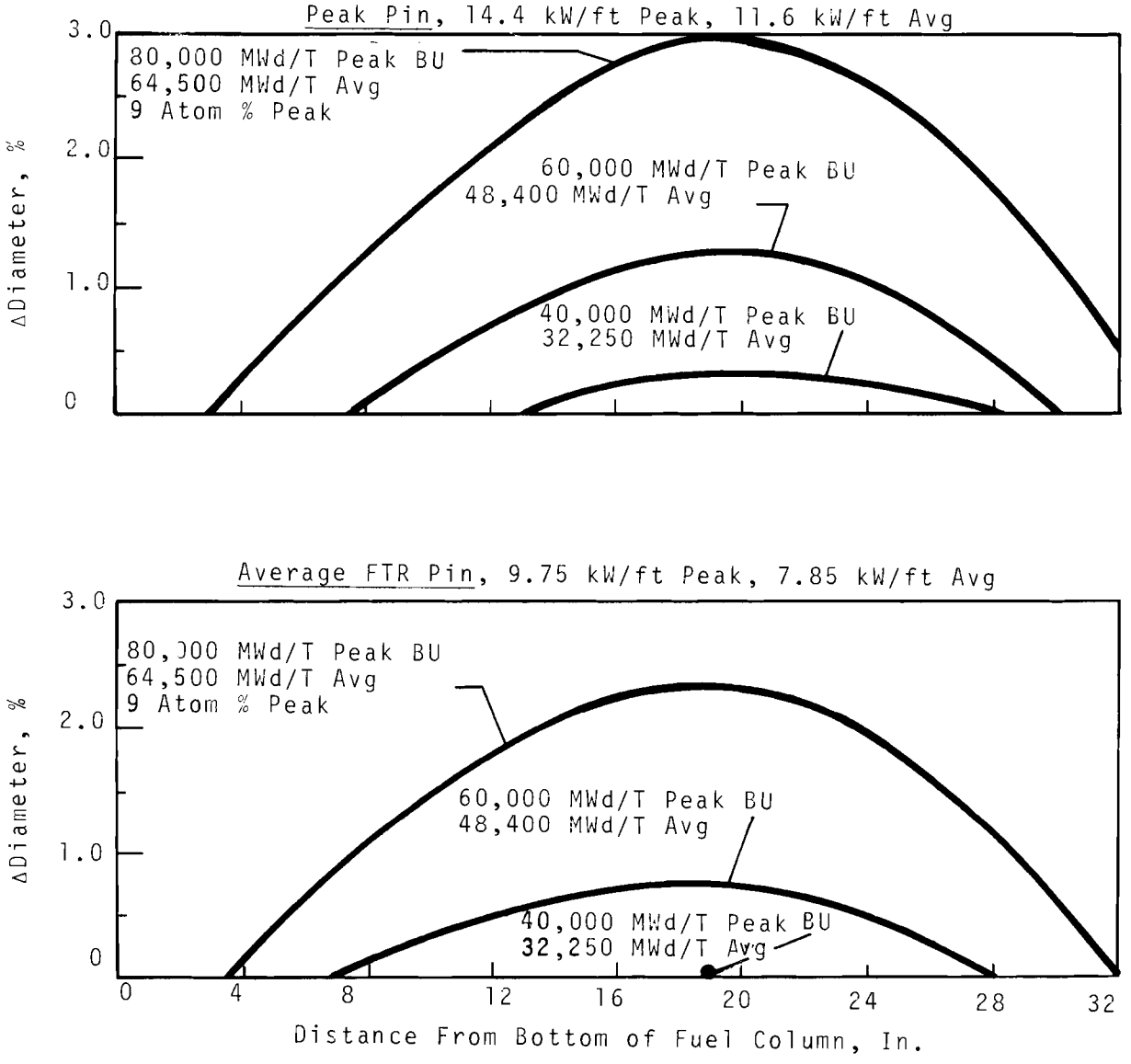

FIGURE 52. FTR Pin Diameter Increases at Various Burnups

Figure 53, a cross-plot of Figure 52, shows the calculated peak diametral growth as a function of burnup.

Comparison of XG06 derived data with the Delta-D plot in Figure 50 shows the numbers generated from two independent sets of data to be at least consistent. The Delta-D, due to cladding swelling in the XG06 specimens, was probably quite small since the peak cladding fluence was only about 3.34×10^{22},[28] and a recent measurement of austenitic stainless steel material irradiated in EBR-II to a fluence of $\sim 2.8 \times 10^{22}$ revealed a density decrease of only 0.37%.[29] On the other hand, the DFR irradiated fuel specimen (from which the equation was derived) received a fluence of about 5.32×10^{22}.[30]

MECHANICAL ANALYSES RELATIVE TO FUEL PIN DEFORMATION

Pin Displacement Analysis

W. E. McClung

A reduction in flow area and pin displacement will occur if the pins in the subassembly grow diametrally to 3%. Three percent is used as the upper limit for swelling as predicted from the U.K. data.

An analysis of a portion of the proposed subassembly in which all pins have the wire wrap in line at the tri-cusp pinch point indicates that a small change in diametral growth can have a large effect on the flow channel area. When the pins have diametrally grown beyond a point where there is continuous contact along a whole row, the pins displace into the coolant channel. It was decided to consider a model with the pins moving in the manner shown in Figure 54. The length of the center two rows, Row D, Row 1, will differ slightly due to the rounding of the ends in Row D (see Figure 55).

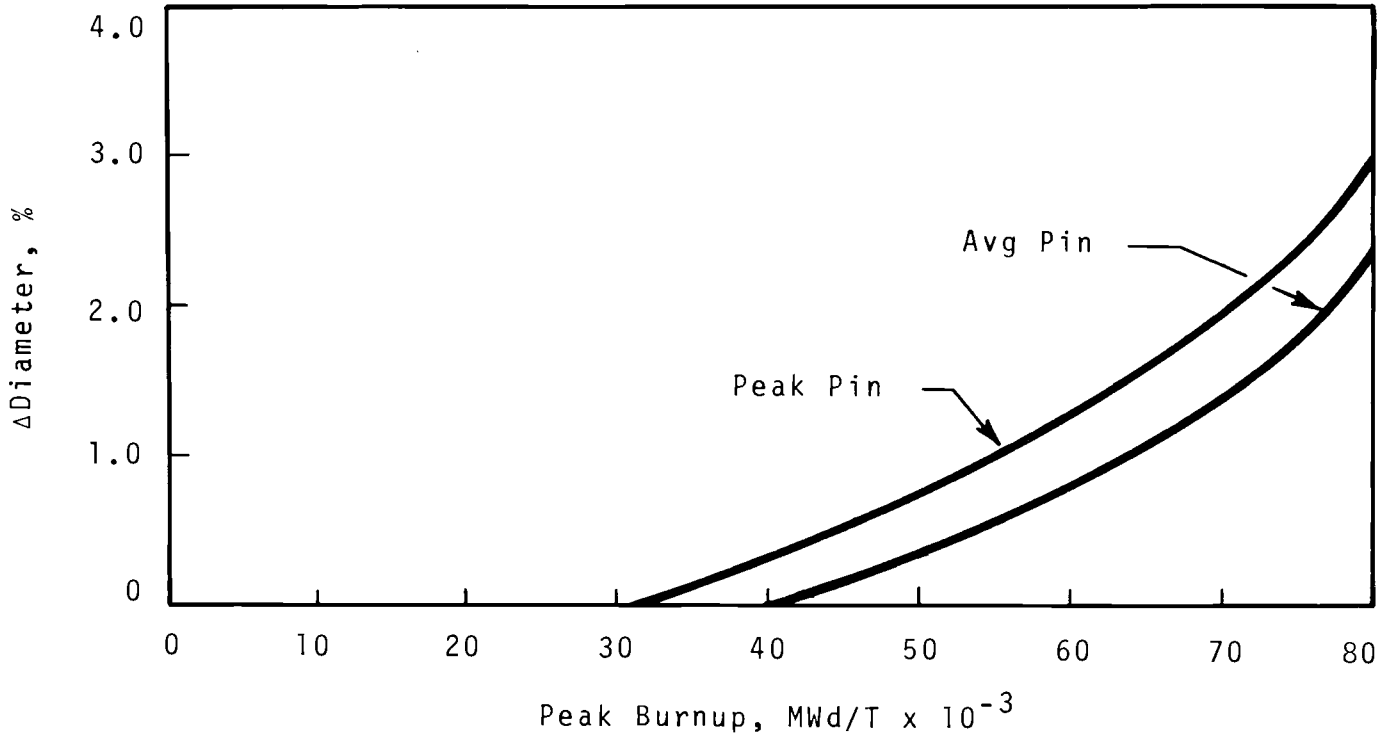

FIGURE 53. Peak Diametral Increase in FTR Fuel Pins Based Upon Empirical U.K. Relationship Adjusted for Difference in Clad Fluence

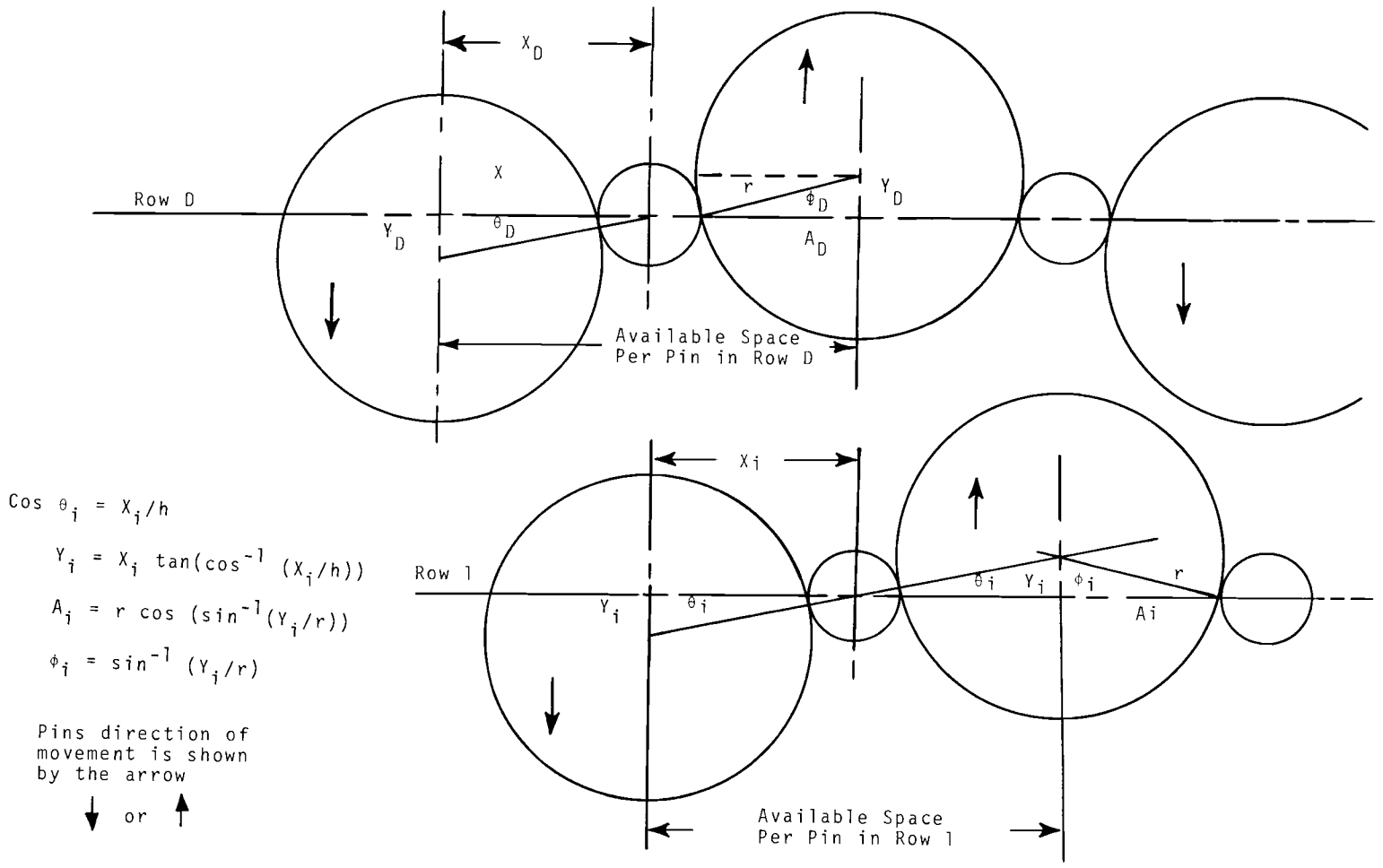

FIGURE 54. Fuel Pin Movement in Row Model

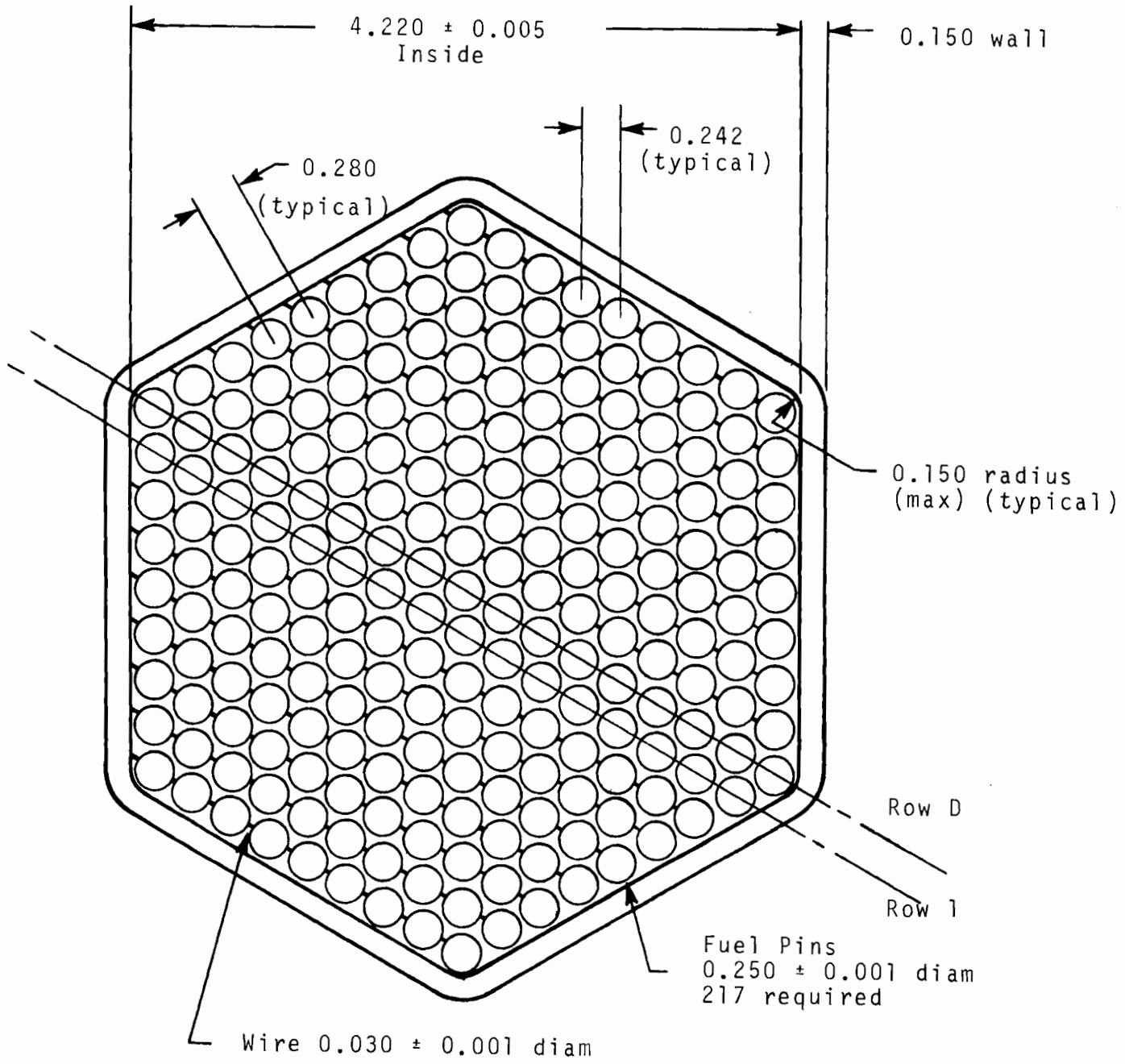

FIGURE 55. Representation of Pin Row Length Differences

The lateral displacement or offset was determined by using the following equation.

$$\text{Cos } \theta_i = \frac{x_i}{h}$$

$$y_i = x_i \tan\left(\text{Cos}^{-1} \frac{x_i}{h}\right) \quad : \text{ Lateral displacement of a pin}$$

$$\phi_i = \sin^{-1} \frac{y_1}{r} \quad : \text{ Angle used to determine the the area of the pin remaining in the region under discussion.}$$

At this point, it became necessary to find the portion of each pin still remaining in the flow channel during lateral movement of the pin. The areas were then summed and subtracted from the area of the trapezoid as follows:

$$\text{Flow channel area} = \text{area of trapezoid} - \left\{9\left[\text{pin area} - \frac{r^2}{2}\left((180 - 2\phi_D)\, 0.01745 - \sin 2\phi_D\right)\right] + 8\left[\frac{r^2}{2}\left((180 - 2\phi_D)\, 0.01745 - \sin 2\phi_D\right)\right] + 8\left[\text{pin area} - \frac{r^2}{2}\left((180 - 2\phi_1)\, 0.01745 - \sin 2\phi_1\right)\right] + 8\left[\frac{r^2}{2}\left((180 - 2\phi_1)\, 0.01745 - \sin 2\phi_1\right)\right] + \frac{33}{2}\,(\text{wire wrap area})\right\} .$$

ϕ_D = angular displacement of the pins in row D

ϕ_1 = angular displacement of the pins in row 1

$\phi_D \neq \phi_1$

Sample Calculation for a 2% Diametral Growth

	New Pin Diameter	$\theta_i = \text{Cos}^{-1} \frac{x_i}{h}$	$y_i = x_i (\text{Tan } \theta_D)$	$\theta_i = \sin^{-1} \frac{y_i}{h}$	$180 - 2\phi_i$
Row D	0.255	$\text{Cos}^{-1} \frac{0.14218}{0.1425}$ $\theta_D = 3°49'$	$0.14218 \text{ Tan } \theta_D$ $= 0.009485$	$\sin^{-1} \frac{0.009485}{0.1425}$ $\theta_D = 4°16'$	$180 - 8°32'$ $= 171°28'$
Row 1	0.255	$\text{Cos}^{-1} \frac{0.1429}{0.1425}$ No displacement because pin + wire does not fill the available space	$0.1429 \text{ Tan } \theta_1$ $= 0$	$\sin^{-1} \frac{0}{0.1425}$ $= 0$	$180 - 0$ $= 180$

Area of trapezoid = 1.14929 in.^{2}

Flow channel area =

$$1.14929 - \Big\{9\left[0.051076 - 0.008128\ (2.99265 - 0.1481)\right] + 8\left[0.008128\ (2.99265 - 0.1481\right] + 8\left[0.051076 - 0.008128 \cdot (3.142)\right] + 8\left[0.008128\ (3.142)\right] + 0.011665\Big\}$$

$$= (1.14929 - 0.011665) - 0.844859$$

$$\simeq 0.292766 \text{ in.}^2$$

Figure 56 shows relative pin movement versus pin diametral growth for rows 1 and D. Figure 57 shows the change in flow area as a function of pin diametral growth.

CONCLUSIONS

That the pins will displace in a uniform spiral pattern has been demonstrated both analytically in this section, and experimentally in the preceding material. Additionally, this performance has been corroborated by data presented in Reference 30. The

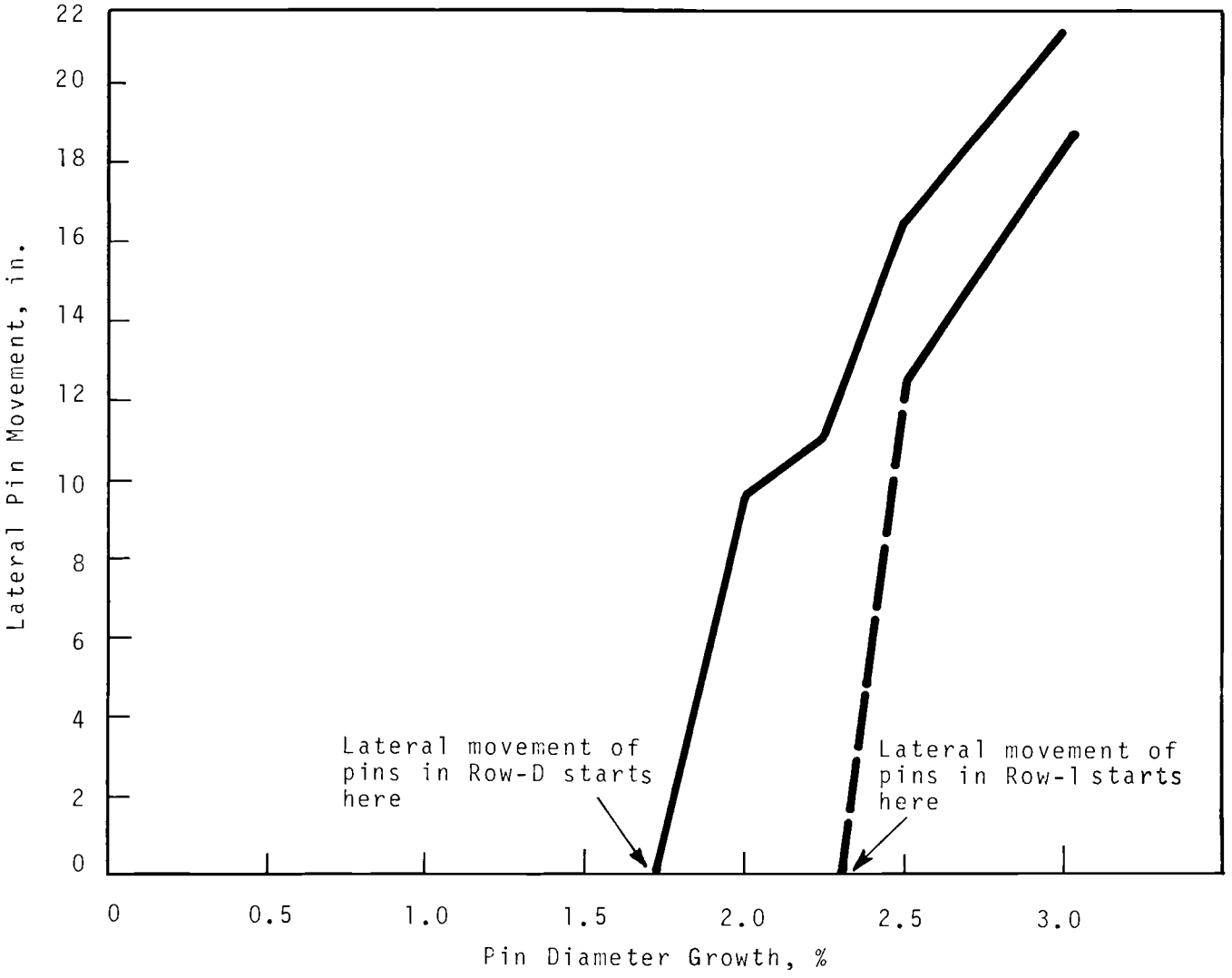

FIGURE 56. Pin Movement Versus Percent Pin Growth Nominally Dimensioned Subassembly

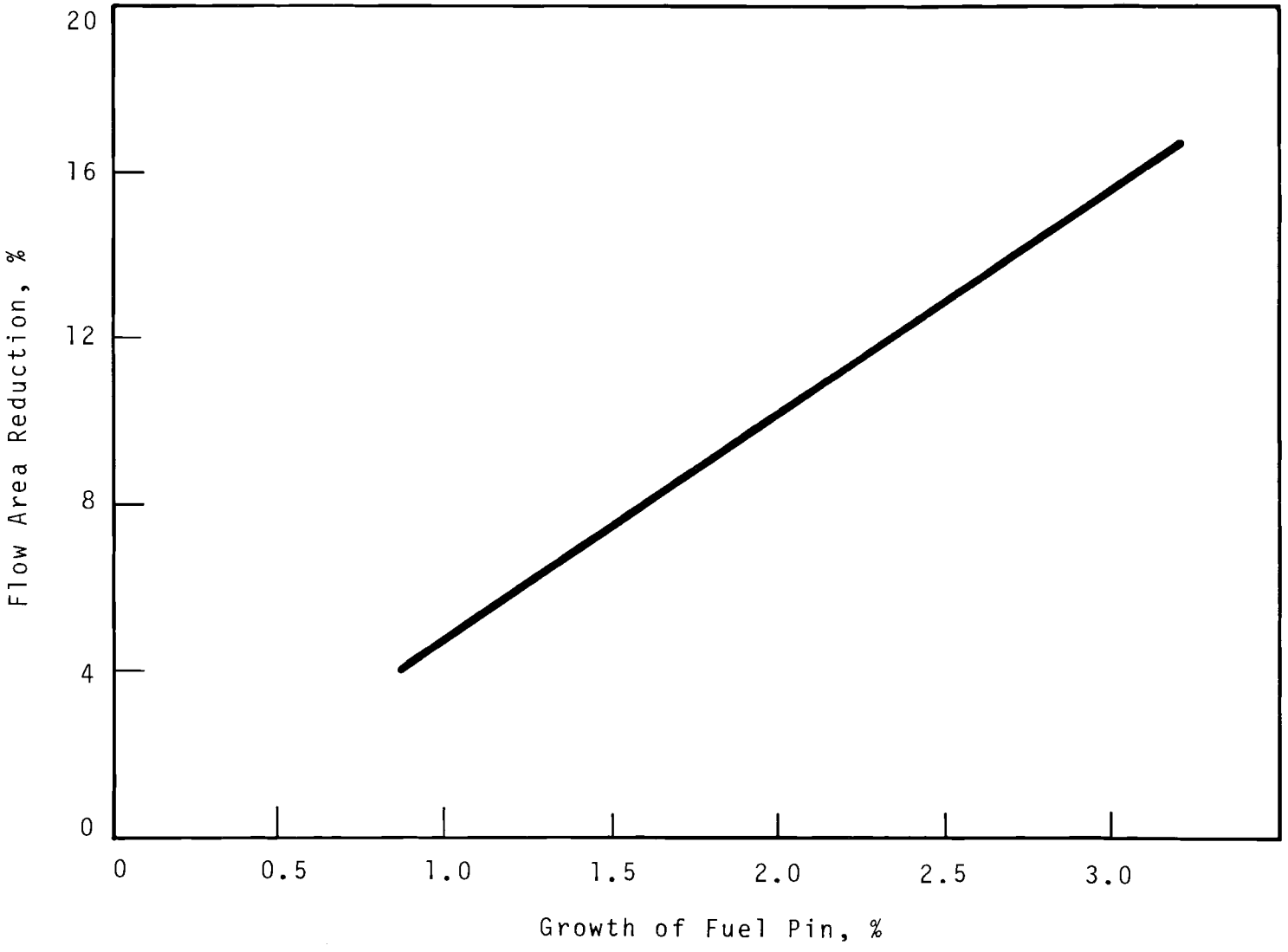

FIGURE 57. Flow Area Reduction Versus Percent Fuel Pin Growth

deformation due to the ML-1 assembly in Reference 30 was attributed to differential thermal expansion, but the net effect is similar to pin diametral growth from the standpoint of the spiral displacement pattern.

Stress Analysis for Pin Displacement Due to Diametral Growth

J. B. Shafer

Calculated values of the diametral increase of the peak burnup FTR fuel pin are repeated from Figure 58a. An investigation of the interaction between the expanded fuel pin and the spiral wire wrap has been made. Assuming that the spacer wires do not swell, the hexagonal flow duct will be filled when each of the 217 fuel pin diameters has increased by 1.075%, based on a 3σ statistical minimum of the assembly clearance. At that amount of strain, the fuel pins will become "cramped" between spacer wires at locations 2 in. apart along the length of the fuel pin. Subsequent fuel pin growth will cause the fuel pin to be displaced in a horizontal plane and to bend into a spiral pattern. The displacement at these cramped locations can be expressed as:

$$Y = \frac{D}{2}\left[2\varepsilon_R(x) + \varepsilon_R^2(x)\right]^{\frac{1}{2}}$$

where: Y = displacement of the fuel pin from the centerline of the row. (see Figure 54)

D = Pin Diameter

ε_R = radial strain as a function of the axial distance along the fuel column, x.

Differentiating the displacement expression twice with respect to x yields an expression directly proportional to the bending stress curve shown in Figure 51a. Note that the calculated bending stresses were based on 30-mil spacer wires and a peak burnup of 80,000 MWd/T, with the profiled radial strain of up to 3%.

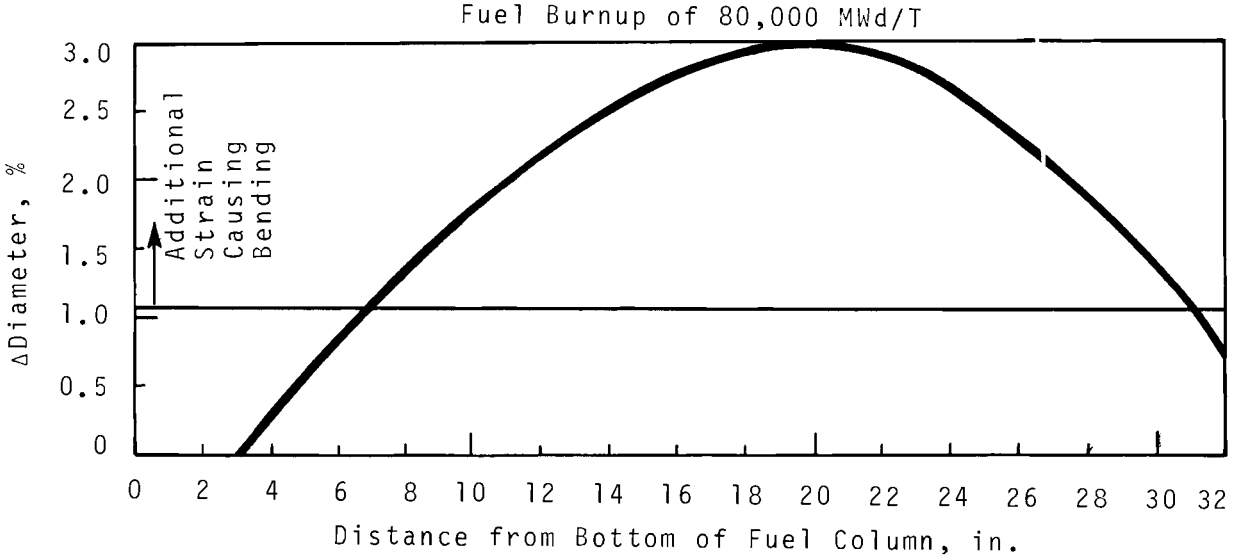

FIGURE 58a. *Calculated Radial Strain Distribution Based on U.K. Empirical Equation for Maximum Fuel Burnup of 80,000 MWd/T*

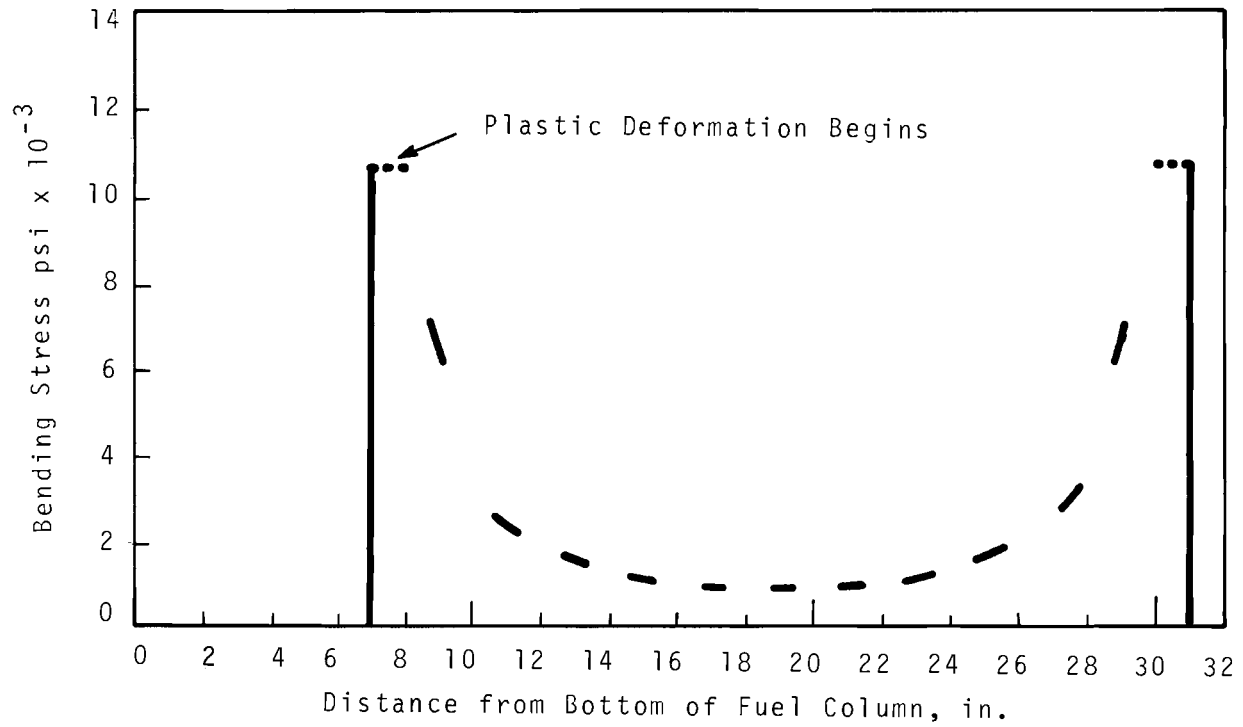

FIGURE 58b. *Calculated Bending Stress at Cramped Locations Only Versus Distance Along Fuel Column*

The bending stress curve (Figure 58b) shows that large elastic stresses may develop at the cramped locations where the radial strain gradient is high with resultant plastic deformation of the cladding. Note that the value of the bending stress is highly dependent upon the shape of the strain distribution curve. The basis for this calculated strain distribution is somewhat uncertain and these bending stresses are believed to be extreme values. Determining the effect of pin displacement on pin life and the coupling of this stress with the thermal, diametral growth, and other stress-producing phenomena will be accomplished in the latter part of FY 1968.

MECHANICAL TESTS FOR FUEL PIN BEHAVIOR DURING PIN DEFORMATION

R. J. Lobsinger

Simulated fuel pin swelling tests were performed to determine the effect of diametral changes on wire-wrapped pins. Burst tests were initially used to evaluate this effect. Empty, wire-wrapped cladding tubes were internally pressurized with gas. Figure 59 shows a typical result of this test. The failed tube burst at a pressure of 10,200 psig. Release of contained gas caused the failure zone to propagate as shown. The second tube was pressurized to 8000 psig for 1 min. In neither case did wire wrap-produced deformation of the tubes occur. Subsequent tests were performed on simulated fuel pins using water-filled compartments in the fueled region. Fuel expansion was simulated by freezing or heating. These tests demonstrated axial shortening of the cladding tubes during unrestrained (unzoned) pressurization. This condition promotes loosening of the wire wrap and tends to obscure interaction effects.

Axial shortening during diametral expansion may be atypical of reactor behavior. Therefore, a zoned-expansion

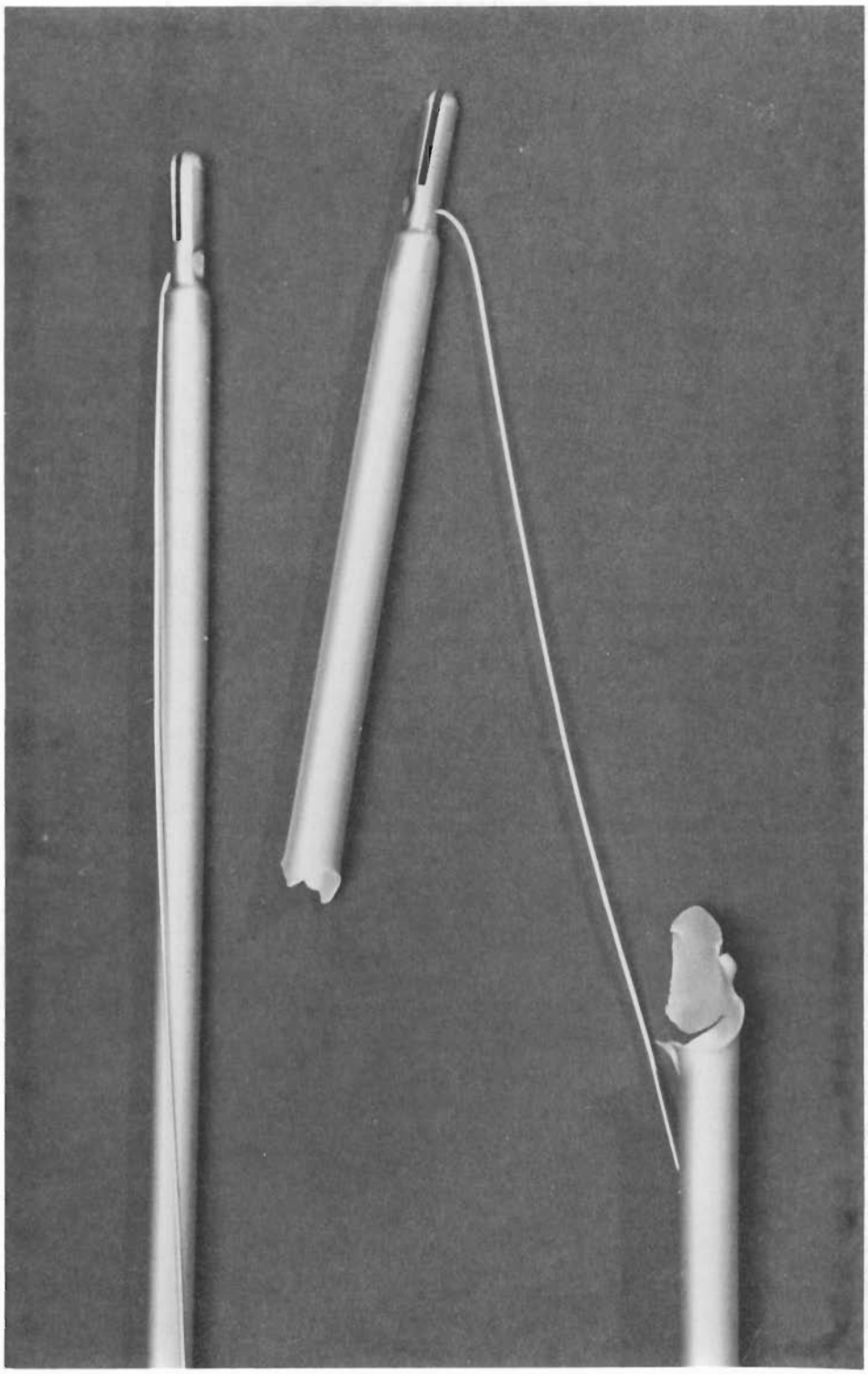

FIGURE 59. Wire-Wrapped Burst Specimens

7-pin subassembly was fabricated using non-fueled 304 SS cladding of 0.250-in. OD by 0.016-in. wall containing a water-filled compartment in the simulated fuel region. The pins were wire-wrapped with 0.030-in. wire, assembled in a prototypic array, and constrained in a tight-fitting cylindrical shroud tube to prevent radial movement. Axial shortening was prevented by constraining the pins axially. The assembly was heated in an electric furnace to 500 °F to permit the water to expand and produce a 2 - 2 1/2% diametral increase. Removal of the tight shroud tube was accomplished with no more difficulty than originally required for assembly.

Examination of the "fuel" pins disclosed no cladding depressions because of wire wrap-to-tube mechanical interaction. As shown in Figure 60, the pin bending occurred following the spiral wire wrap in the swollen region, thus permitting accommodation for the diametral changes and supporting the analytical prediction of this behavior as previously discussed in this section. It is therefore concluded that moderate fuel pin swelling can be accommodated by a contortion of the fuel subassembly. Further tests defining behavior of reduced ductility cladding are planned. Determination of the bending stresses imposed on the cladding will be needed to properly design the fuel pin for reliable operation.

FUEL PIN-SPACER INTERACTION, THERMAL DIFFERENCE EFFECTS

Pin-Wire Differential Thermal Expansion/Stress

J. B. Shafer

An investigation determined spacer wire tensile stress due to the differential thermal expansion between the wire and fuel pin. Calculated values of the average clad temperature, the temperature difference between average clad temperature and spacer wire temperature, and spacer wire tensile stress are shown, respectively, in a, b, and c of Figure 61. These

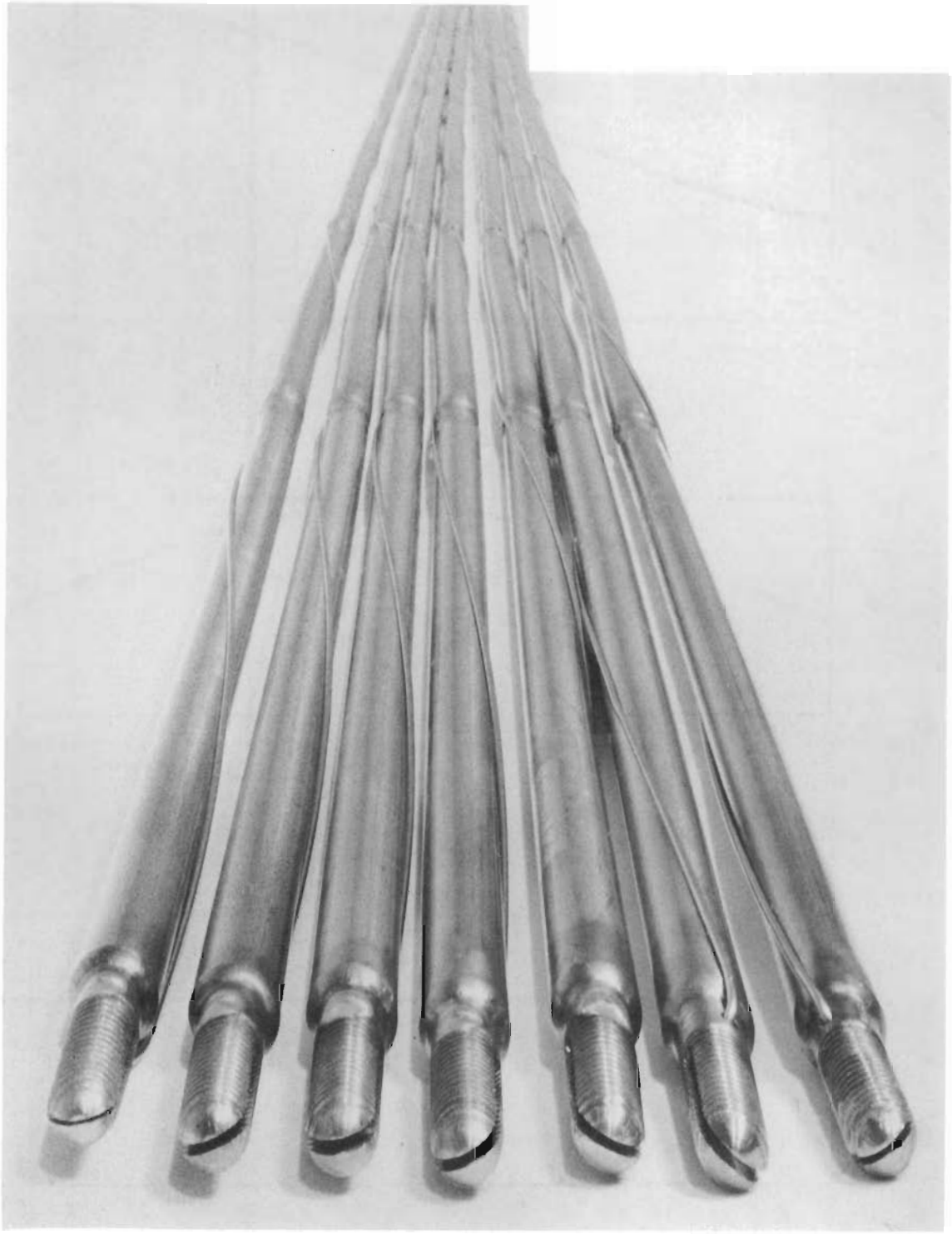

FIGURE 60. Effect of Swelling Upon Pin Bundle Behavior

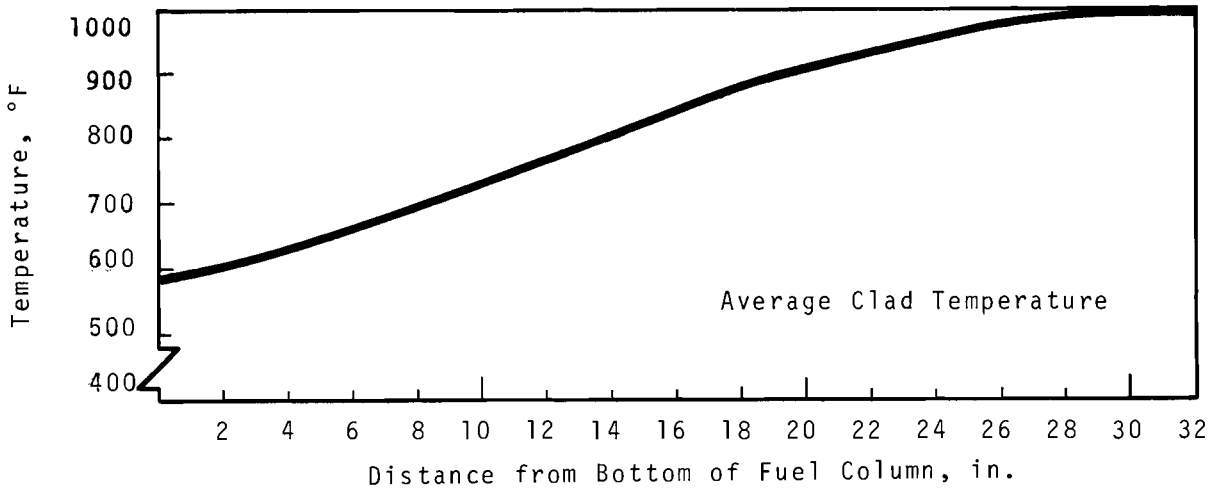

FIGURE 61a. Average Clad Temperature

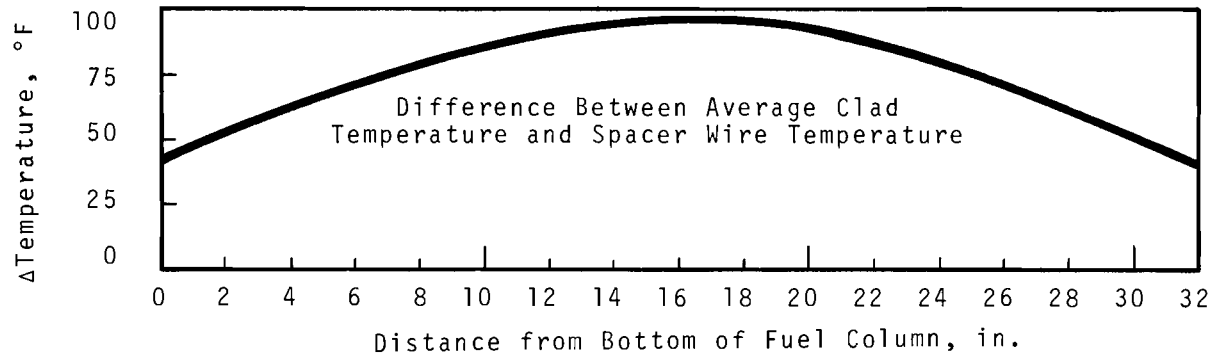

FIGURE 61b. Difference Between Average Clad Temperature and Spacer Wire Temperature

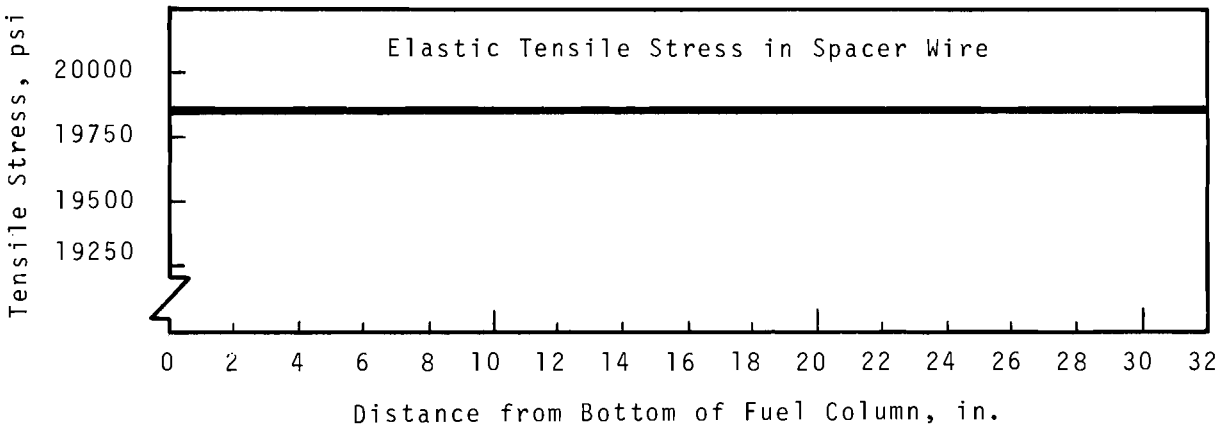

FIGURE 61c. Elastic Tensile Stress in Spacer Wire

calculations are based on the following:

- Both spacer wire and fuel clad behave elastically.
- Spacer wire temperature is equal to the outside temperature of the fuel clad.
- Clad temperature is based on an average of ID and OD temperatures.
- The spacer wire is free to slide over the clad.
- Net elongations of both the wire and clad are the same.

It may be concluded from b and c of Figure 61 that the tensile stress in the spacer wire is largely dependent on the temperature difference between the spacer wire and fuel clad. Further evaluations of pin and spacer behavior and possible operating problems due to the differential temperatures are underway.

Fuel Pin Bowing Due to Flow Induced Temperature Gradients

R. J. Jackson and W. H. Sutherland

An analysis of fuel pin thermal bowing was performed and reported.[31] This work was based upon an estimated maximum temperature difference across a fuel pin of approximately 38 °F. It also assumed fuel pin supports at 6-in. inline intervals. This resulted in a maximum fuel pin deflection of 0.00016 in. and a stress of 4200 psi. Since that work, Kolesar has completed a more rigorous analysis of the temperature gradient across the hottest peripheral fuel pin. These calculations indicate this temperature gradient to be in the range of 140 °F to ∿350 °F. The extremes on this range result from the assumptions regarding dimensional tolerances and mixing values. The deflection and the thermal bowing stress of the fuel pin resulting from these temperature gradients are shown in a and b, respectively, of Figure 62.

The deflections are small and pin touching considerations seem unwarranted. The stress in the extreme case will cause some plastic deformation if these temperature gradients are reached

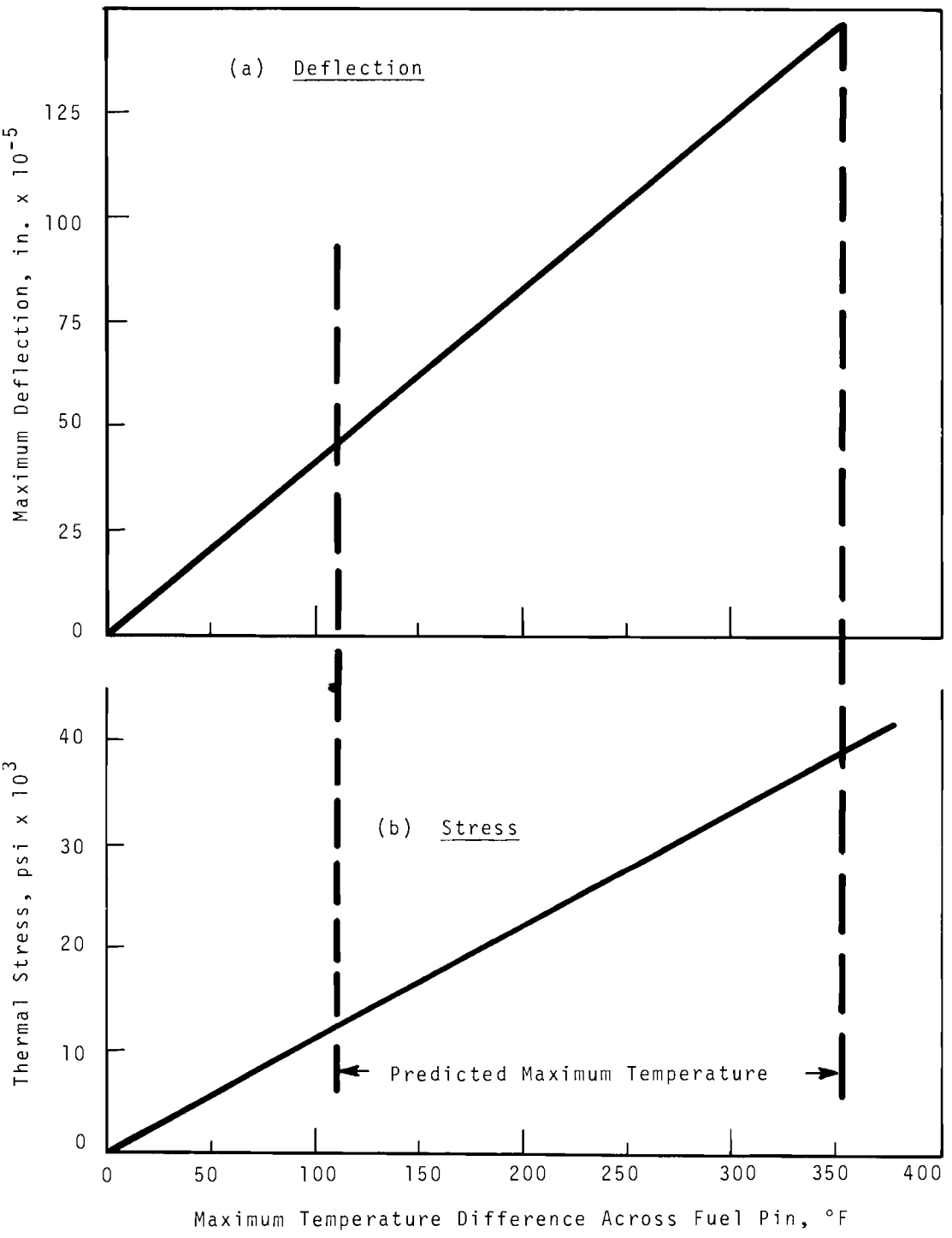

FIGURE 62. Stress and Deflection Based Upon 6 Inch Span of FTR Fuel Pin

early in life. This fuel pin, if irradiated for a sufficient time at low temperature, would experience radiation enhanced yield strength. Thus plastic deformation would be prevented if the subassembly were repositioned at a higher point in the core so as to experience these extreme temperature gradients.

Differential Temperature-Induced Pin Touching

M. T. Jakub and T. J. Bennett

Thermal distortion causing pins to touch is reinforced by the temperature gradient set up across the fuel pin due to the differential coolant flow. Since one side of the fuel pin is significantly hotter than the other side, the temperature difference will cause the pin to bend as in a bimetallic strip.

The temperature difference needed to cause pin touching is predicted by a formula developed in Reference (32):

$$\Delta T = \frac{(\delta \sqrt{3})(OD)}{\alpha_T \quad ab} \quad \frac{1/4 + 1/3\ a/b}{1/9 + 1/8\ a/b}$$

where ΔT = temperature difference in °F

δ = wire wrap thickness

OD = pin outer diameter

α = coefficient of linear expansion

a = half of unsupported length

b = unsupported pin length

Pin touching as a function of ΔT and wrap pitch for a 0.25-in. diam pin with a 30-mil wire wrap is shown in Figure 63. It may be seen from this analysis that the previously described peripheral fuel pin gradients may be sufficient to cause these pins to touch their neighboring internal pins. Further analysis of this problem is continuing.

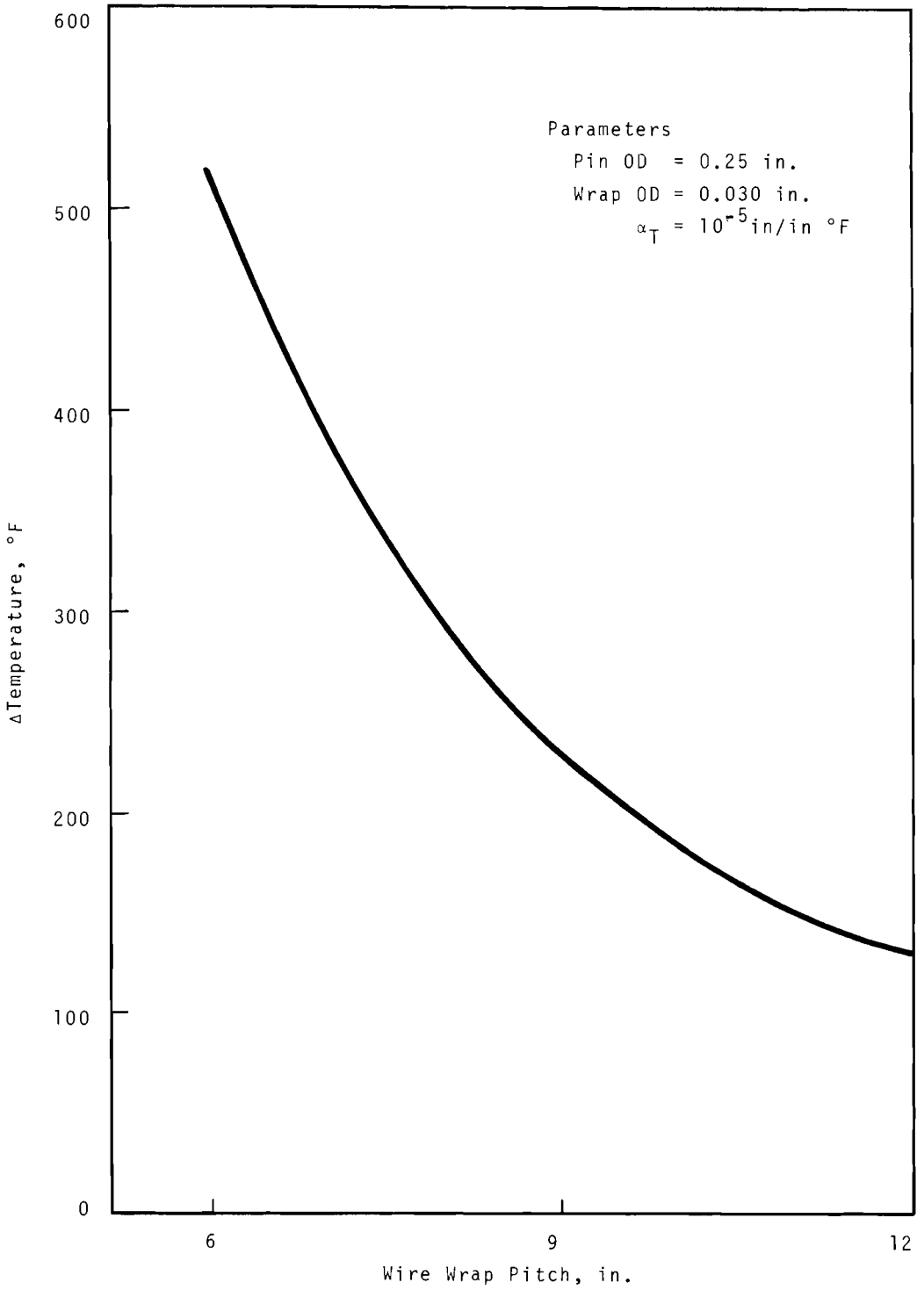

FIGURE 63. Pin Touching ΔT Versus Wire Wrap Pitch

FUEL PIN-SPACER VIBRATION CHARACTERISTICS

M. A. Fischer, G. L. Fox, N. L. Johnson, W. H. Sutherland

Vibration Testing and Analyses

Two pins have been tested, one with and one without the wire wrap. In addition, a solid rod and a thin wall tube were tested and theoretical comparisons were calculated.

Lumped mass models of a solid rod and a fuel pin were set up for a matrix analysis by means of the SAMIS code. Both the rod and fuel pin were unsupported except at the ends. Three sets of end conditions considered for the fuel pin were (1) both ends fixed (F-F), (2) one end fixed and one end pinned (F-P), and (3) both ends pinned (P-P). The analysis indicated that, compared to the solid rod, the fuel pin had shifted nodal points and unequal amplitudes of vibration, with the larger amplitudes at the lighter weight end. Figures 64 and 65 show this for the second and third vibration modes, respectively. Table VI presents a summary of the calculated and test data.

Under (F-F) conditions, odd numbered modes of vibration should require relatively low levels of force and even numbered modes relatively higher levels. Data were obtained in the form of plots of force level versus frequency for a range from 5 to 500 Hz. These data are shown in Figures 66 through 69.

Values for the first modes (fundamentals) may not be exact. The force levels are so low that minor transducer mass effects become proportionately large. Also, the frequencies are approaching the lower limit of the equipment. Above the first mode, the experimental data for all items show pairs of frequencies very close together. For the rod and the tube, these pairs occur between theoretical values. The apparent discrepancy between their experimental and theoretical frequencies can be reconciled as follows: First, a general dynamics theorem states that when an additional constraint is applied to a system, its natural

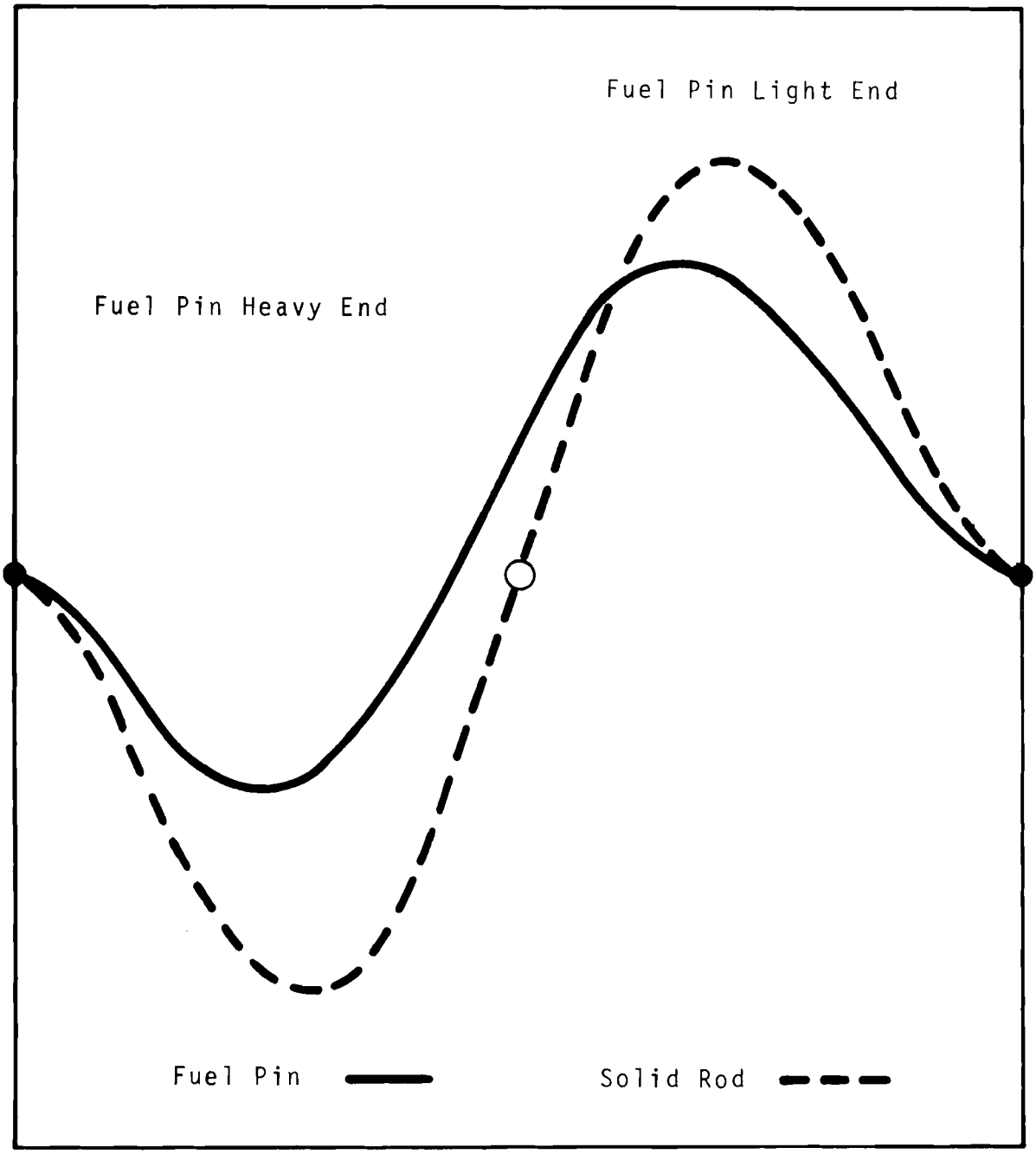

FIGURE 64. Second Vibration Mode Comparison

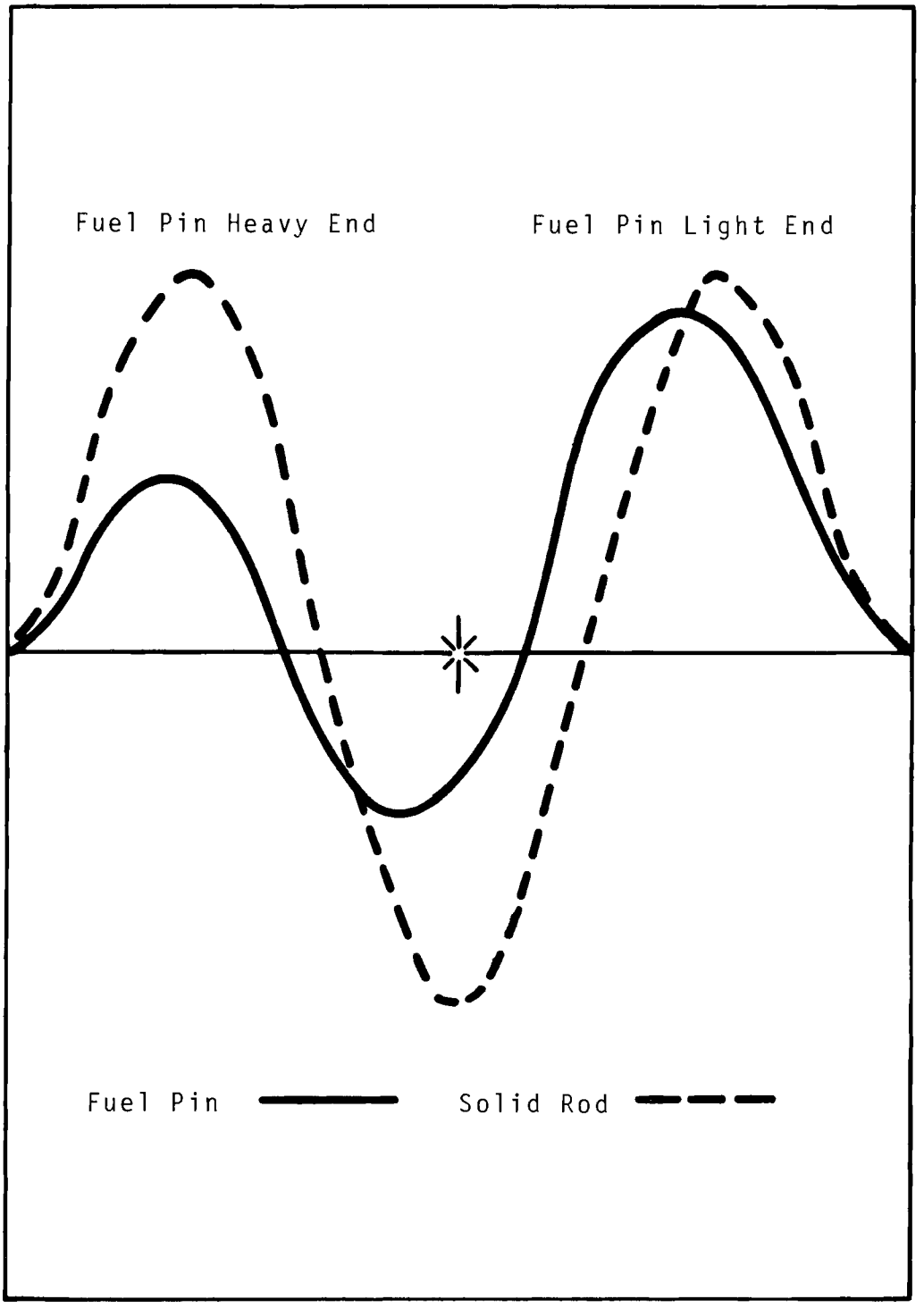

FIGURE 65. Third Vibration Mode Comparison

TABLE VI. Calculated and Test Vibration Data for Clad Tubes, Fuel Pins, and Solid Rods

	Hollow Tube*, cps		Fuel Pin, cps					Solid Rod*, cps		
					Theoretical Lumped Mass				Theoretical	
Mode	Experimental	Theoretical	Experimental (No F-F Wires)	Experimental (Fixed-Fixed)	Fixed-Fixed	Fixed-Pinned	Pinned-Pinned	Experimental	Exact	Lumped Mass (20)
1	7.2	9.5	6.3	6.3	6.29	4.77	2.82	8.5	8.04	8.05
2	37	26.1	20.5	19.5	19.9	16.5	13.1	32	22.1	22.2
3	39	51.2	21.5	20.5	38.1	32.1	27.7	35	43.5	43.5
4	105	84.8	35	35	62.8	56.8	49.8	87	71.8	71.9
5	110	126	37	37	92.4	84.9	77.6	91	107	107.4
6	210	176	52	51	132.0	123.4	113.2	160	149	149.9
7	220	235	54	53	164.9	151.8	145.0	175	199	199.4
8					200.7	199.0	188.0			255.6
9					265.7	244.5	244.3			318.5
10					323.1	313.6	313.6			387.4

* *Same dimension as reference fuel pin*

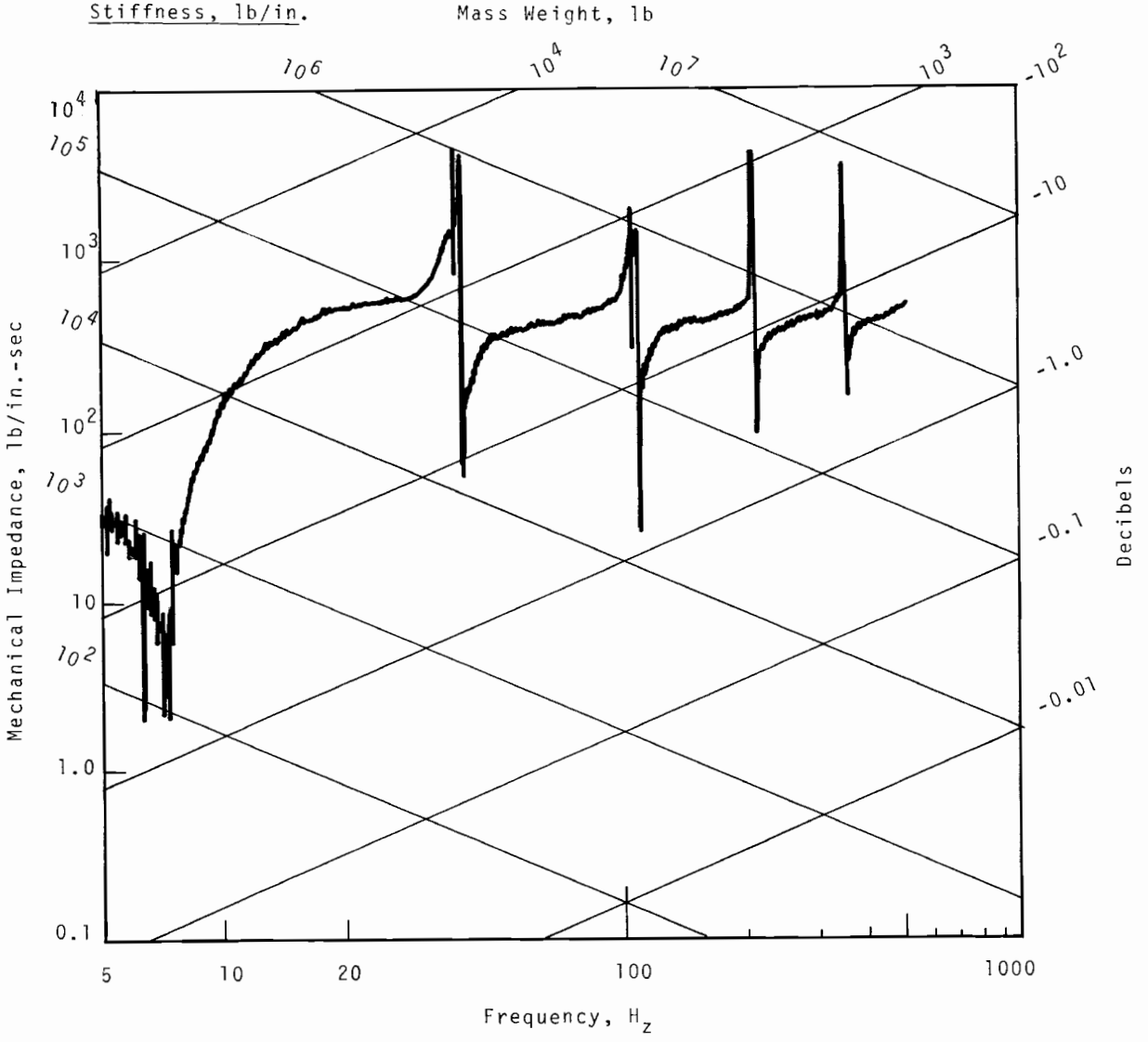

FIGURE 66. Hollow Rod (Thin Wall) Force Level

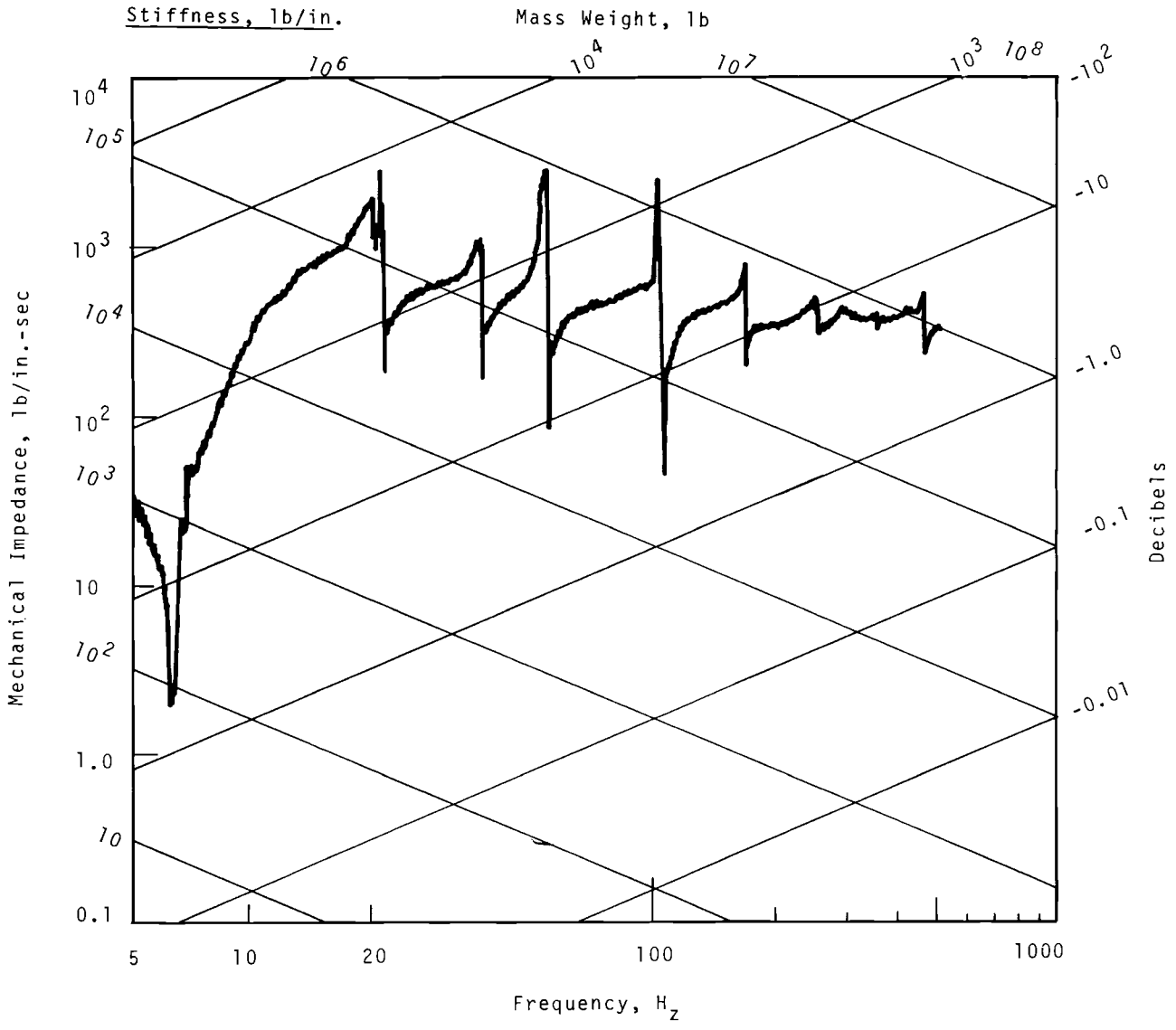

FIGURE 67. Fuel Pin (Without Wire) Force Level

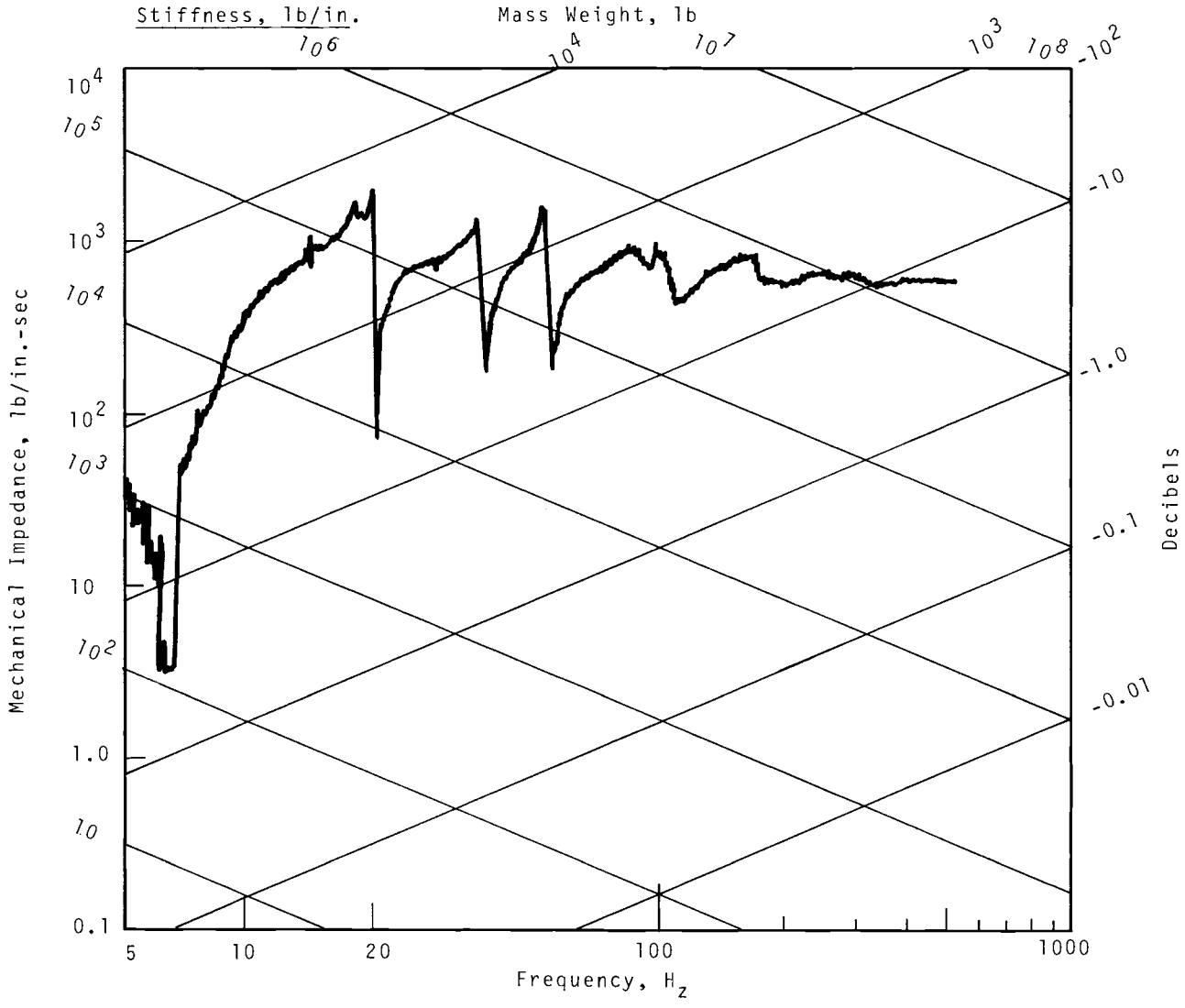

FIGURE 68. Fuel Pin (With Wire) Force Level

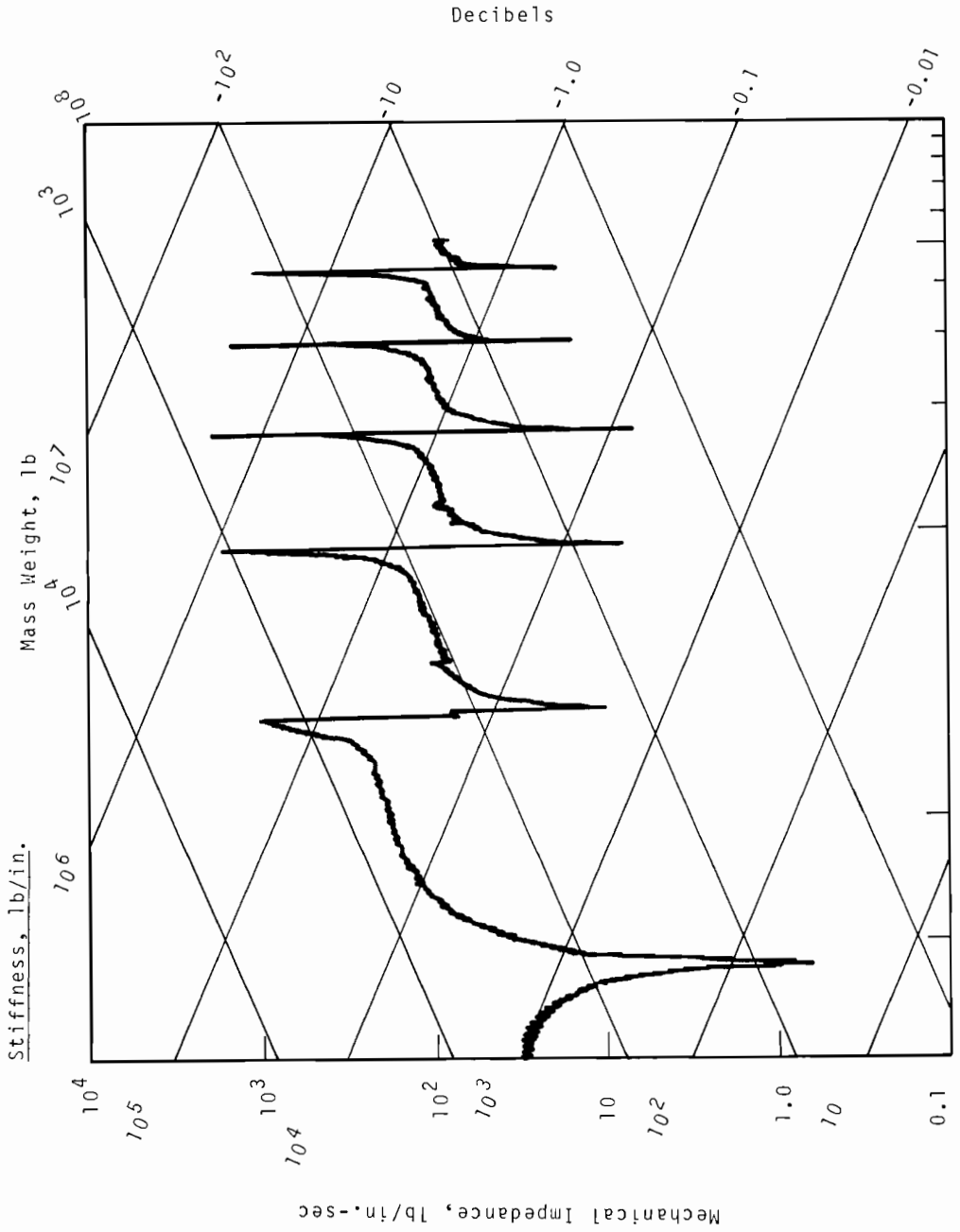

FIGURE 69. Solid Rod Force Level

frequencies must lie between those of the original system. The attachment for driving the test items provides an additional constraint. The test set up will be altered to eliminate this constraint. Second, harmonic distortion from additional degrees (rotational) of freedom can also alter the observed natural frequencies. Finally, the theoretical calculations assume perfect fixity at the ends, although, in reality, perfect fixity cannot be achieved.

The frequency-impedance plots show that the fuel pins vibrate in a manner very similar to the rod and tube. The preliminary use of testing rods and tubes is therefore worthwhile in developing techniques and exploring instrumentation possibilities. The effect of the wire wrap, also apparent, is minor in respect to frequencies but is more noticeable for force levels, especially at the higher frequencies.

Flow Induced Fuel Pin Vibration

The fuel pin vibrations were simulated with a shaker, and different data readout circuits were attached to a conductivity cell to measure displacements. The data circuits were evaluated for sensitivity, noise rejection, and introduction of harmonics. A bridge circuit appears to give the best definition of the data.

A vibration analysis was performed for a full length fuel pin with multiple supports. For this system, the natural frequencies were compared to a simply supported beam with a length the same as the distance between wire wrap supports. The first modes for both systems have comparable frequencies. However, the frequency of the second mode of the simply supported beam increased by a factor of 4, while the multisupported fuel pin frequencies increased only about 10 to 15%. This result is attributed to the second mode amplitude form of a simply supported beam which first occurs at one span rather than along the whole fuel pin length.

Then, at higher modes of the multisupported pin, this second mode amplitude form covers more and more spans, i.e.

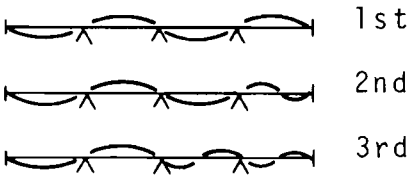

Thus a multisupported fuel pin may be excited at a range of frequencies between those obtained at the first and second mode shapes of a simply supported beam.

A new vibration test fixture, now being manufactured, will permit the testing of pin bundles as well as individual pins. Nineteen wire-wrapped model fuel pins manufactured for use with this fixture are now on hand. This test assembly will be used for development of instrumentation for the full scale vibration-hydraulic tests planned in late FY 1968.

SODIUM EFFECTS

M. K. Millhollen

A seven-pin cluster was fabricated and subjected to flow testing in the PNL isothermal sodium test loop. The pin cluster consisted of seven 0.200-in. diam pins (304 SST), each containing 17.5 in. of 0.168-in. diam depleted UO_2 pellets to simulate the mass and vibration characteristics of mixed oxide pellets. The overall length of the cluster was 24 in. A shortened cluster was used to keep the loop pressure drop at the required test coolant velocity level. The pin spacing was maintained by a 0.040-in. diam wire wrap on a 12-in. pitch.

The flow duct was a hexagonal stainless tube of 0.703 in. inside dimension across the flats. The duct was fabricated by draw sizing a 1-in. x 0.065-in. walled stainless steel tube. The duct was equipped with 18 tubes 1/8 in. in diameter

penetrating the wall of the basket for attaching pressure sensing probes (water test only).

The seven-pin sodium flow test cluster was recently removed from test in flowing sodium after 240 days (5760 hr) at a velocity of ∿25 fps and a temperature of 1060 °F. Carbon was maintained to <20 ppm, and oxygen to <10 ppm. Tests of small pin clusters using grid spacers will follow this test. Full scale tests of subassemblies in sodium will take place in the Core Component Test Loop at ANL.

Measurements on individual rods and wires showed no obvious decrease in diameter. Rod numbers, put on the rods by the grit blast method, are still visible. Inasmuch as these marks are normally 0.0001 in. deep, diametral wear on the fuel rod surfaces may be considered less than 0.0002 inch. Figures 70, 71, and 72 show the cluster as it now appears. No evidence of wire erosion, corrosion dimensional change, or wire wrap loosening was apparent.

The seven-rod cluster will be re-inserted in the hexagonal flow basket and the basket will be placed back in the loop after the new pump is installed. This pump will provide a sodium flow of higher velocity than the 27-30 fps range. The test will be completed after 12 full flow months of testing.

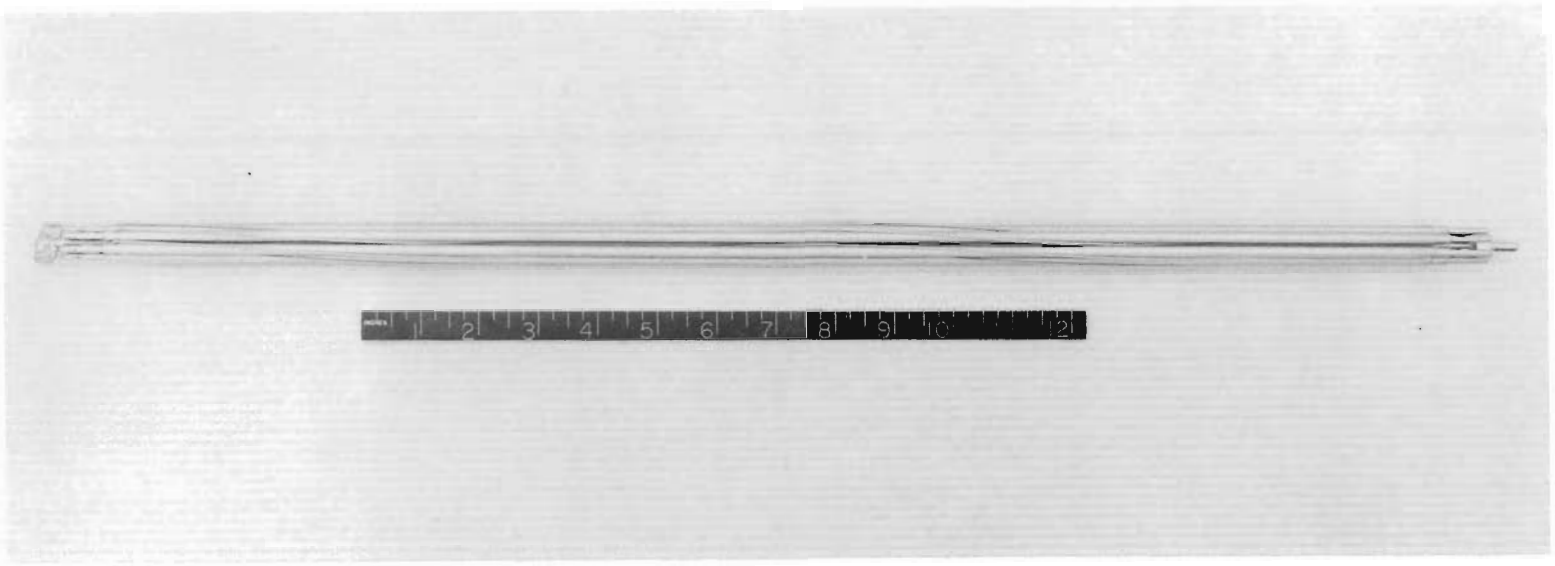

FIGURE 70. Seven Pin Sodium Test Assembly After 5760 Hr at 25 FPS and 1060 °F

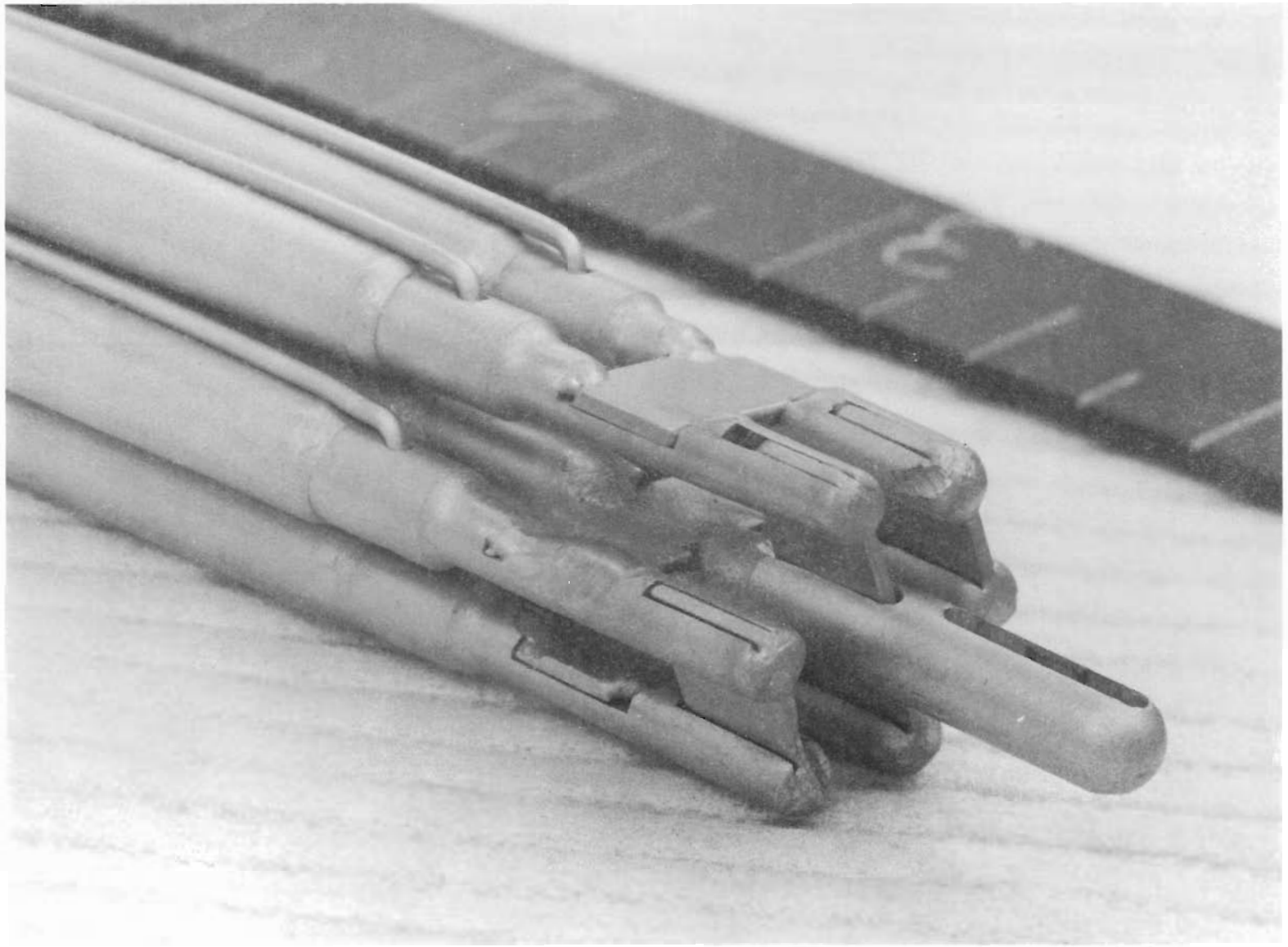

FIGURE 71. Seven Pin Sodium Test Assembly After 5760 Hr at 25 FPS and 1060 °F

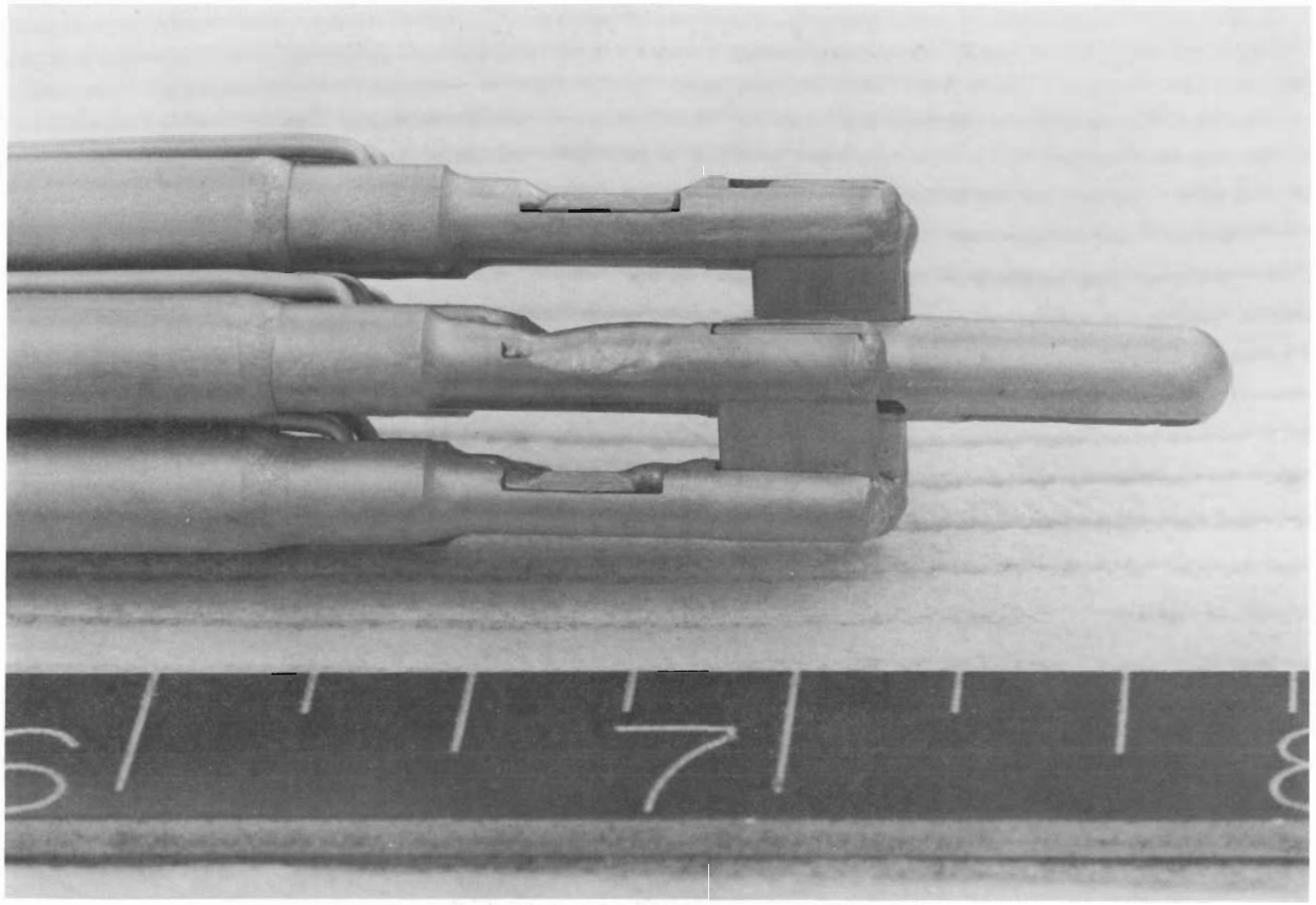

FIGURE 72. Seven Pin Sodium Test Assembly After 5760 Hr at 25 FPS and 1060 °F

REFERENCES

1. *A-0035-R, Conceptual Component Design Description for the First Core Fuel Assembly. No. 35. Pacific Northwest Laboratory, Richland, Washington, January 29, 1968.*

2. *FFTF Control Rod Drive Mechanism and Pin Spacer Studies, WARD-30, Prepared Under Contract AT(30-1)-3684, Westinghouse Electric Corporation, Advanced Reactors Division, P. O. Box 158, Madison, Pennsylvania 15663.*

3. *J. J. Edwards, E. A. Fischer, W. H. Jens, J. B. Nims, R. G. Pallmer, A. A. Shoudy, and R. C. Williams. Fast Reactor Fuel Cycle Cost and Temperature Coefficient of Reactivity for PuO_2-SS and PuO_2-UO_2, APDA-154. Atomic Power Development Associates, Inc., Detroit, Michigan, April 25, 1963.*

4. *P. D. Cohn. FTR Fuel Design and Analysis Hydraulic, Sodium, and Mechanical Testing, BNWL-599. Pacific Northwest Laboratory, Richland, Washington, February 1968.*

5. *G. M. Hesson, A. Padilla, and J. M. Yatabe. Unpublished Data. Pacific Northwest Laboratory, Richland, Washington, April 1967. (Thermal-Hydraulics Development).*

6. *A. N. de Stordeur. "Drag Coefficients for Fuel Element Spacers," Nucleonics, vol 19. no. 6. June 1961.*

7. *G. M. Hesson and C. W. Angle. Unpublished Data. Pacific Northwest Laboratory, Richland, Washington, March 13, 1967. (Internal letter to M. K. Millhollen: Pressure Drop of 7-Pin Test Section).*

8. *R. D. Benham. A Simplified Method for Programming a 7090 Computer for Simulation of Dynamic Systems, HW-80246. Available from Clearinghouse for Federal Scientific and Technical Information, Springfield, Virginia, February 6, 1964.*

9. *K. Rehme. The Measurement of Friction Factors for Axial Flow Through Rod Bundles with Different Spacers, Performed on the INR Test Rods, EURFNR-142 P. Karlsruhe. November 10, 1965.*

10. *Primary Examination of Experimental Prototype Fuel Pins Discharged from Dounreay Fast Reactor in August, United Kingdom Atomic Energy Establishment, Dounreay, Caithness, Scotland, 1965.*

REFERENCES

11. D. S. Rowe. A Cross-Flow Mixing Between Parallel Flow Channels During Boiling, Part I. COBRA - Computer Program for Coolant Boiling in Rod Array. BNWL 371, Part I. Pacific Northwest Laboratory, Richland, Washington, March 1967.

12. D. S. Rowe and C. W. Angle. Crossflow Mixing Between Parallel Flow Channels During Boiling, Part II. Measurement of Flow Enthalpy in Two Parallel Channels, BNWL 371 PT2. Pacific Northwest Laboratory, Richland, Washington, December 1967.

13. FFTF Monthly Informal Technical Progress Report, BNWL-603. Pacific Norhtwest Laboratory, Richland, Washington, November 9, 1967.

14. FFTF Monthly Informal Technical Progress Report, BNWL-659. Pacific Northwest Laboratory, Richland, Washington, January 8, 1968.

15. FFTF Monthly Informal Technical Progress Report, BNWL-712. Pacific Northwest Laboratory, Richland, Washington, March 7, 1968.

16. Andrew Padilla, Jr. "Analysis of Coolant Mixing in the FFTF Fuel Bundle", to be presented at American Institute of Chemical Engineers at the Tenth National Heat Transfer Conference and Exhibit Symposium on Heat Transfer in Fast Reactor Technology at Philadelphia, Pennsylvania. August 11-14, 1968.

17. L. F. Moody. "Friction Factors for Pipe Flow," Trans. Amer. Soc. Mech. Engrs., vol. 66, p. 671. 1944

18. S. F. Armour and D. L. Smith. MANTA-Mixing Analyzed Nodal Thermal-Hydraulic Analysis, GEAP-4805. General Electric Company, Schenectady, New York. February 1965.

19. Fast Flux Test Facility Conceptual Design Description for the First Core Fuel Assembly No. 35, Pacific Northwest Laboratory, Richland, Washington, November 10, 1967.

20. Unpublished Data. Pacific Northwest Laboratory, Richland, Washington, April 1967. (Fast Flux Test Facility Monthly Informal Technical Progress Report).

REFERENCES

21. W. W. Little, et al. FTR Reference Nuclear Parameters and Parametric Studies, S-3 of 6, Preliminary Issue Support Document for A-0036, Pacific Northwest Laboratory, Richland, Washington, November 12, 1967.

22. FFTF Monthly Informal Technical Progress Report, BNWL 772. Pacific Northwest Laboratory, Richland, Washington, May 7, 1968.

23. O. E. Dwyer. "Analytical Study of Heat Transfer to Liquid Metals Flowing In-Line Through Closely Packed Rod Bundles," Nucl. Sci. Eng. vol. 24, p. 347. 1966.

24. R. C. Deissler and M. F. Taylor. Analysis of Fully Developed Heat Transfer and Flow in an Annulus with Various Eccentricities, NACA-TN-3451, pp. 4-8. Lewis Flight Propulsion Laboratory, Cleveland, Ohio, May 1965.

25. M. B. Bader and G. L. O'Neill. "EVESR Power Distribution and Thermal-Hydraulic [Hydraulic] Analysis", Nucl. Eng. and Design. vol. 6, pp. 115-133. 1967.

26. R. E. Bardsley, C. A. Burgess, and H. G. Powers. Proposed Program for Development of the Capability to Manufacture Complete Driver Fuel Subassemblies, March 8, 1968.

27. T. T. Claudson, R. E. Peterson, and J. E. Hanson. Trip Report: U.S. FFTF Fuels and Materials Team Trip to the United Kingdom and France, BNWL-569. Pacific Northwest Laboratory, Richland, Washington, December 1967.

28. Fast Flux Test Facility, Monthly Informal Technical Progress Report, December 1967, BNWL-659. p. 3.54. Pacific Northwest Laboratory, Richland, Washington, January 8, 1968.

29. J. J. Holmes. Unpublished Data. Pacific Northwest Laboratory, Richland Washington, (Personal Communication to J. E. Hanson)

30. J. S. Brunhouse, A. B. Burgess, G. T. Geering, S. Nakazato, and G. W. Titus. Army Gas-Cooled Reactor Systems Program In-Pile Test of Prototype ML-1 Fuel Elements, IDO-28616. Idaho Operations Office, Idaho Falls, Idaho, June 1964.

REFERENCES

31. *Fast Flux Test Facility Monthly Technical Progress Report, BNWL-686. Pacific Northwest Laboratory, Richland, Washington, January 1968.*

32. *M. T. Jakub and W. H. Sutherland. Unpublished Data. Pacific Northwest Laboratory, Richland, Washington, February 28, 1968. (Core Radial Constraint Theory and Applications to the FTR).*

DISTRIBUTION

No. of Copies

OFFSITE

1 AEC Chicago Patent Group
G. H. Lee

30 AEC Division of Reactor Development and Technology
M. Shaw, Director RDT
Asst Dir for Nuclear Safety
Analysis & Evaluation Br, RDT:NS
Environmental & Sanitary Engrg Br, RDT:NS
Research & Development Br, RDT:NS
Asst Dir for Plant Engrg, RDT
Applications & Facilities Br, RDT:PE
Components Br, RDT:PE
Instrumentation & Control Br, RDT:PE
Liquid Metal Systems Branch, RDT:PE
Asst Dir for Program Analysis, RDT
Asst Dir for Project Mgmt, RDT
Liquid Metals Projects Br, RDT:PM
FFTF Project Manager, RDT:PM (3)
Asst Dir for Reactor Engrg
Control Mechanisms Br, RDT:RE
Core Design Br, RDT:RE (2)
Fuel Fabrication Br, RDT:RE
Fuel Handling Br, RDT:RE
Reactor Vessels Br, RDT:RE
Asst Dir for Reactor Tech
Coolant Chemistry (RDT)
Fuel Recycle Branch (RDT)
Fuels & Materials Br, RDT:RT
Reactor Physics Br, RDT:RT
Special Technology Br, RDT:RT
Asst Dir for Engrg Standards

1 AEC Idaho Operations Office
Nuclear Technology Division
C. W. Bills, Director

1 AEC San Francisco Operations Office
Director, Reactor Division

No. of Copies	
4	AEC Site Representatives Argonne National Laboratory Atomics International Atomic Power Development Associates General Electric Co., Sunnyvale
2	Argonne National Laboratory R. A. Jaross LMFBR Program Office
6	Atomics International D. J. Cockeram (5) Liquid Metal Engrg Center R. W. Dickinson (1)
1	Atomic Power Development Associates Document Librarian
2	Babcock & Wilcox Co. Atomic Energy Division S. H. Esleeck Boiler Division T. P. Farrell
3	Bechtel Corporation J. J. Teachnor (2) D. H. Weiss
1	Combustion Engineering, Inc. (AEC) 1000 MWe Follow-On Study W. P. Staker, Project Manager
2	Gulf General Atomic Incorporated (AEC) D. Coburn
5	General Electric Co., San Jose Sunnyvale, California Karl Cohen (3) Bertram Wolfe (2)

No. of Copies

1 Idaho Nuclear Corporation
D. R. deBoisblanc

1 Nuclear Systems Programs
P.O. Box 15132
Cincinnati, Ohio 45215
D. H. Ahmann

1 PNL Representative
N. A. Hill (ZPR-III)

1 Stanford University
Nuclear Division
Division of Mechanical Engrg
R. Sher

5 Westinghouse Electric Corp.
Atomic Power Division
Advanced Reactor Systems
J. C. R. Kelly

ONSITE-HANFORD

1 AEC Chicago Patent Group
R. K. Sharp (Richland)

4 AEC Richland Operations Office
FFTF Program
J. M. Shivley

4 AEC Site Representatives - PNL
P. G. Holsted (2)
L. R. Lucas
A. D. Toth

51 Battelle-Northwest
E. R. Astley
J. M. Batch
T. J. Bennett
C. L. Boyd
C. A. Burgess

Battelle-Northwest (contd)

A. C. Callen
J. R. Carrell
T. T. Claudson
P. D. Cohn
D. L. Condotta
R. R. Cone
E. A. Evans
L. M. Finch
M. A. Fischer
G. L. Fox
S. M. Gill
B. R. Hayward
R. J. Hennig
P. L. Hofmann
R. J. Jackson
M. T. Jakub
B. M. Johnson
N. L. Johnson
D. C. Kolesar
D. L. Koreis
G. A. Last
R. J. Lobsinger
W. E. McClung
W. B. McDonald
M. K. Millhollen
R. E. Peterson
H. J. Powers
J. B. Shafer
D. W. Shannon
D. E. Simpson
W. H. Sutherland
J. C. Tobin
K. G. Toyoda
J. H. Westsik
J. F. Wett
D. R. Wilson
J. M. Yatabe
FFTF Files (2)
Technical Information (5)
Technical Publications (2)